Review Article

Zummurd Al Mahmoud, Mohammed Asmael*, Rosli Ahmad, Saeid Sahmani, Kamila Kotrasova*, Mária Mihaliková, David Hui, and Babak Safaei*

Recent developments in ultrasonic welding of similar and dissimilar joints of carbon fiber reinforcement thermoplastics with and without interlayer: A state-of-the-art review

https://doi.org/10.1515/rams-2024-0077
received February 26, 2024; accepted December 10, 2024

Abstract: Ultrasonic welding (USW) is utilized to join identical and non-identical materials, with and without a thermoplastic composites or thermoset composites coupling layer, or with different shapes of energy directors or adhesive materials. Due to its emerging structure, joining carbon fiber (CF)-reinforced polymer has become imperative due to the developed concerns in different industrial and manufacturing sectors. This review article covers all types of joined CF-reinforced polymers, including similar/dissimilar CF-reinforced thermoplastics or CF-reinforced thermosets joined by USW, considering different types of USW (spot welding, continuous welding). This review considers various welding process parameters and their impacts on welding quality, welding strength, and mechanical and microstructure characterizations of the welded joint. Also, improving the USW joints and their challenges are discussed. The fabrication processes of the polymer matrix composite and various polymers are addressed. In addition, the recyclability of CF-reinforced polymer is highlighted. A key finding from this review is that polyetheretherketone and both types of nylon (PA6 and PA66) show high exceptional characterizations, making them more favorable for developing CF-reinforced thermoplastics over other types of polymers. While a unique co-curing process must be completed for the adhesive material before performing the USW, welding energy is the most effective process parameter that enhances the mechanical properties when using adhesive bonding before USW.

Keyword: polymer matrix composites, interlayer, welding quality, lap shear strength, spot welding

*** Corresponding author: Mohammed Asmael,** School of Mechanical and Aerospace Engineering, Queen's University Belfast, Belfast, BT9 5AH, United Kingdom; Advanced Composites Research Group, School of Mechanical and Aerospace Engineering, Queen's University Belfast, Belfast, BT9 5AH, United Kingdom, e-mail: m.asmael@qub.ac.uk
*** Corresponding author: Kamila Kotrasova,** Institute of Structural Engineering and Transportation Structures, Faculty of Civil Engineering, Technical University of Kosice, Vysokoskolska 4, 04200, Kosice, Slovakia, e-mail: kamila.kotrasova@tuke.sk
*** Corresponding author: Babak Safaei,** Department of Mechanical Engineering, Eastern Mediterranean University, Famagusta, North Cyprus via Mersin 10, Turkey; UNESCO-UNISA Africa Chair in Nanosciences and Nanotechnology, College of Graduate Studies, University of South Africa, Muckleneuk Ridge, PO Box 392, Pretoria, South Africa, e-mail: babak.safaei@emu.edu.tr
Zummurd Al Mahmoud: Department of Mechanical Engineering, Eastern Mediterranean University, Famagusta, North Cyprus via Mersin 10, Turkey
Rosli Ahmad: Department of Manufacturing and Industrial Engineering, Faculty of Mechanical and Manufacturing Engineering, University Tun Hussein Onn Malaysia, Parit Raja, 86400, Batu Pahat, Johor, Malaysia
Saeid Sahmani: Department of Civil Engineering, School of Science and Technology, The University of Georgia, Tbilisi, 0171, Georgia; Center for Advanced Materials and Structures, School of Science and Technology, The University of Georgia, Tbilisi 0171, Georgia
Mária Mihaliková: Institute of Materials and Quality Engineering, Faculty of Materials, Metallurgy and Recycling, Technical University of Kosice, Letna 1/9, 04200, Kosice, Slovakia
David Hui: Department of Mechanical Engineering, University of New Orleans, New Orleans, LA, 70148, United States of America

Abbreviations

AM	additive manufacturing
AF	aramid fiber
BO	Bayesian optimization
CF	carbon fiber
CFRP	carbon fiber-reinforced polymer
CFRTP	carbon fiber-reinforced thermoplastic
CFRTSC	carbon fiber-reinforced thermoplastic composite
CFRTS	carbon fiber-reinforced thermoset

CF/Ep	carbon fiber/epoxy
CNT	carbon nanotube
CUSW	conventional ultrasonic welding
CTT	cross tensile test
DSW	double spot welding
DLS	double-lap shear
ELF	Elium® film
ELP	Elium® particle
ED	energy director
EMMA	mendable polymer, poly [ethylene-co-(methacrylic acid)]
Ep	epoxy
FRC	fiber-reinforced composites
FRTP	fiber-reinforced thermoplastic
FRP	fiber-reinforced polymer
FE	finite element
FED	flat energy director
FSW	friction stir welding
GA	genetic algorithm
GF	glass fiber
GFRP	glass fiber-reinforced polymer
GNP	graphite nanoplatelet
HAZ	heat-affected zone
HHT	Hilbert-Huang transform
HFUSW	hollow fixture ultrasonic welding
HNT	halloysite nanotube
IPS	interposed sheet
IW	induction welding
LSS	lap shear strength
LW	laser welding
ML	machine learning
MF	mechanical fastener
MSW	multi-spot welding
MWCNT	multi-walled CNT
NC	nanocomposite
NF	nanofiller
NFRC	natural fiber-reinforced composite
NSM	near-surface mounted
NN	neural network
NL	nonlinear
PBF	powder bed fusion
PC	polycarbonate
PEI	polyetherimide
PFRP	polymer fiber-reinforced polymer
PMC	polymer matrix composite
PCM	polymer-coated material
PMMA	polymethyl methacrylate polymer
POF	plastic optical fiber
PVA	polyvinyl alcohol
PVB	polyvinyl butyral
rCF	recycled carbon fiber
RF	reed flour
RTM	resin transfer molding
RW	resistance welding
SSW	single spot welding
SE	steam-exploded
S-USW	water-submerged ultrasonic welding
SVM	support vector machine
TOF	Time-of-flight
TPC	thermoplastic composite
TP	thermoplastic
TSC	thermoset composite
UF	ultimate failure
UFL	ultimate failure load
USW	ultrasonic welding
VaRTM	vacuum-assisted resin transfer molding
VMD	variational mode decomposition
2D	two-dimensional

1 Introduction

1.1 Ultrasonic application and ultrasonic welding (USW) for polymers

USW is a speedy process of joining materials. It can be used for joining alloy/composites and composite/composite. USW is considered as a solid-state welding method that is defined as a sustainable welding process [1]. It is worth mentioning that the USW is one of the most promising fusion bonding processes. Nonetheless, the fusion bonding technologies consist of USW, induction welding (IW), and resistance welding (RW) techniques [2]. The basic concept of USW is based on the ultrasonic wave, which is same as any other ultrasonic process machine (based on ultrasonic wave) applications. Figure 1 illustrates the current applications of various ultrasonic machines for polymer industries. As shown in Figure 1, the major applications of ultrasonic for polymers can be classified into four main categories, which are fabrication process, welding, defect detection, and cleaning. However, each classification can be further classified as shown.

Furthermore, the USW main principle is based on very high frequency usually 20 kHz, associated with very low amplitude at the joining surface interface of the adherends to be welded. In the USW process, the vibrations are converted to heat between the two joining surfaces, which melt the thermoplastic composites (TPCs) and enable the joining [3–6], where the vibration energy leads to a surface asperity deformation, which disperses into heat. In consequence, the heat melts the surface asperities, which then flow, expanding the interfacial area, which permits the molecules of the polymer chains to diffuse [7]. High

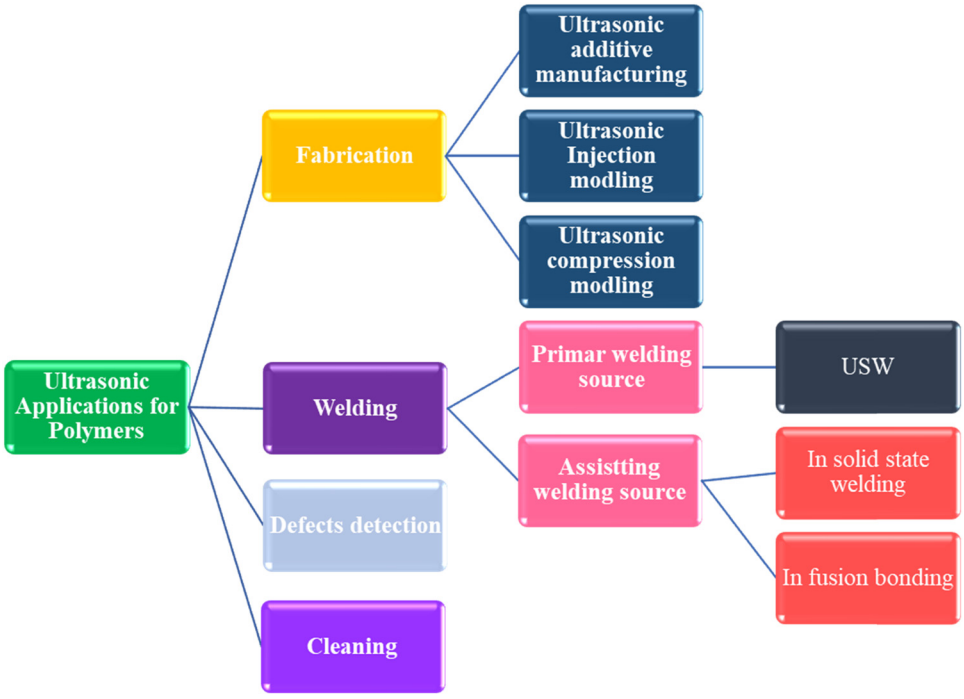

Figure 1: Applications of ultrasonic in polymers.

amount of frequency in kHz in the oscillation of the USW to the stacked specimens, frictional heat will be generated by the plastic boundaries, which melt and form the joint [4]. A schematic representation of USW machine with its components is given in Figure 2. The generated frictional heat is caused by the transmission of the mechanical vibration, which helps in melting the TPCs causing them to flow, which will cause the interfacial bond between the two specimens to join. This heating mechanism is classified as surface friction as well as viscoelastic friction [8,9]. Mainly, the viscoelastic heating became governing when the temperature reached the glass transition temperature, is the reason of providing the absolute heating during welding process [8]. As shown in Figure 2, the USW machine consists of generator, transducer, booster, sonotrode, and fixture. The generator converts the electrical power to high electrical energy at 20–40 kHz. The transducer works as a converter, which alters the high frequency electrical pulses to a mechanical vibration. The amplitude of this mechanical vibration is further increased or decreased by the booster. In consequence, the mechanical oscillations are transferred to the specimens by the sonotrode. However, the specimens remain stable by the fixture on the anvil [10]. Besides, the welding process consists of a solidification phase, which is a consequence of the vibrational phase, in which the heat is generated. Further, the vibration energy is transfererred to the sontrode, which creates the welded zone by heating the surface [11].

The USW has the potential for extensive applications, particularly in lightweight vehicle structures, owing to its good strength and stiffness [12,13], as well as in the marine industry [14]. The global market scale of USW technology is demonstrated in Figure 3 [15,16]. As shown in Figure 3, the applications of joining polymers by USW are much greater than those of metals. Besides, a substantial increase in the

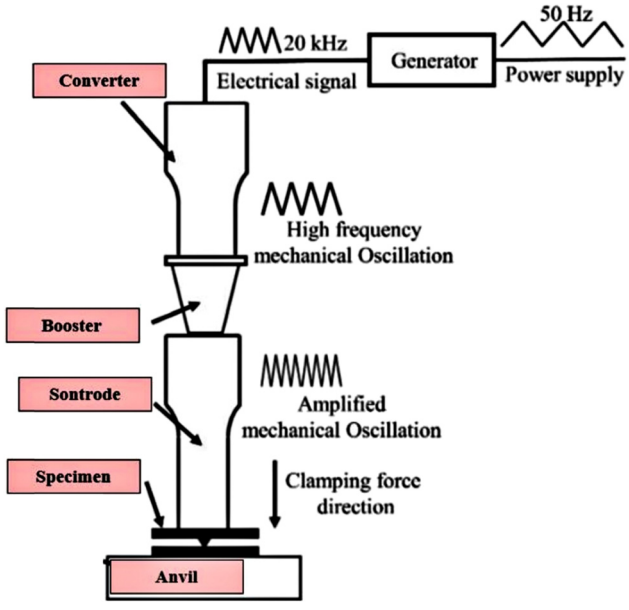

Figure 2: The schematic of USW [20].

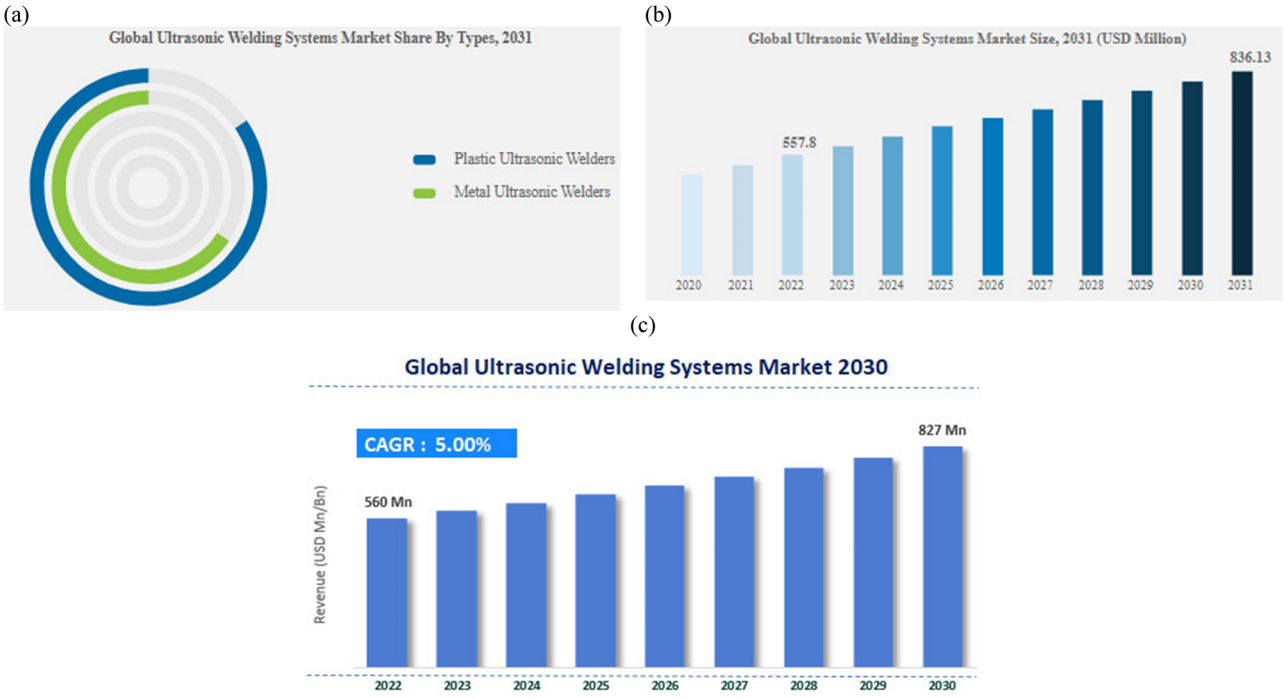

Figure 3: The global market scale of USW technology: (a) The development of USW in polymers and metals and (b and c) the annual global market of USW in various application sectors [15,16].

global market is observed, where in 2022, the market size reached 550–560 million US dollar, while it is estimated to reach 825–840 million US dollar in 2030. However, the first publication regarding USW of TPCs was recorded in 1989 published by Benatar and Gutowski [17], where the processing information was highlighted, and the obtained outcomes were significant. Nonetheless, the USW has many advantages, *e.g.*, it is a time-saving method and an economical technique for joining polymer composites [18], and disadvantages, *e.g.*, it is mainly used for welding small areas and it can be used under some conditions for welding larger areas [19]. Further advantages and drawbacks of USW are illustrated in Figure 4.

From literature records, Sandeep and Natarajan [21] presented a review that focused on investigating the recent developed joining methodologies for carbon fiber (CF)-reinforced polymer (CFRP)/Al-joined hybrid structures. Liu *et al.* [22] presented a comprehensive review to examine the metal/fiber-reinforced thermoplastic (FRTP) joined by USW. Abbas *et al.* [23] explored the developments in USW of joining lightweight alloys. Furthermore, Pramanik *et al.* [24] studied the earlier available joining techniques that were utilized in joining CFRP/Al. Besides, Fan *et al.* [25] presented a review study focused on considering various joints

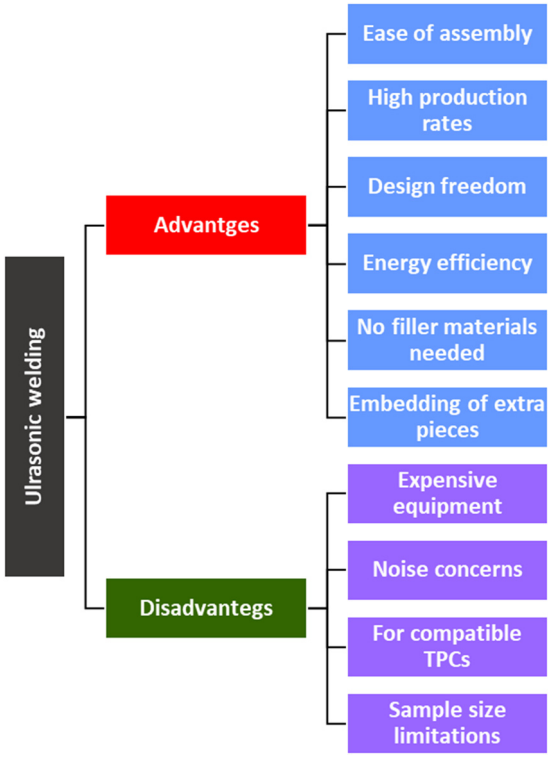

Figure 4: The advantages and disadvantages of USW process.

joined by implementing the ultrasound vibration. The dissimilar joining of carbon fiber-reinforced thermoplastic (CFRTP) with metals by laser welding (LW) has been reviewed by Jiao *et al.* [26]. Additionally, Acherjee [27] reviewed the parameters, process monitoring, and quality attributes of laser transmission welding used for similar and dissimilar joining of polymer/polymer and polymer/metal. Moreover, Li and Palardy [28] reviewed the methodologies, which are currently used to monitor the damage caused by fiber-reinforced polymer (FRP) joints. However, Li *et al.* [29] accomplished a comprehensive review that focused on examining the mechanical features as well as the behavior of structural health monitoring of carbon nanotube (CNT)–FRP composites. An evaluation between different types of joining approaches used to join TPCs and thermoset composites (TSCs) was published earlier. As findings, the USW was found to be most suitable in some essential factors of joining performance, processing time, minimal surface preparation, *in situ* inspection production environment, and reproducibility [30]. However, a short review study has been accomplished by Forintos and Czigany [31], who investigated the applications of CFRPs and highlighted the electrical characterizations of the CF reinforcement. Zeng *et al.* [32] inspected the impact of fiber interfacial and the mechanical responses of CFRP reinforced with gelatin-CNTs. In addition, the welding methodologies that were implemented in joining polymers for biomedical applications were stated by Amanat *et al.* [33]. Nonetheless, Hamza and Jalal [34] accomplished a comprehensive review that covered the PCs joined by friction stir proceeding. Asmael *et al.* [35] performed a review study that investigated the enhancements in tensile features of the CFRP joined by friction welding. Meanwhile, El-Sayed *et al.* [36] presented a review study focused on friction stir welding (FSW) in joining metallic materials. Wang *et al.* [37] reviewed the TPCs reinforced with various types of fibers and joined by USW. Zhao *et al.* [38] presented a study that covers the recent progress in USW in joining various fiber-reinforced polymer composites. Nagarajan and Manoharan [39] presented a comprehensive review that studied various types of joining and welding used in joining metal with polymer in a hybrid structure. Besides, Ni and Ye [40] reviewed various Al alloys joined by USW where the macrostructure, microstructure, and mechanical characterizations of the weldment were addressed. Moreover, Bose *et al.* [41] accomplished a recent review study which focused on the latest improvements in the USW of polymers and polymeric composites that investigate specific types of TPCs reinforced with CF and glass fiber (GF). Besides, for obtaining superior mechanical properties, Mirzaahmadi *et al.* [42] added TiO_2 and CuO nanoparticles to the polyvinyl chloride interface of the ultrasonically welded GF-reinforced polymer (GFRP) at optimum process parameters. However, Mahato *et al.* [43] presented a review paper exploring fibrous PC materials' mechanical response (static and dynamic) under various environmental circumstances and mainly to define the failure modes. Meschut *et al.* [44] accomplished a comprehensive review that focused on joining by plastic deformation. Additionally, Luckachan and Pillai [45] performed a comprehensive review for the purpose of investigating eco-friendly polymers and their developed perspective. Besides, the recent developments in eco-friendly sustainable materials such as bamboo and wood and their modification processes were investigated and comprehensively reviewed by Paul *et al.* [46]. Moreover, Alhijazi *et al.* [47] presented a comprehensive review investigating the latest improvements in palm fiber composites. In a further study, Odesanya *et al.* [48] revised several types of natural fiber-reinforced composite (NFRC) implemented in ballistic functions. Besides, based on high demands on natural fiber such as bamboo, it is essential to develop the bamboo material properties. Accordingly, Sun *et al.* [49] presented a comprehensive review that explored the nanotechnology applications in improving the bamboo material properties in different aspects. However, Gandini and Belgacem [50] presented a review on the preparation process for producing polymers generated from sustainable resources. In addition, to overcome the defects of NFRC, Hosseini *et al.* [51] presented a comprehensive review that focused on exploring the enhancements of fiber/natural-fiber treatment on the mechanical and physical characterizations of NFRC. Accordingly, several treatment processes were discussed, such as NaOH, polyvinyl alcohol, steam-exploded (SE) treatment, fungicide solutions, plasma treatment, distillate treatment, and chemical coupling agents. Nonetheless, Rafiee and Shahzadi [52] presented a comprehensive review on the investigation of the mechanical characterizations of polymer reinforced by nanoclay. Hosseini *et al.* [53] presented a comprehensive study that focused on exploring the behavior of fiber-reinforced composites (FRCs) laminated with CNT. Francisco *et al.* [54] presented a comprehensive review addressing the enhancement of various nanocomposites (NCs) (tubes, particles, and layers) on polyamide NCs. Gu and Gu [55] reviewed the methodologies utilized in investigating the microbiological degradation and the deterioration of numerous polymers with different grades of degradability. Anugrahwidya *et al.* [56] presented a comprehensive review that focused on investigating the performance of starch-based bioplastics embedded with fiber and nanoparticles. SJ and Natarajan [57] presented a review study that focused on recently developed joining techniques for joining Al to polymer/CFRP for hybrid lightweight structures.

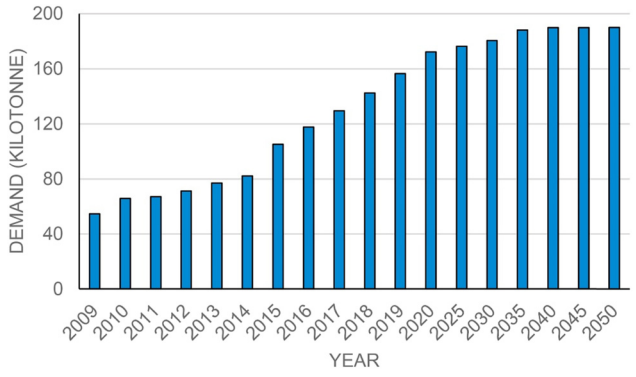

Figure 5: The annual global demand on CFRP in kilo tons [61].

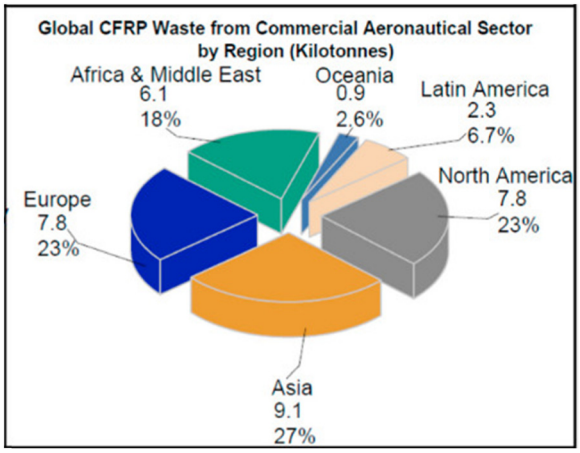

Figure 6: The global estimation of CFRP wastes in 2050 from the aeronautical sector by region [61].

Furthermore, Xiao *et al.* [58] explored the latest improvements in the mechanical characterization of hybrid fiber metal laminates reinforced polymers and their applications in automotive industrial sector. A comprehensive review has been accomplished to investigate the current techniques for curing the deformation process of CF-reinforced resin composites and their challenges. Also, Zhang *et al.* observed that the significant parameters that affected the curing deformation were variable and varied by changing the process and environmental conditions [59]. However, Yu *et al.* [60] performed a novel review study that investigates the preparation processes as well as the regulations of cellulose materials for developing cellulose/epoxy (Ep) composite which overcome the disadvantages of CF/Ep composite such as high costs. Furthermore, due to the global high demand on CFRP as shown in Figure 5 where a yearly gradual increase can be observed, Zhang *et al.* [61] presented a comprehensive review that focused on the recyclability of CFRP. In addition, the global estimation of CFRP wastes in 2050 from the aeronautical sector by region is predicted and plotted in Figure 6, the maximum waste is estimated to be in Asia followed by Europe. While, the lowest is estimated to be in Oceania. Besides, a further analysis of capital investments in CFRP in various sectors is illustrated in Figure 7. It is seen that highest capital investment is recorded by aerospace and defense sectors, while the lowest is in marine sector.

Meanwhile, this state of art review is considered as the first comprehensive review that covers the joining process of similar and dissimilar CFRP weldment produced by USW, considering single, double, multi, and continuous welding. In this context, the enhancement of process

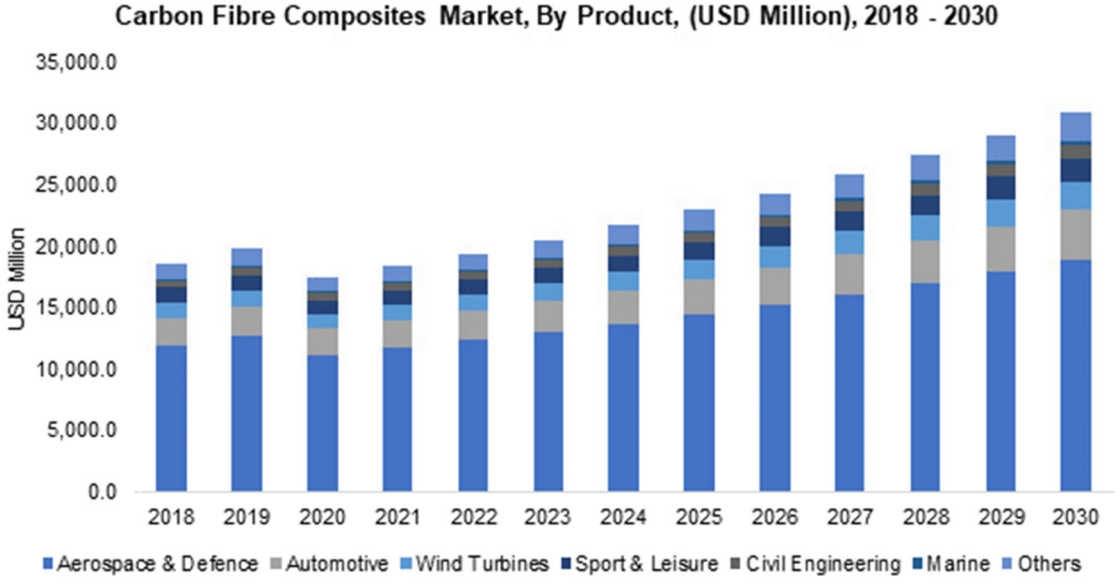

Figure 7: The annual capital investments in CFRP in various sectors [62].

parameters on the microstructure and mechanical characterizations, and welding quality is discussed. Besides, it highlights the influence of using energy director (ED) or interlayer and the consequence of preheating and heat treatment on the weldment strength and quality. The various fabrication processes and other welding processes are also briefly addressed, besides highlighting the challenges faced by USW.

1.2 Comparison of USW and other joining approaches

The USW has become more attractive to use in different industrial applications due to its several advantages over regular welding processes such as FSW, shield metal arc welding, *etc.* Apart from the USW advantages mentioned in Figure 4, it also requires a very short welding time (a few seconds) and does not require the usage of another material as gas tungsten arc welding or between the interface as required in other welding techniques such as RW, as well as the welding strength is very close to the neat polymer strength [63]. Additionally, the most unique advantage of USW over other welding processes is that the potential of *in situ* observation is automated through process data [64], *e.g.*, a strong relationship among the response of a microprocessor-controlled welder and the physical variations at the welding interface for USW using flat energy director (FED) [65]. Furthermore, joining TPCs by USW has the advantage of the absence of forging material on the welding interface, such as metal mesh, and other welding features like significant welding joint quality [64]. Accordingly, a comparison study was performed between the strength joint by adhesive bonding and by USW, the joint was in between C/Elium® [66]. The results showed that ultrasonically welded composite joints had a 23% higher lap shear strength (LSS), as shown in Figure 8. It has been found that the optimal welding time for an ultrasonic welded junction was 1.5 s, compared to 10 min for an adhesively bonded joint. Besides, it has been reported that it is necessary to perform a co-curing process to coat the TSCs with a rich layer of TPCs for the purpose of achieving a sufficient adhesion in between TPC and TSC polymers for the welding process, such as USW [67,68]. In addition, by implementing the adhesive joining technique, numerous bonding defects may occur in the bonded joints, which consequently affects the bonding quality, such as porosity, inadequate adhesive, and cracking [69]. However, the basic steps of adhesive bonding and types of adhesive joints are shown in Figure 9. Nevertheless, the quality of adhesive bonding can be established either by physical breaking or by observing the number of adhesive-bonded joints [70]. Additionally, by generating a hybrid joining technique that consists of adhesive joining followed by USW, the uncured adhesive bonding in the USW process is uninspected due to the high damping property, which will dramatically reduce the ultrasonic signal, and subsequently, the inspection sensitivity [71]. However, this effect can be mitigated by squeezing the melted adhesive out by using the pressure of the sonotrode in the USW. The formatted weld nugget may use to overhaul the partially adhesive bonded joints under the appropriate USW process parameters [70]. Furthermore, Zhang *et al.* [70] implemented the USW to repair a previous joint of CFPA6 by adhesive bonding.

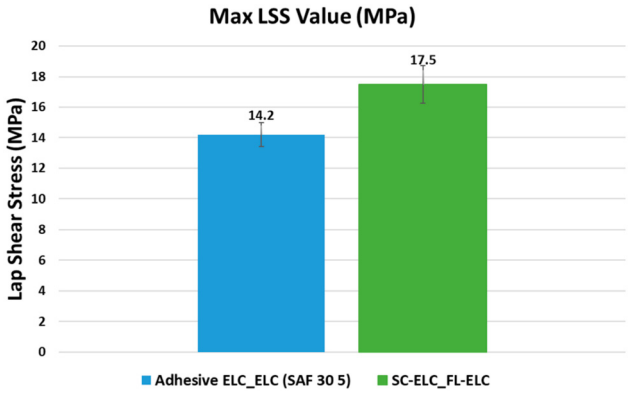

Figure 8: A comparison of the LSS between welded and adhesively bonded laminate joints for C/Elium®, under USW conditions of 1.5 s, 3 bar, and 75% amplitude (48 μm) [66].

Moreover, an evaluation between the strength and stiffness of CFRTP and CFRTP joints by USW spot welding and by mechanical fasteners (MFs) with double-lap shear (DLS) and pull-through test had been carried out [72]. However, on comparing the results of LSS in MPa of APC-2 laminates (polyetherimide, PEI film) joined by USW, RW, IW, MFs, adhesive bonding, and bulk heating, the results of USW show to be the most significant joining process and the most studied method on average compared to other methods [73–76]. A recent review shows that, given the capacity to transmit loads and create a homogenous junction that maintains structural integrity, adhesive bonding is mostly preferred to mechanical joining due to the lower cost and less assembly weight. However, fusion bonding approaches such as USW, IW, and RW have great potential for applications requiring quick processing times, such as wind turbine blades, automotive bulkheads, aerospace fuselages, and surfboards, which require large volumes of material. The advantages of fusion bonding methods include lower surface preparation necessities, recyclability, reprocessing,

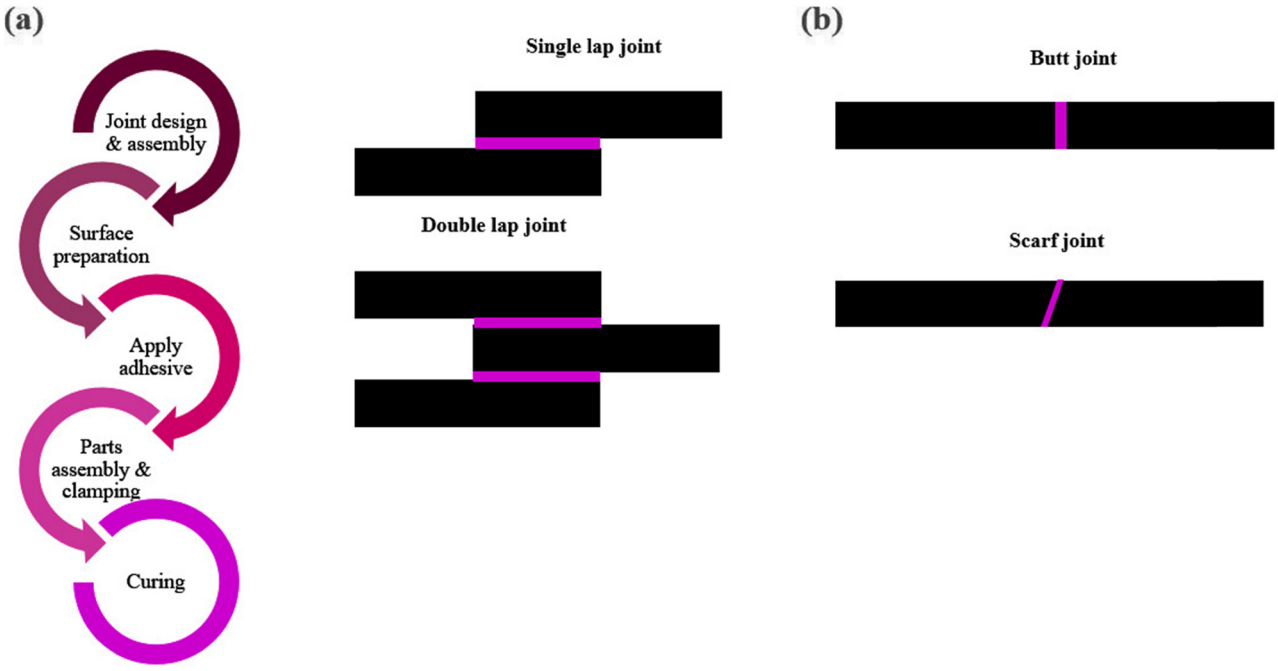

Figure 9: (a) Steps of adhesive joining and (b) types of adhesive joints.

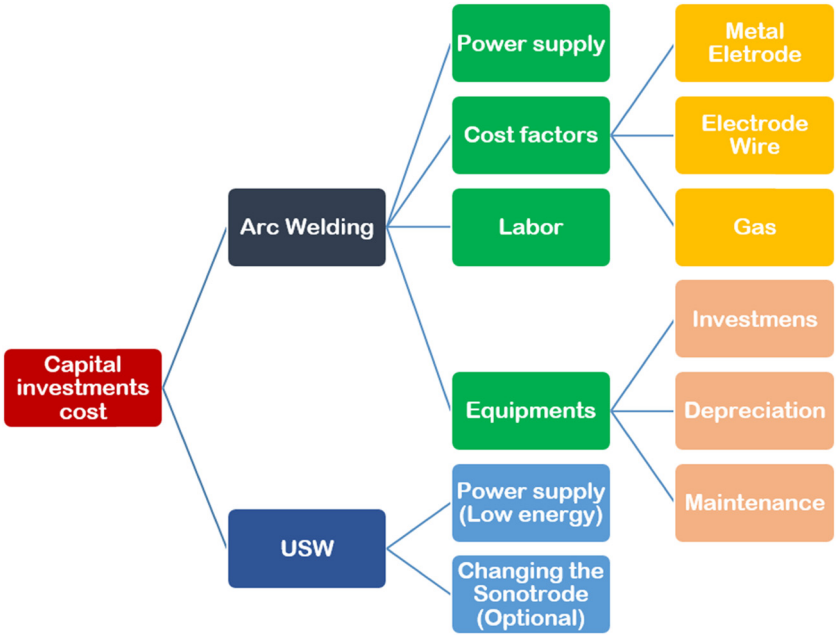

Figure 10: A comparison between capital investments cost of arc welding and USW technologies.

and enhanced integrity/durability over other joining processes [76]. Furthermore, a comparison between the capital investment costs of arc welding and USW is shown in Figure 10. Besides, the USW consider as one of the sustainable welding process. The sustainability criteria in welding is shown in Figure 11.

1.3 Polymers and polymer matrix fabrication

1.3.1 TP polymer

The advantages of TPCs over other polymers are that they are cost-effective in manufacturing, and have excellent

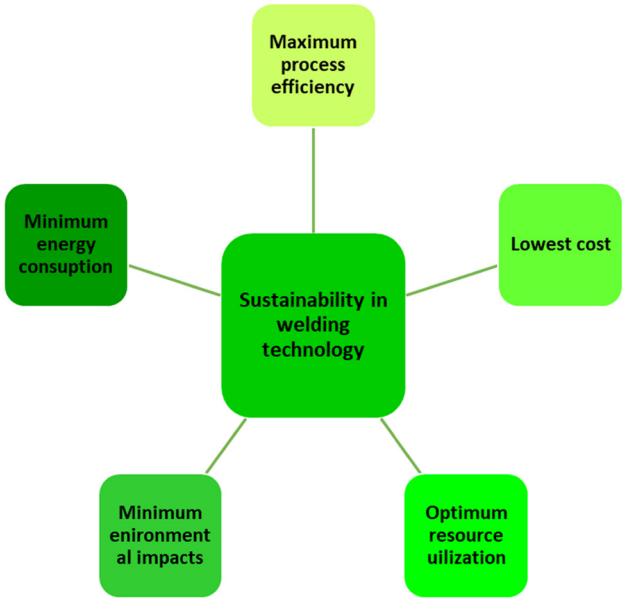

Figure 11: Sustainability in welding technology.

impact resistance and recyclability [72,77–79]. Moreover, consolidation under elevated/high pressure and heat after welding through melting is a unique advantage for TPCs [80]. Table 1 presents the properties of TPs used in the USW process, followed by the most favorable types of TPs to fabricate with CF and joined by USW. As observed from Table 1, there is a considerable variation in the values of density, Young's modulus, processing temperature, melting and glass transient temperatures of the TPCs, which are based on the unique structure of each TPC. All mentioned properties are classified as the most important properties that influence the USW process since they directly impact weldability, melting, crystallization, phase transformation, and the thermal cycle. The importance of maximum operational temperature during USW is based on the purpose and the nature of using the TPCs as a reinforcement of the CF or as an ED or interlayer coupling, considering that the melting must be generated in the ED or interlayer before the adherent, which means that the melting temperature of the interlayer is supposed to be less than that of CFRTPs. Besides, the maximum operational temperature significantly enhanced the material flow in the welding zone. However, considering the density and Young's modulus is essential because it may affect the USW process factors, such as required welding power and welding time. Moreover, the glass transition temperature gives an indication of where the chains of polymer starts to move [81]. In addition, the glass transition temperature is directly affected by the crystallinity in semi-crystalline polymers [82]. Based on these, the material properties of TPCs must be studied

Table 1: Properties of TP polymers employed in USW processing

Types of polymers	Abbreviation	Density ($kg \cdot m^{-3}$)	Young's modulus at room temperature (GPa)	Glass-transition temperature (°C)	Processing temperature (°C)	Melting temperature (°C)	Ref.
Elium		1181.33 ± 20.43	0.0033	97.9	85	NA	[98]
High-density polyethylene	HDPE	940–970	0.6–1.1	−100	90	130	[99,100]
Low-density polyethylene	LDPE	910–955	0.1–0.3	−100	88	110	[100,101]
Acrylonitrile butadiene styrene copolymer	ABS	1,080	1.9–2.0	100	75	125	[100,102]
Polyamide (Nylon 6)	PA6	1,084–1,230	1.5–3.0	45	80–160	221	[103,104]
Polycarbonate	PC	1,196	2.2–2.4	149	100–140	149	[100,105]
Polyetheretherketone	PEEK	1,260–1,300	3.7	143	250	343	[106,107]
Polyetherimide	PEI	1.27	3.3	215	170	340–360	[108–110]
Polyethylene terephthalate	PET	1,333–1,365	2.7–4.1	70	150	240	[100,111]
Polymethyl methacrylate	PMMA	1,170–1,230	2.2–3.8	105	80–100	130–160	[112,113]
Polypropylene	PP	900–920	2.55	(−25)	85–120	170	[100,114–116]
Polyphenylene sulfide	PPS	1,350	3.8–4.2	85–90	218	280–285	[117–119]
Polyvinyl chloride	PVC	1,385–1,440	2.5–4.0	80	60	160	[120–122]
Polyvinylidene fluoride	PVDF	1,750–1,800	1.2–1.6	−35	148–190	100	[123,124]
Polystyrene	PS	1,050–1,080	2.4–3.5	95	105	240	[100,125]
Styrene-acrylonitrile copolymer	SAN	1,070–1,080	3.9	115	85	160–260	[126,127]

intensely before performing the USW process. Furthermore, Elium is a novel acrylic TP resin developed by ARKEMA. The advantage of Elium over other kinds of TPs is that it can be cured at room temperature [63]. The mechanical features of Elium® with various fiber reinforcements studied in various literature are fracture toughness [83], tensile [84], flexure [85,86], impact [87,88], and vibration [89]. Also, their mechanical properties are similar to TSCs' mechanical properties. Shogren *et al.* [90] explored the enhancement of orientation on the microstructure and mechanical characterizations of the polylactic acid (PLA)/starch composite filaments produced by the extrusion (twin screw) methodology. Chen *et al.* [91] inspected the ability to enhance the toughness of polyethylene terephthalate (PET), where the outcomes showed a significant enhancement in the mechanical properties. Additionally, the results of that study are considered as an initial step for future application of the PET. However, by reinforcing the TPCs with CF to develop the CFRTPs, the CF was found to develop the mechanical behavior of polymers [92]. Likewise, Kord *et al.* [93] considered the enhancement of multi-walled CNT (MWCNT) on the dynamic behavior of PCs made of PP/reed flour (RF). The outcomes show that the MWCNT has a negative effect on some properties and a positive effect on other properties simultaneously. However, the treated polyetheretherketone (PEEK) by ultraviolet irradiation with carbon/Ep prepregs has been used as a direct co-curing process between the interfaces of TSCs/TPCs [94]. Conversely, Talbott *et al.* [95] recorded that due to reducing the PEEK's crystallinity, the tensile strength, shear strength, and modulus of elasticity will all decrease. Besides, a review has examined the mechanical behavior of CF/PEEK in biomechanical applications [96]. By using the PEI as a coupling layer for carbon/PEEK, there may be a high-performance PEI-PEEK exploit caused by the molecular inter-diffusion between the adhesive and the adherend as a consequence of the total miscibility of PEI and PEEK over the melting temperature of the layer [97].

Remarkably the TPCs became highly attractive over TSCs in different manufacturing sectors, owing to their high damage tolerance, cost-effective manufacturing, and welding process [2,80,128]. Numerous fusion-bonding techniques that are founded on altered heating mechanisms such as ultrasonic, microwaves, laser, IW, FSW, and hot gas and plates can be used to join the TPCs [80,129–131]. Anaç [132] investigated the mechanical characterization of similar/dissimilar polymers joined by FSW. Based on the literature, the TPCs are considered a semi-crystalline natural structure that enhances the mechanical features, such as shear strength, stiffness, fracture toughness, the interfacial strength of fiber/matrix, and chemical resistance. Besides, the industrial applications of polymers and polymer matrix are becoming widespread in industrial manufacturing, such as railway [133], automotive [134], aerospace [135,136], elastomeric shape memory, and its application [137,138], as well as biomedical [139]. Popp and Drummer [140] performed joining process of carbon fiber-reinforced thermoplastic composites (CFRTSCs)/steel through infrared heating and undercutting pin structure. Hussen *et al.* [141] presented an experimental and developed analytical model to investigate the peeling strength of a composite structure consist of multilayer hybrid textiles and coated with PVC, that was joined by using USW process. However, the most commonly used PC matrix-reinforced fibers are CF, GF, and aramid fiber (AF), as shown in Figure 12 with their specifications and compared with TPCs reinforced with TPC polymer fiber-reinforced polymers (PFRPs) and their specifications [135]. Researchers and industries show more interest in CF than other fibers due to their superior mechanical characteristics. For modern and next-generation structures, the CFRTPs are a significant candidate and have higher productivity than the CFRTSCs due to their fast formation by injection molding and press molding. However, Wang *et al.* [142] investigated the thermal characterizations and the fusion performance at the interface of CFRTP (CFPEEK) enhanced by heat input and joined through IW with CF subsector. Besides, Liu *et al.* [143] studied the compression behavior and impact resistance of CFPEEK laminates experimentally, followed by repairing with hot-press fusion with various stacking arrangements. The authors observed that 20–30% of development was achieved in compression residual strength by the repairing process.

1.3.2 Polymer matrix's fabrication

The CFRP, TPCs and TSCs which joined by USW can be fabricated in various approaches. In this context, a brief discussion about the fabrication process implemented in the preparation of CFRP and polymer matrix is presented in this section. There are several methods to fabricate the CFRPs, such as vacuum-assisted resin transfer molding (VaRTM), which is considered as one of the fabrication techniques with the lowest cost [144,145]. Moreover, Francis *et al.* [146] presented a comprehensive review that focused on enhancing disparity in the composition of material characteristics and the performance of PEEK and then exposed the association with additive manufacturing (AM) processability of such composites. Besides, the study highlighted the challenges faced in the production of PEEK by AM. However, despite the remarkable advantages of fabricating PCs by AM

over traditional manufacturing processes in terms of mechanical behavior, it still has some drawbacks. Darji *et al.* [147] presented an inclusive review that addressed the essentials and sorts of current AM PCs. It also investigated the present cutting-edge studies as well as progress. Besides, the gaps in the mechanical properties of PCs fabricated over several AM methods, such as powder bed fusion, material jetting, material extrusion, sheet lamination, *etc.*, were also highlighted. Furthermore, in the prospective of producing polymer matrix, which is created by embedding fibers, Figure 13 illustrates a summary of the most utilized fabrication processes for TPCs [135]. Furthermore, Iwata *et al.* [148] employed a microstructure that includes a protrusion and is produced by AM to enhance the CFRTPs joined with Al by solid-state approaches. Pinto *et al.* [149] recorded that due to the adaptability and remarkable inherent qualities, two-dimensional (2D) materials have become a highly potential class of additives in the field of PCs, which in consequence allows the researchers to develop various NCs that might be used in a wide range of multipurpose implementations. The effectiveness of these NCs strongly depends on the integrity of the 2D materials, the relationship with the polymer matrix, distribution, and the form when implanted in the polymer. Additionally, one of the most essential key factors for achieving multipurpose applications in PC NCs is how the nanofillers (NFs) are embedded in the polymer matrix. These NCs are usually created through three various technologies, as shown in Figure 14, where red, green, and yellow signify the advantages and disadvantages of each process. However, Azizli *et al.* [150] presented a novel PA6/PLA nanocomposite by utilizing the graphene oxide and poly ethylene-butyl acrylate-glycidyl methacrylate with superior mechanical characterizations. While a PLA reinforced with halloysite nanotube (HNT) through melt-blending the PLA matrix with the HNT was studied by Murariu *et al.* [151].

Furthermore, the generated polymer matrix's mechanical, physical, and microstructural characterizations were investigated. The production of the polymer matrix composites (PMCs) by utilizing microwave energy has been revised by Naik *et al.* [152]. Meanwhile, Melentiev *et al.* [153] reviewed the capability of employing polymer metallization, counted as one of the AM process techniques for producing polymers and PCs. Nonetheless, Gupta *et al.* [154] presented a review study for exploring the benefits of producing CFRPs by utilizing the near-surface mounted (NSM) methodology. Additionally, it has been observed that the NSM method influences the shear strength, fatigue resistance, durability, and flexural capacity of the CFRPs. Besides, it highlighted the bonding performance and failure mode of the CFRPs. However, the most commonly utilized geometrical structure is the sandwich composite structure owing to its advanced energy absorption capabilities and mechanical properties, which depend on the core and face sheet material characteristics as well as the strength between the core-inner face sheet as recorded by Patekar and Kale [155].

Furthermore, various reviews were published in the field of investigating the fabrication process utilized for producing polymer matrix. For instance, Miranda Campos *et al.* [156] investigated the TPC matrix formed by implementing the resin transfer molding (RTM) method. Moreover, Eratbeni and Rostamiyan [155] developed a novel model of sandwich panels made of CFRPs with rhombus cores. Also, the achieved outcomes of the vibrational analysis performance of the novel sandwich structure were compared and validated arithmetically and experimentally with the traditional elliptical sandwich structure. Besides, the CFRTPs are appropriate for mass-produced products and high-end production [6,157–159]. Additionally, by comparing the CFRPs with conservative metals, it is observed that CFRPs

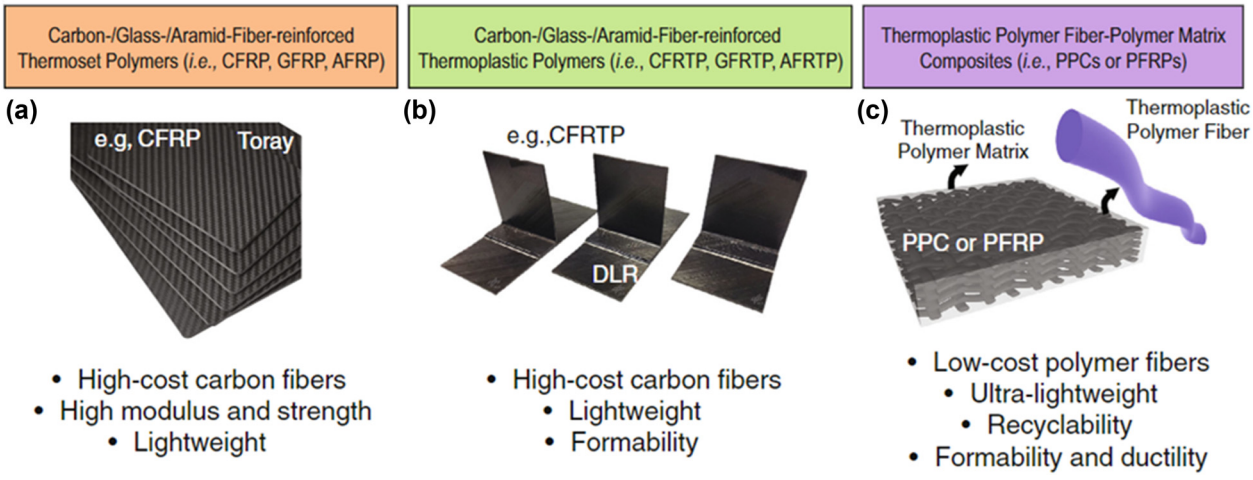

Figure 12: The most commonly used PC matrix reinforced fibers with their specifications and compared with (a–c) TPCs reinforced with TPC polymer fiber (PFRPs) specifications [135].

have comparatively higher tensile strength and stiffness, outstanding corrosion properties, impact as well as lower densities [160]. Sawpan [161] stated that while embedding the FRP into the water, the composite thermal and mechanical characterizations are exposed to vary owing to the diffusivity of water molecules and ions into the polymer matrix. An occurrence of hydrolytic reaction, a reaction between sodium ions, which is one of the solution components, and hydroxyl ions, will be generated for electrical charge balancing, which will cause an osmotic condition, as a consequence, a considerable pressure will be generated that will cause degradation in the mechanical features of CFRP [162] as well as GFRPs [163]. Moreover, Cheng *et al.* [164] analyzed a chain reaction of a cross-linked network in CFRP by reaction kinetics models of CFRP to define the degradation of CFRP immersed in supercritical fluids. It is observed that the CFRP deterioration was caused mainly by the scission of the C–C, C–O, and –O– bonds in the longitudinal chain region and the C–N bond in the cross-linked segment of an Ep resin curing system.

1.4 USW for TPC and TSC

In spite of all welding techniques that may be used in joining TPCs, such as FSW, LW, RW, and electromagnetic welding [165–168], the USW accomplished advanced benefits for welding the TPCs including reliability; cleanliness; harmlessness, which allows *in situ* monitoring; and less welding time [169,170]. Additionally, in certain circumstances, it is possible to perform the joint by USW at a temperature below the melting point of the weldment while maintaining a high welding quality distinct from other welding methods [171]. Joining polymers by the USW has been prevalent and used in various industrial applications for many decades [172–175]. Furthermore, there are several differences between the joining process of TPCs by USW and the joining process of metals by USW [176,177]. For instance, Abbas *et al.* [178] performed a dissimilar metal joint Al/Cu by USW while considering increasing the welding contact area. Besides, a study investigated the USW of plastic optical fibers (POFs), which are

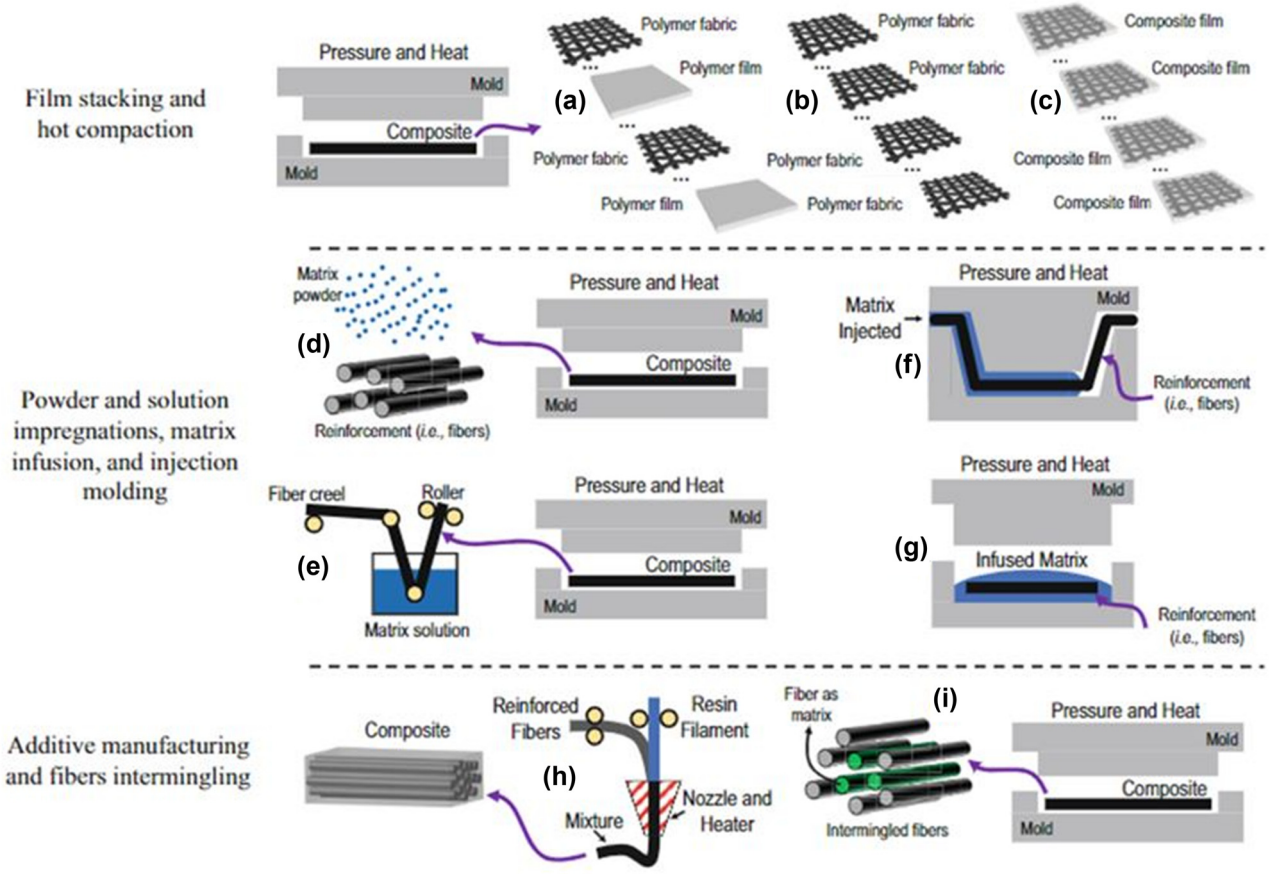

Figure 13: The most utilized fabrication processes for TPCs: (a) Film stacking, (b) hot compaction utilizing polymer fabrics only, (c) jot compaction utilizing composite films; (d) powder impregnation, (e) solution impregnation, (f) injection molding, (g) matrix melt impregnation or infusion, (h) AM *via* fused deposition molding; and (i) fiber intermingling [135].

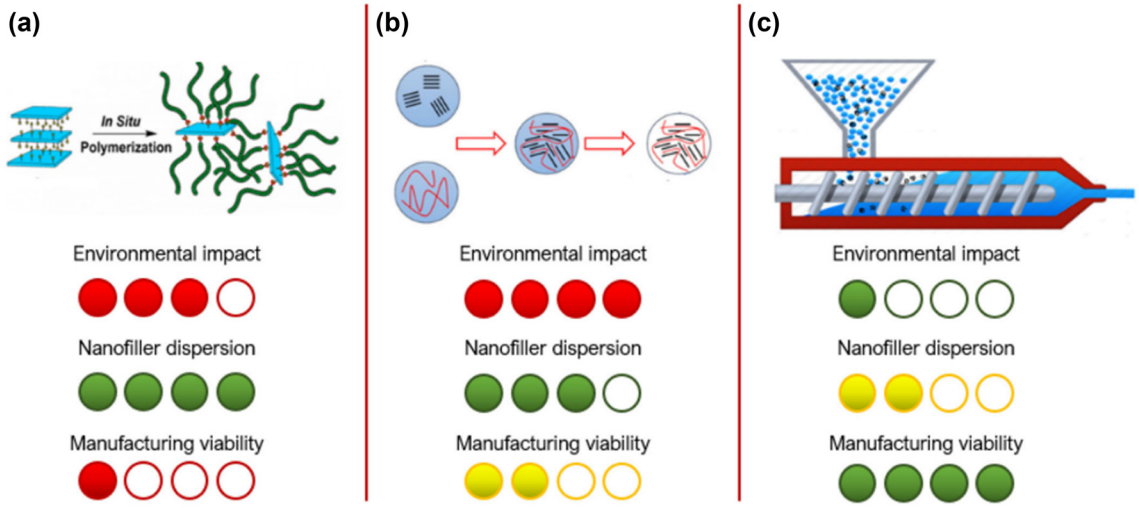

Figure 14: The various technologies for producing polymer NCs, addressing their major advantages (green) and disadvantages (red): (a) *in situ* polymerization, (b) solvent casting, and (c) melt compounding [149].

made of polymethyl methacrylate polymer (PMMA) joined with CFRPs fabricated by using VaRTM (Ep resin)/thermoset plastic. It has been noticed that the POFs melted and firmly welded to the CFRP, and it experienced the deformation of the CFRP. While no changes were noticed in the CFRP, it remained in the same state without melting [179]. Nevertheless, the USW compared with other fusion bonding techniques, such as adhesive bonding and MFs, by using the APC-2 laminates (PEI film) system has been examined [30,180]. Bonding TPCs by TPC films as hot melt adhesive by fusion bonding has been examined; with high interest in USW technology, the bonding was accomplished for similar and dissimilar materials [2]. Meanwhile, Biswal *et al.* [181] utilized the USW to join vitrimer composites with GF and CF. Sadeghi *et al.* [182] joined GF/PA6 by USW through using FED to concentrate the interface heat, where the optimum welding time was found to be 1.8 s at which the welding strength reached 24.46 MPa. Moreover, the welding process of dissimilar materials is more sensitive than welding similar materials, as a primary necessity, the melting temperature for both materials must be identical with a temperature variation less than 20°C [183]. The interest in dissimilar welding TPCs to TSCs and TPCs to metal has been widely studied by many researchers [184–190]. The dissimilar USW joins metal to TPCs, and TPCs to TSCs [185]. However, as a demonstration in USW, the strength of the composite interface is correlated with the molten polymer flow [17]. A rich coupling layer of TPCs must be included in the un-cured TSCs, owing to the fact that TSCs by itself is not weldable; so the coupling layer must be added to achieve weldability [5]. As mentioned in the literature, the curing reaction can be done only for TSC resins, but the process was referred to as (co-curing) [191]. Furthermore, several publications focused on finding a strong method to connect the TSCs with the coupling layer during the co-curing process [94,191–193]. The polyethersulfone, PEI, and polysulfone are examples of TP resins and share a typical amorphous nature. Besides, they have also been reported as a compatible common Ep system [193–195]. Elsewhere, at appropriate process parameters, the interface between ultrasonic oscillation and TPCs will result in vibration energy that disperses as heat, which elevates the temperature of the plastic to a suitable level to endorse fusion bonds between the workpieces [9]. On the other hand, a novel study on hybrid welding of CFRTP established that the location of failure and the final thickness of the weld line were significantly influenced by the welding technique used as well as the initial thickness of the TPC film. The welding procedures were found to be made more accessible by thicker TPC films [196]. Liu *et al.* [197] investigated the nonlinear (NL) friction performance of CFPA6/Al joined by USW. Lionetto *et al.* [198] performed a joining process of CF/Ep/Al alloys by using hybrid USW with single-spot. Besides, Shi *et al.* [199] performed a dissimilar joint by using the USW through joining CF/PA66 to 6061Al by using ED made of PA6, where the effect of various process parameters and the impact of ED crystallinity on the welding joint strength were examined. Similarly, Kalyan Kumar and Omkumar [200] joined the CF/PA6 by USW while implementing interfacial coating instead of single ED, where the interfacial coating layer behave as an insulator, which avoids the galvanic corrosion in the joint and the fretting damage. Furthermore, Huang *et al.* [201] employed a hybrid joining technique, combining the plastic deformation and chemical bonding to join CFRTSs with thin metal sheets.

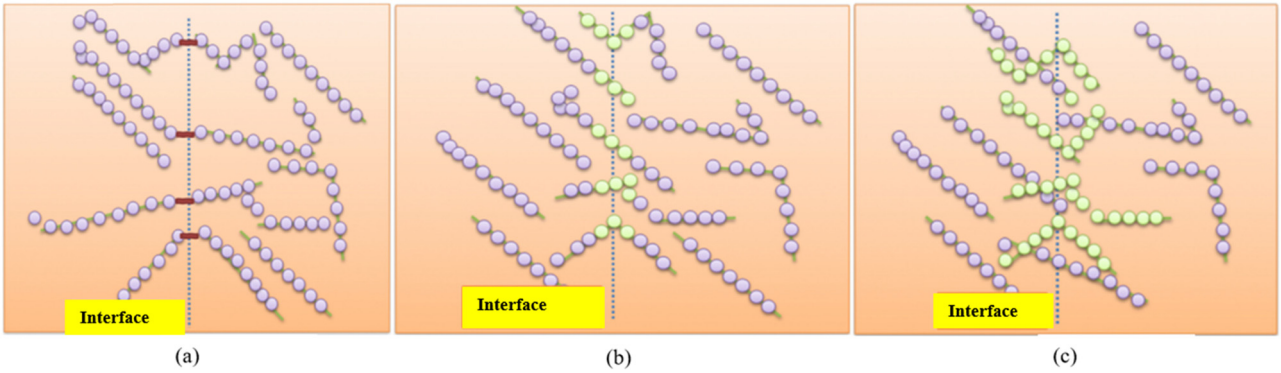

Figure 15: A graphical representation of the interface of the polymer–polymer bonding processes: (a) molecular bonding, (b) chain interdiffusion, and (c) chain entanglements [206].

Reisgen *et al.* [202] implemented a novel technique for embedding metallic elements through the PMCs to join metals to polymers with FRC using traditional joining methods. Furthermore, by investigating the welding performance of the semi-crystalline polymers, Xue *et al.* [203] revealed that the chain mobility of semi-crystalline polymers remarkably decreased, since in autohesion process, the interdiffusion of polymer chain and the crystalline structures' presence are considerably limited. On the other hand, Lamèthe *et al.* [204] explored the polymer dynamics subjected to the PEEK matrix composite welding. The obtained results show that the essential factors that influence the interface strengthening are the crystallization and the interdiffusion. Additionally, Kurtz and Devine [205] reported that when the polymer surface cool rapidly by the injection molding components, a thin layer of amorphous structure will form at the surface, which is further explained by Awaja [206] to have a remarkable influence on the self-bonding progressions, since the crystallinity content of the surface layer affects the inter-diffusion of molecules. For example, the graphical representation of the interface of polymer–polymer bonding processes is illustrated in Figure 15. Moreover, it has been reported that the crystallinity highly influenced the interfacial shear strength of CF/polyphenylene sulfide (PPS) and CF/PEEK [207,208].

1.5 Recyclability of CFRPs

As the global market demand increases, capital investments as well as the wastes of CFRP are increasing annually, which cause the necessity of recyclability of CFRPs to become essential. The waste of CFRP is considerably important due to challenges and difficulties of it is huge volume [209]. Besides, the maximum amount of CFRP wastes is from aerospace industries [210]. In addition, it is necessary to recycle this type of waste considering the cost-effectiveness and environmental impact [211]. The CFRP wastes can be classified into two groups, which are new scraps and old scraps [212]. However, the necessity of recyclability of CFRPs is also due to the great amount of

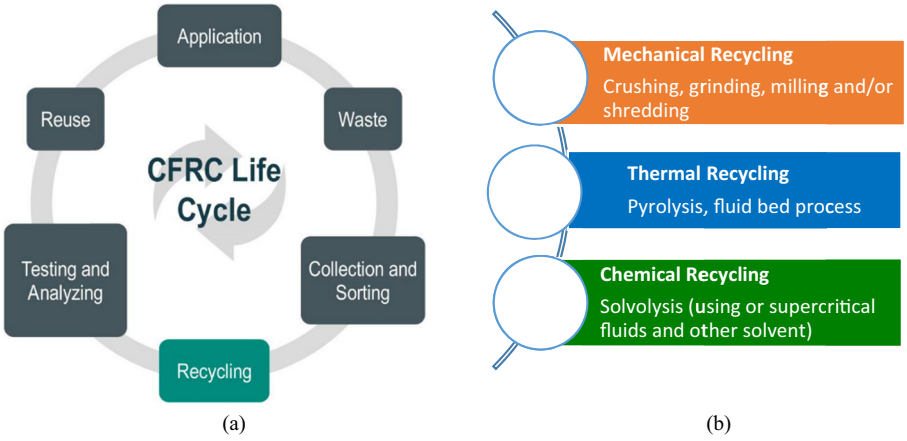

Figure 16: (a) The CFRP life cycle and (b) the most used recycling methods for CFRP [215].

consumed energy that is required to fabricate 1 kg of CFRP which is around 28 MJ [213]. The life cycle and the most used recycling method for CFRPs are shown in Figure 16. Also, further classifications of CFRC waste and scrap managements are shown in Figure 17. The mechanical recycling technique considered efficient in managing the increasingly great volume of CFRP waste based on grinding the CFRCs into minor pieces [214]. Nonetheless, the amount of materials, which are processed by the mechanical recycling, can be utilized as a partial reinforcements in further productions, which in consequence will restrict the combination in new materials [209]. Meanwhile, it is recommended to use the chemical recycling for long fibers [215]. However, with the recent progress in recycling manufacture field, it was noticed that the recycled carbon fibers (rCFs), achieved by implementing the solution degradation or pyrolysis methodologies, has lower resin content and good adhesion to the resin which subsequently augment the mechanical characterizations of the CFRP [216]. Additionally, researchers show interests in studying mechanical and electrical properties and the environmental impact of cementitious composites reinforced with rCFs. Recently, Vidal *et al.* [217] proposed the enhancement of binders made of ionic dynamic networks on the processing, properties as well as recyclability of CF/Ep. Though each recycling process has it is own advantages and limitations and its own specific properties such as energy demand in mechanical recycling [218], fiber recovery and their retain characterizations [211], global impact and cost analysis must be considered before starting the recycling process [212,215].

There are many factors that restrict the recyclability of CFRP, such as the initial steps before recycling process, namely, identification, assembly, and separation are a considerable challenge [219], the difficulty of having the same significant mechanical properties of CFRP after recycling process [220], the cross-linked combination between the CF and TSs lead to more difficulties in treating the waste [221]. Further limitations facing the CFRP recyclability are illustrated in Figure 18. However, the recycling approaches of CFRP are promising in terms of reducing the greenhouse gas emissions, resource depletion, and energy usage [214]. Besides, the financial feasibility is directly associated with the consumed energy cost and raw material cost.

2 Types of USW and types of joints in USW

Mainly, the joints of polymers by USW can be achieved in two techniques: with and without ED. In both techniques, the direction of ultrasonic vibrations is average to the welded surface, which is unsuitable for a flat surface. Therefore, in the first type of joint by USW, a sharp wedge protrusion, which is ED, is needed, where it connects the outer surfaces of the welding piece to the other welding piece outer surface. Although shear joint is the second type of joint by USW, in this type of joint, the welding joint processes can be proceeded without the ED, and the

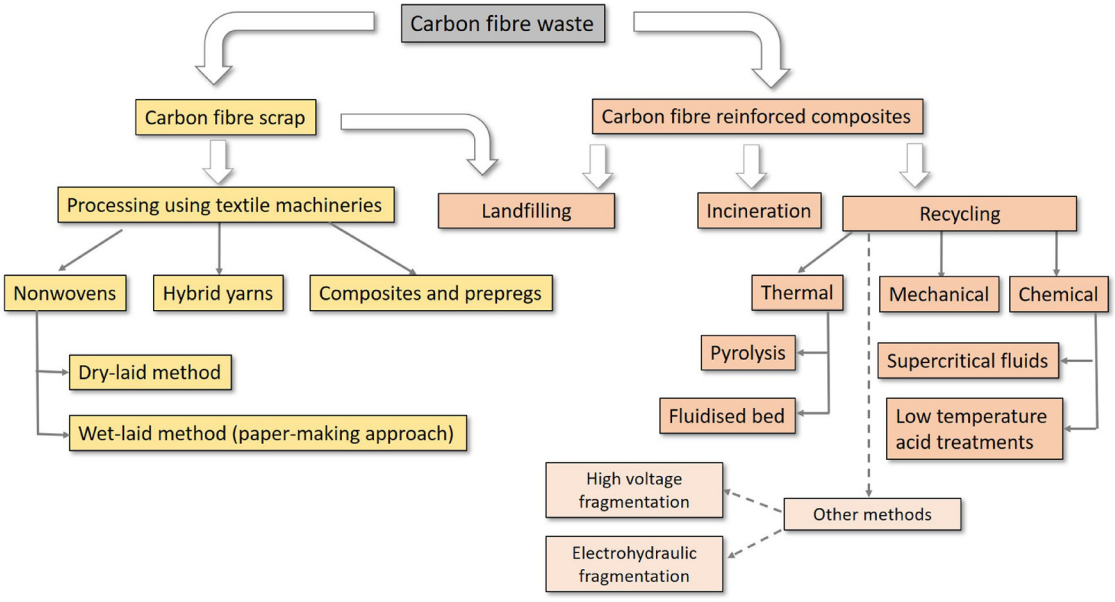

Figure 17: The waste of CFRC and dry CF scrap management routes [214].

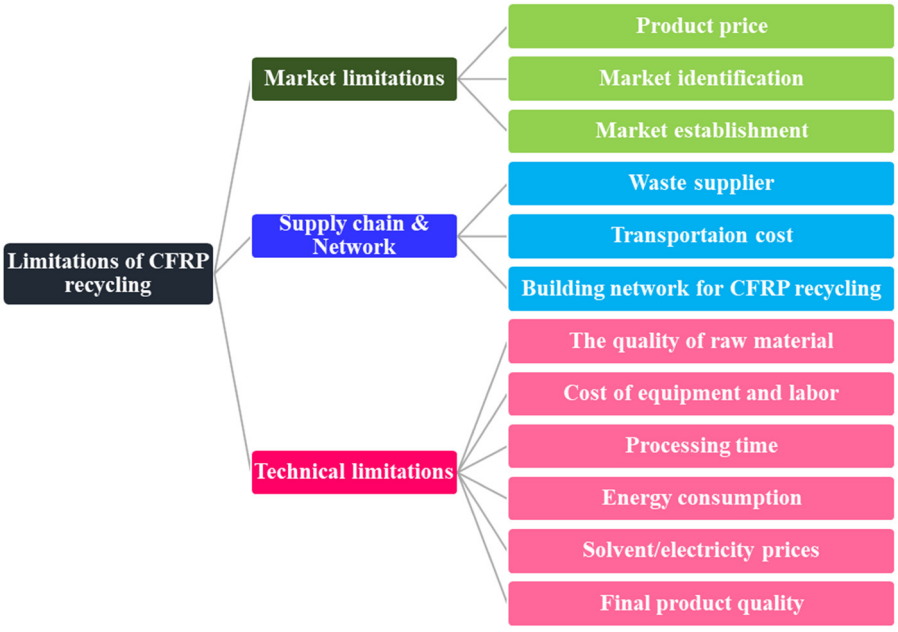

Figure 18: The limitations of CFRP recycling.

direction of ultrasonic vibration is directly parallel to the coupling surface. Also, in this type of joint, the frictional shear force causes heat generation in the mediator to be welded [175]. Figure 19 shows schematic of shear and butt joints in USW. However, the ED in butt joint can be designed in various geometries, and Figure 20 shows some examples of ED shapes [222].

2.1 Types of USW machines and welding tools

Commercially, a variety of USW machines are available; the main differences in USW machines are energy output, maximum force, amplitude, and range of frequency, although all these parameters are adjustable. The USW machines generally consist of the generator, transducer, booster, and sonotrode [223–226]. Figure 21 illustrates the USW machine components' structure and schematic [227]. Mainly, all USW machines provide the same variable adjustable process parameters, although there are some differences in their range. However, the USW machines are classified into two types based on the oscillation direction as shown in Figure 22 [228]. As realized from Figure 22(a), the oscillation direction in polymers joining is perpendicular to the welding zone, where the high vibrational frequency transmission causes a heat generation at the interface which melts the TPCs and makes the TPCs to flow and form the bond between the two specimens to be welded [185]. Besides, from Figure 22(b), the oscillation direction in metal joining (similar joint or dissimilar metal to TPC) is parallel, which influences the interaction area between the sonotrode and the specimens, in which the friction action at the surface makes the solid-state bond to

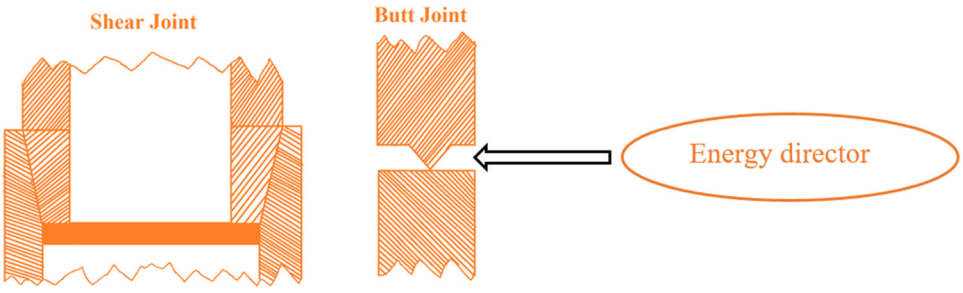

Figure 19: The schematic of shear joint and butt joint in USW.

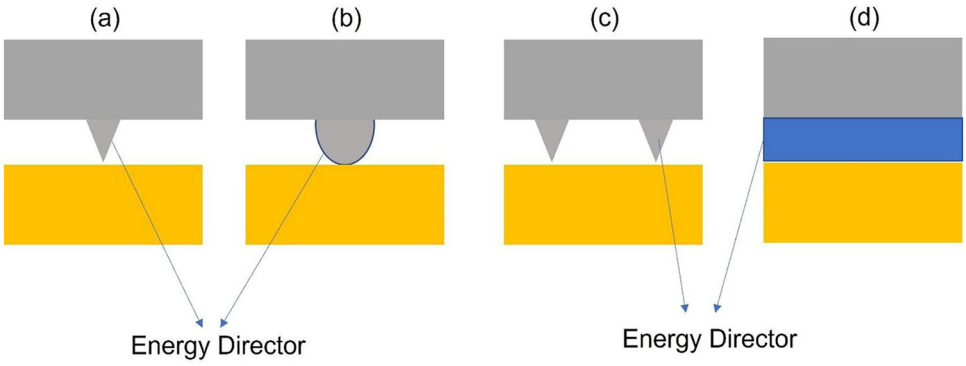

Figure 20: Schematic of various shapes of ED in USW: (a) single triangle shape, (b) round/semi-circle shape, (c) multi triangle, and (d) flat film [222].

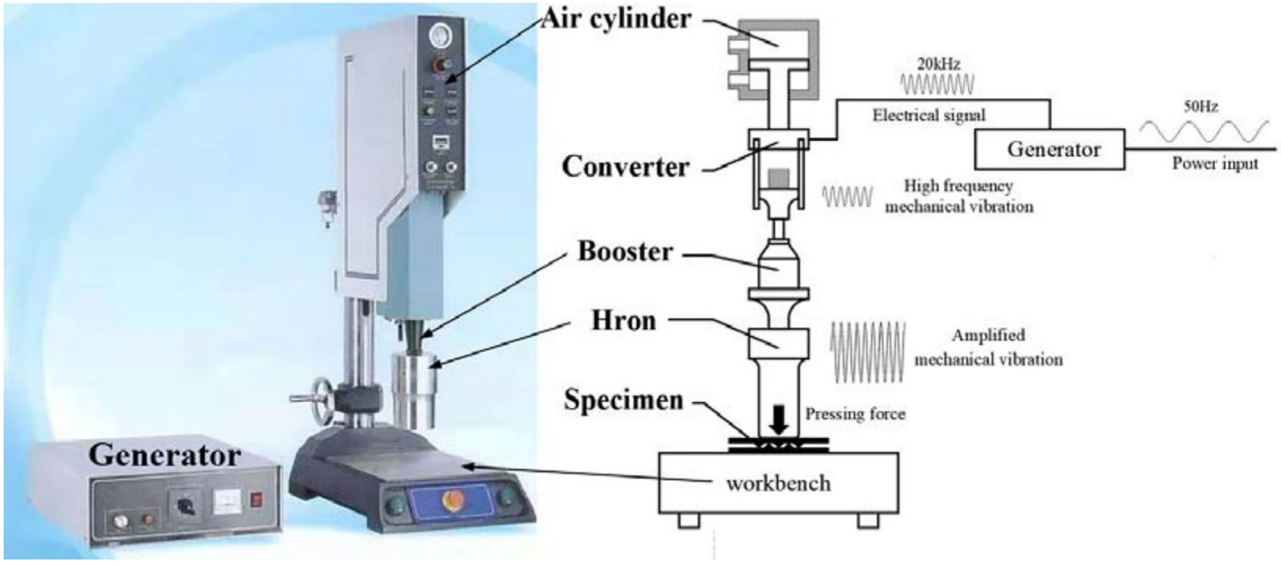

Figure 21: Structure and the schematic of USW machine component [227].

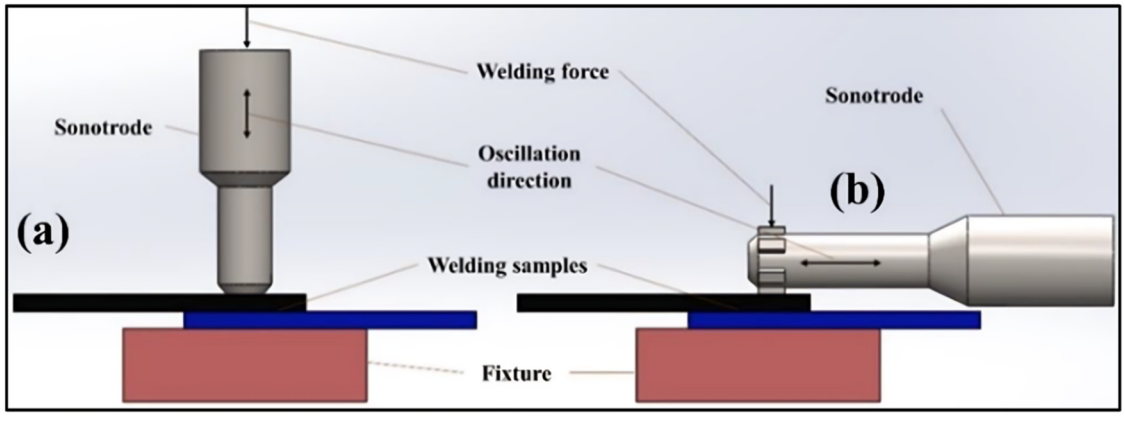

Figure 22: Types of USW machine based on oscillation direction: (a) USW machine for joining polymers and (b) USW machine for joining metals (similar/dissimilar) [228].

Table 2: Classification of CFRP joined by USW based on type of USW machine without using ED or an interlayer

USW type	CFRP matrix	Parameters							Shape of sonotrode and number of spots	Summary	Ref.
		Welding/ holding time (s)	Welding force/ pressure	Overlap area (mm^2)	Amplitude (μm)	Power (W)	Vibration time (ms)	Energy (J)			
20 kHz Rinco Dynamic micro-processor controlled	CF/Elium	1–5.5	3–4 bar	25.4 × 25.4	33, 49	NA	NA	NA	Square SSW	USW with Elium is more efficient than adhesive bonded and takes less time	[63]
	Output	– Static LSS for Elium® composite with integrated ED (ELC-IED) = 18.86 ± 0.14 MPa – Static LSS for Elium® composite with flat laminates (ELC-FED) = 14.04 ± 0.01 MPa – Static LSS for adhesively bonded joint = 14.2 MPa – ELC-FED samples have lower fatigue life at all stress levels compared with adhesive bonded joints – 2SH-ELC_SH-ELC – Samples have higher fatigue life at all the stress levels as compared to the adhesive bonded								Shear Cusps and fiber impingement has been formed, the ED was used as ELC-IED and ELC-FED	
20 kHz Rinco Dynamic micro-processor controlled	CF/PEI	Travel (12–100)%	300, 1,500 N, 0.9 and 2.8 MPa	12.7 × 25.4	51.8–86.2	(51–83)% of 3,000 N = 100%	250 (5.1)–1,928 (4.7)	433 (5.7), 1,466 (6.7) (COV, %)	Cylindrical SSW	Study the weld strength of USW for continuous-fiber reinforced TPCs with FED. To check the possibility of maximum weld strength by using the power and displacement to set the optimum parameters	[64]
	Output	– Welding force and vibrational amplitude effects on the welding time and welding power – Force and amplitude has no impact on weld strength									
20 kHz Rinco Dynamic micro-processor controlled	CF/PEEK	4	1,500 N	25.4 × 25.4	60.8	NA	NA	600	Cylindrical SSW	The USW was compared with mechanically fastened joints. By mechanical test (DLS and PT), fractographic analysis, mechanical behavior, failure modes, and damage affected zone	[72]
	Output	– In both test D = 10 mm in USW twice bigger than the Hi-Lok fasteners – In DLS test the stiffness was higher with 88% in USW – The most critical failure mode in USW were found as intra-laminar failure in both DLS & pull-through (PT) testes – In PT of USW the joint stiffness is higher with 113.5% compared with mechanically fastened									
20 kHz Rinco Dynamic 3000	CF/PEI	NA	300–1,500 N, 1.6 MPa	12.7 × 25.4	51.8–86.2	3,000 W	354 (4.1)–2,305 (12.9)	NA	Cylindrical SSW	Investigate the relation between power and displacement data and the transformation formation at the interface during USW	[65]
	Output	– High amplitude effect on peak power – The power and displacement help in finding the optimum set of parameters, also ease of *in situ* monitoring of USW – The relation between welding time and power has been studied									
Rinco 3000 microprocessor-	CF/PEI Cetex	4	500 N	NA	86.2	NA	400, 450 s	NA	Cylindrical SSW	Compared three different thickness of	[238]

(Continued)

Table 2: *Continued*

USW type	CFRP matrix	Parameters							Shape of sonotrode and number of spots	Summary	Ref.
		Welding/ holding time (s)	Welding force/ pressure	Overlap area (mm^2)	Amplitude (μm)	Power (W)	Vibration time (ms)	Energy (J)			
controlled ultrasonic welder										PEI. Study the effect of thickness of FED on the generated heat during the USW	
	Output	– The power and displacement curves for the two samples of 0.25 and 0.5 mm thickness show typical behavior – At thickness = 0.06 mm, heating and melting of ED and adherents occur simultaneously, while in thicker ED, first it heats and melts and then substrates during the process								Further research in small thickness is needed	
20 kHz Branson 8200	CF/PEI	3.5	4 MPa	25.4 × 15	50	1,000 W	NA	NA	Rectangular SSW	The weld quality and strength were investigated. For four different types of ED	[3]
	Output	– The overlap length has changed in each triangular energy director – A remarkable reduction in the disturbance in the outer layer of welded fibers – A lack of observation in mechanical properties caused by the random sample selection								Surface were compared and for each type, 8–15 samples were welded and compared. With two modes of failure in the LSS test The relation between ED orientation & the direction of load, the size & EDs distribution	
KZH-2026 multifunction UW	CF/PA66	NA	0.17 MPa	25 × 38	25	NA	NA	3,000	Cylindrical SSW	Investigate the moisture impact failure mode analysis	[239]
	Output	– A proportional linear relationship between amplitude and joint strength. – Amplitude highly impacts the welding quality – At low humidity, 1 wt% of the peak load of the welded joints was slightly affected, while by increasing the humidity, ≥1.7 wt% of the peak load started to decrease – By increasing the welded area, the peak load decreases – The Hydrogen bonds in polymers is affected by the water molecules								Generate mathematical modeling (findings damping properties) On amplitude During welding Moisture enhances interfacial fracture and decreases welded total area	
	CF/PA6 Output	3	150 N	12.7 × 12.7	50	NA	NA	NA	Square SSW	Investigate the USW of short CF with and	[240]

(Continued)

Table 2: *Continued*

USW type	CFRP matrix	Parameters							Shape of sonotrode and number of spots	Summary	Ref.
		Welding/ holding time (s)	Welding force/ pressure	Overlap area (mm^2)	Amplitude (μm)	Power (W)	Vibration time (ms)	Energy (J)			
iQ Servo USW machine (Dukane,IL) 20 kHz		– The weld strength and the generated heat during USW are highly affected by the changes in mechanical and viscoelastic properties – Annealing has an impact on morphological parameters – As a final result, increasing α/γ ratio and uniform DoC improve the efficiency of USW – High mechanical and viscoelastic properties significantly enhance welding strength and reduce the variation in weld strength								without ED, which affects the morphology of materials & its elasto-viscoplastic behavior	
Branson Ultrasonics 2000 IW/IW+	CF/PP, CF/PA	1.5 holding time 1	800–3,200 N, trigger force 220–870 N	10 × 25–30	(30.4–32)	NA	NA	NA	Rectangular, continuous welding	Investigate the USW quality and tensile properties for sandwich structures made of multi-layer CF and TPCs polymer foils (PP/PA)	[241]
Herrmann Ultraschall HiQ DIALOG 1200	CF/PP, CF/PA	0.65 holding time 2	600 N, trigger force 220–870 N	10 × 25–30	30.0	NA	NA	NA			
Herrmann Ultraschall HiQ DIALOG 6200	CF/PP, CF/PA	(4.5–16.0) Holding time 5	2,000 N, trigger force 500 N	10 × 25–30	30	NA	NA	NA		three different USW machines have been used with five different sample structures and different parameter sets	
	Output	– Samples of the PA matrix show higher tensile strength than PP matrix – The maximum tensile strength was at fiber content of 39 wt%, four layers of polymer foils and three layers of CF, the thickness of each layer is 100 μm									
Branson 2000IW+ Ultrasonic Welder	CF/ PP, CFPA	1.5 holding time 1	1,800–3,200 N, trigger force 220–870 N	10 × 25–30	(30.4–32.0)	NA	NA	NA	Rectangular, continuous welding	Four different USW machines have been used to fabricate CF with TPCs films (PE/ PA/PP)	[242]
				10 × 25–30						By studying the mechanical properties, the maximum strength has been achieved by using the PA of nine layers fabricated with eight layers of CF in both cases unidirectional plates and multi-durational	
Herrmann Ultraschall HiQ DIALOG 1200	CF/PP	0.65 holding time 2.0	500 N and trigger force 600 N	NA	30	NA	NA	NA		The discontinuous and continuous USW were discussed	

(Continued)

Table 2: *Continued*

USW type	CFRP matrix	Parameters							Shape of sonotrode and number of spots	Summary	Ref.
		Welding/ holding time (s)	Welding force/ pressure	Overlap area (mm^2)	Amplitude (μm)	Power (W)	Vibration time (ms)	Energy (J)			
Herrmann Ultraschall HiQ DIALOG 6200	CF/PA	3–16 holding time 5	500/ 2,000–2,000 N and trigger Force 500–1,200 N	NA	20–30.6	NA	NA	NA			
	Output	The maximum tensile strength was recorded by PA and the CFRP density was 1.336 gm^{-3} at fiber content of 33 wt %, nine layers of polymer foils and eight layers of CF, with the thickness of each layer 100 μm									
KZH-2026 multifunction	CF/PA66	2.1 for CUSW 1.7 for HFUSW	0.16 MPa	38 × 25	NA	NA	NA	NA	Cylindrical SSW	A comparison between CUSW and HFUSW has been established HFUSW record higher ED at the faying interface with 25%, and the experimental results proven HFUSW is more efficient in machine protection and energy efficiency	[243]
	Output	– In both types of USW, there is a proportional relationship between peak load and weld time									
20 kHz Rinco Dynamic microprocessor-controlled ultrasonic	CF/PSS	4	1,500 N	SSW = 25.4 × 25.4 DSW = 50 × 25.4	60.8	3,000	NA	350–420	Cylindrical SSW, DSW	The effect of optimum energy and displacement on welded area and failure in both cases SSW and DSW by the USW boundary condition. Have impact on optimum energy requirement and quality	[170]
	Output	– At displacement controlled welding, D_{opt} = 0.23 mm in SSW UFL = 3578.7 ± 162.3 N (4.5) COV, %; Welded area = 95.4 ± 7.3 (7.6)COV, % and in DSW UFL = 7037.5 ± 467.8 N (6.6)COV, % and Welded area = 196.3 ± 14.3 (7.3) COV, % – At energy controlled welding E_{opt} = 420 J in SSW UFL = 3834.1 ± 272.7 N (7.1) COV, %; Welded area = 100.2 ± 9.1 (9.1)COV, % and in DSW UFL = 5838.3 ± 780 N (13.3) COV, % and Welded area = 160.2 ± 8.9 (5.5) COV, %									
20 kHz Rinco Dynamic microprocessor controlled ultrasonic welder	CF/PEI	NA	1,500 N	12.7 × 25.4	36.3	3,000	NA	NA	Rectangular SSW	Investigate the amplitude transmission during welding The hammering phenomenon occurring due to high frequency	[244]

(Continued)

Table 2: *Continued*

USW type	CFRP matrix	Parameters							Shape of sonotrode and number of spots	Summary	Ref.
		Welding/ holding time (s)	Welding force/ pressure	Overlap area (mm^2)	Amplitude (μm)	Power (W)	Vibration time (ms)	Energy (J)			
										which may have effect on heating efficiency was studied	
	Output	– Due to the heat generation based on the interface heating, there was a reduction in hammering effect – By experiment, the maximum power reached 1,300 W within a vibration time of 2–3.5 s while in simulation it reached 1,600 W at vibration time of 0.13 s and at 0.52 s								An experimental study of USW with high-frequency laser sensor followed by mathematical modeling and FFT to improve metaphysical FEM	
Oscillator JS3600s and a press machine, JP80s, a digital phase-locked-loop frequency tracking, 15.15 ± 0.15 kHz	CF/PA6	5	400–940 N	25 × 25	90	NA	NA	(200, 450, 650, 800), (450, 650, 800)	Square SSW	The LSS and cross tensile tests have been used to investigate the CFRTP welded by USW, the effect of FED and welding energy on the joint strength have been studied	[6]
	Output	– The cross-ply laminates have a higher stress range than twill woven laminates – Linear behavior was observed for load displacement curves maximum load 400kN with and without FED – The shear strength is higher with FED at 650 and 800 J by LSS2								Welding efficiency, welding quality, and fracture surface were observed	
20 kHz Rinco Dynamic microprocessor-controlled ultrasonic welder	CF/PPS	4	1,500 N, rate change 1,000 N	SSW 25.4 × 25.4, DSW 25.4 × 50	60.8	3,000	NA	NA	Cylindrical SSW, DSW, MSW	Study the mechanical behavior of SW single-lap joints and compare with mechanical fastened counterparts. Both single and double row joints were examined while varying the displacement	[236]
	Output	– The impact of increasing the number of rows or increasing the distance between inter row were the same – The capacity of carrying load of the spot welding was identical with mechanical fastened joint – By increasing the inter-row distance, the welded area increases in DSW – Double spot joint is much more efficient than single spot and it is compatible with mechanical fastened joint									
20 kHz Rinco, 3000 microprocessor-controlled ultrasonic welder	CF/PPS	NA	1,000, 300	NA	86.2–52.8	3,000	400, 1,500	NA	Cylindrical SSW	The impact of welding force & vibration amplitude on crystallinity have been investigated	[245]
	Output	– At low amplitude and welding force the cooling rate decrease to 16.9°C which leads to larger heat affected zone – Increasing cooling rate will decrease PPS crystallinity – An imperfect and a predominantly amorphous crystal produced by high amplitude and welding force									
	CF/PPS	10	500 N 1.6 MPa	12.7 × 25.4	80	NA	NA	NA	Rectangular SSW, continuous welding	A comparison between static USW and	[246]

(Continued)

Table 2: *Continued*

USW type	CFRP matrix	Parameters							Shape of sonotrode and number of spots	Summary	Ref.
		Welding/ holding time (s)	Welding force/ pressure	Overlap area (mm^2)	Amplitude (μm)	Power (W)	Vibration time (ms)	Energy (J)			
HiQ DIALOG 6200, Herrmann Ultrasonics	Output	– In static USW the consolidation pressure = 0.4 & 0.6 MPa and a reduction in strength, but it increases with pressure ≥1.6 MPa – High quality in CUSW was observed by applying consolidation pressure 1.6 MPa and length 400 mm								continuous USW to improve the quality of CUSW by adding consolidator. The effect of consolidation pressure on the quality of static USW before CUWS	
20 kHz USW machine (HiQ DIALOG SpeedControl Herrmann Ultraschall	CF/PEEK	0–8	500 N	12.7 × 25.4	86.2	NA	NA	NA	Rectangular SSW	The effect of misalignment between adherends on SUSW CFPEEK adherends with a flat PEEK ED has been investigated by studying eight different cases, the power peak and time flow were predicted by using numerical cycle strain	[247]
	Output	– The stiffness of the top adherend increased by decreasing clamping distance – A longer flow time may peak power and less uniformed fracture surface achieved by less clamping distance and the opposite is correct – The effect of angle between the adherends can be reduced by increasing clamping distance – The angle between adherends have effect on the process									
USW Servo Welder 20 kHz	CF/PA6	0–0.42	2,400 N	NA	50–90	NA	Plunging speed 0.1–1.5 $mm \cdot s^{-1}$	200–1,200	Cylindrical SSW	Investigated the CF/PA6 welded by USW without ED and the vibrations were separated into four stages based on physical states and contact temperature. The impact of the following parameters on the bonding efficiency and the welding process has been studied: amplitude, welding energy, trigger force, and plunging speed	[248]
	Output	– By increasing sonotrode displacement and welding time, temperature increase until it reaches the maximum point in the beginning of stage 4, then it starts to decrease slightly – The power increase by increasing time until stage 3, then it fluctuates downward – By increasing welding energy, the effect of sonotrode indentation shows to increase and the melted area in the welded material increases and a squeezed-out material was observed – The amplitude was supposed to be within a limited range; low amplitude may lead to loss of input energy, while high energy may destroy the welder – The servo driven welder without ED has many advantages									

(Continued)

Table 2: *Continued*

USW type	CFRP matrix	Parameters							Shape of sonotrode and number of spots	Summary	Ref.
		Welding/ holding time (s)	Welding force/ pressure	Overlap area (mm^2)	Amplitude (μm)	Power (W)	Vibration time (ms)	Energy (J)			
Dukane ultrasonic welder 20 kHz	CF/PA6	3	Trigger force 300 N	38 × 38	35	NA	Plunging speed 0.004 $in{\cdot}s^{-1}$	400–1,400	Cylindrical SSW	More than 100 samples were studied, 2 set of samples were tested and after USW process, the machine learning (ML) approaches were applied by using the artificial neural network and random forest (RF); aiming to predict failure load and welding quality concurrently	[249]
	Output	– 1,200 J found to be the optimum value of power – The performance of RF was very close to the real experiment (for welding quality) – Failure load results show that the predicted results were very close to that of real experiment – During the USW process, the energy and displacement increased with time								15 experiments were run for the welding process under displacement-controlled mode and the rest under energy-controlled mode. The welding process has been done without ED	
iQ Servo UltrasonicWelding machine 20 kHz	CF/PA6	6	Trigger force 200 N	NA	33	NA	Welding speed 0.3 $mm{\cdot}s^{-1}$	200–1,600	Cylindrical SSW	The relationship between process parameters weld quality and joint performance by USW using ML ANN and other methods were investigated by using three welding quality classes to set the algorithm. The microstructure characterization and welding quality were observed in all applied power regions	[250]

(Continued)

Table 2: *Continued*

USW type	CFRP matrix	Parameters							Shape of sonotrode and number of spots	Summary	Ref.
		Welding/ holding time (s)	Welding force/ pressure	Overlap area (mm^2)	Amplitude (μm)	Power (W)	Vibration time (ms)	Energy (J)			
	Output	– At power energy <700 J and welded area of 0–70.9 mm^2 with an interfacial separation failure mode – At power energy 700–1,100 J and welded area of 70.9 mm^2 with nugget shear fracture – At power energy >1,100 J and welded area of 70.9 mm^2 with nugget shear fracture – Under the same selected features, the ANN bidirectional recurrent neural networks has significantly higher categorization accuracy and greatest robust than other methods (SVM and k-nearest neighbors)								The Fisher's ratio combined with innovative clustering overlap analysis were proposed	
HiQ DIALOG 6200, Herrmann Ultrasonics	CF/PPS	4	500–1,000 N	NA	86.2	200–2,500 W	NA	0–1,200	Cylindrical SSW	To study the impact of weld manufacturing defects on guided wave of the USW transmission across the joint, a triangular ED was used in the lower adherends, which enable controlling the production of defective joints, but was not able to detect the unwelded areas	[78]
	Output	– At 619 kHz, the strength of the interaction increases – The characteristic frequency enables the detection of adherend fiber bundle distortion. The detection accuracy for adherend fiber bundle distortion = 100 and 60% for unwelded area – The maximum strain and applied force were found in batch 2 – The extra reflection from overlap edges to interfere constructively caused by the effect of oblique scattering leads to have the highest value of Time-of-Flight (TOF) in batch 3 with 619 kHz – The adherend fiber bundle distortion has higher impact on the frequency spectrum than the unwelded area – By combining TOF and Δf_{ch} the structural monitoring, failure detection, and diagnosing becomes easier								The samples were separated into the batches each with different vibration time and different single-lap shear strength	
Dukane ultrasonic welder	CF/PA6	Holding time 3	Trigger force 300 N	NA	±35	NA	Plunging speed 0.04 $in{\cdot}s^{-1}$	400–1,600	Cylindrical SSW	USW technique has been used to weld CFRP/CFRP and Metal/ Metal For welding PC sheets, 129 weld coupons joining were studied, holding the data signals for time, clamping	[251]

(Continued)

Table 2: *Continued*

USW type	CFRP matrix	Parameters							Shape of sonotrode and number of spots	Summary	Ref.
		Welding/ holding time (s)	Welding force/ pressure	Overlap area (mm^2)	Amplitude (μm)	Power (W)	Vibration time (ms)	Energy (J)			
										force, power, and displacement The outcomes of the welding process were classified into three categories (under weld, normal weld, and over weld) and both power and clamping force at the three classified categories were presented	
	Output	– The maximum power for under weld = 1,550 J at 2–2.3 s – The maximum power for normal weld = approximately 1,490 J at 2.1 s and the second peak power were found around 1,150 J at 3 s – The maximum power for over weld = 1,400 J at 1.7 s and the second peak power were found around 1,160 J at 2.5 s								Different ML. approaches and methods have been applied after the welding process	
The USW machine has been developed in the lab 20 kHz	CF/PPS	NA	500, 1,500 N	CW 12.7 × 220, SW 12.7 × 220 and 12.7 × 15	60, 80	NA	For SW (110–1,000), For DW welding speed (15–55)	NA	Square SSW, Continuous welding	Three combined sets of vibrational amplitude force and power were chosen to investigate the SW and CW to find the difference and the resemblance between both methods and the optimum conditions were studied	[165]
	Output	– The optimum condition in both the welding methods was found to be typically the same, which mean that the melting process kinetics is insensitive to SW/CW – A significant higher LSS of SW than CW; the main reason is due the lack of consolidation during cooling in CW – Maximum LSS in SW = 40 MPa at 500 N, 60 μm, and 910 ms – The power curves morphology is typical for both welding methods – In SW, the material consecutively undergoes all the phases of welding process – In CW, the material pass through phases which has a constant coexistence									
20 kHz Rinco Dynamic 3000 microprocessor-controlled ultrasonic welder,	CF/PPS	0–4	1,500 with increasing rate by 1,000	SSW 25.4 × 25.4, DSW 50.0 × 25.4	51.8–80.8	3,000	NA	NA	Cylindrical SSW, DSW	A PPS spot ED has been used in both SSW and DSW The SSW was carried by using sonotrode with	[231]

(Continued)

Table 2: *Continued*

USW type	CFRP matrix	Parameters							Shape of sonotrode and number of spots	Summary	Ref.
		Welding/ holding time (s)	Welding force/ pressure	Overlap area (mm^2)	Amplitude (μm)	Power (W)	Vibration time (ms)	Energy (J)			
										different diameters, while the DSW was carried by sequential welding and simultaneous welding	
	Output	– The maximum % of power was recorded by using sonotrode D = 40 which is around 62% at 0.5 s, 783 J – For SSW, the maximum total welded area = 400 mm^2 at D = 40 and Optimum displacement = 0.16 mm – For SSW, the highest ultimate failure load = 1,190 N at D = 40 and the highest LSS = 1,500 N at D = 10 – High vibration concentration at ED – For DSW, the highest ultimate failure load = 6,450 N and the highest LSS = 6,500 N at Seq W								By increasing the diameter, the heating rate increased and welding time decreased, which enhance the welding efficiency; but a low weld quality was noticed at the edges	
Branson 2000XD ultrasonic welder 20 kHz	CF/PEEK	NA	Trigger force 150	40 × 40	32, 56	2,500	NA	600–1,800	Cylindrical with different dimensions of SSW	A novel USW was established by using a spherical anvil instead of flat anvil, the enhancement of anvil radius on welding has been studied	[232]
	Output	– The scattered welds were reduced by using the spherical anvil – The welding time decreased in case of using spherical anvil – The welding process was divided into four stages – An interfacial fracture was observed at very high and at very low welding energies – The optimum anvil radius is 300 mm – At welding energy >1,600 J, the failure load = 5,000 N – In both anvil geometries, the power % was found to increase sharply at first time of the process – Shear tensile force increased as a consequence of weld growing in a narrow range of welding energy									
Dukane advanced iQ servo welder 20 kHz	CF/PA6	Holding time 6	Trigger force 100–200 N	38 × 38	33	NA	Welding speed 0.3 $mm{\cdot}s^{-1}$	200–1,600	Cylindrical SSW	The welded composite by USW without ED with different welding parameters has been evaluated in mechanical, microstructure, and thermal prospective	[252]
	Output	– By increasing the welding energy, the welding area increases; maximum welded area 70.9 mm^2 – The maximum welding force 2,500 N achieved at the first 2 s of welding process at 800, 1,000, and 1,600 J – The maximum bonding efficiency is approximately 70%, which is recorded at 1,000 J – Maximum shear load 3389.5 N at 1,000 J – As an overall, the highest temperature = 450°C at 1,200 J – Failure mode classifications; nugget shear fracture, nugget pullout fracture, and interfacial separation									
Dukane iQ Series i220 Ultrasonic	PCABS	4–5	3.5–5 bar	NA	30–50	NA	NA	NA	Cylindrical SSW	The PC and Acrylonitrile butadiene styrene (ABS)	[253]
	Output	– The maximum welding strength = 6.02 $N{\cdot}mm^{-2}$ at 33.14 μm, 4.03 bar, and 3.35 s									

(Continued)

Table 2: *Continued*

USW type	CFRP matrix	Parameters							Shape of sonotrode and number of spots	Summary	Ref.
		Welding/ holding time (s)	Welding force/ pressure	Overlap area (mm^2)	Amplitude (μm)	Power (W)	Vibration time (ms)	Energy (J)			
Spot Welding equipment 20 kHz		– Maximum heat generated = 146.2°C at 40.89 μm, 4.29 bar, and 4.52 s								blends were welded by USW with ED using the injection molding techniques, the effect of USW process parameters on welding strength was studied, the ML techniques ANN and NSGA II were used for optimization	
Acoustic welder (Branson US Corporation) 20 kHz	CF/ Ep-EMAA	30	60 kPa	25 × 25	NA	1.1	NA	NA	Square SSW, MSW	To quantify the healing efficiency of US vibration; two groups of specimens with two different concentrations of EMAA were tested; the EMAA was welded with carbon-Ep to heal it, and it has been proven that USW is sufficient for multi repairs and recoveries in interlaminar fracture toughness. USW can repair composite structure containing mendable polymers (EMAA)	[254]
	Output	– The delamination cracks can be repaired by thermally activated mendable polymer through the high frequency of US and the short duration bursts – The repair efficiency reaches 130% – The repair efficiency by conventional heating through thermal oven is higher than USW – Maximum interlaminar fracture toughness of USW with EMAA content 80% is approximately 0.35 $kJ{\cdot}m^{-2}$ – Maximum. crack opening load = 90 N achieved at the fifth self-healing cycle – EMAA phase has fracture toughness = 2.25 $kJ{\cdot}m^{-2}$ which prevents the initial crack from propagation through the phase – USW can generate the required heat for thermal activation for the reaction = 150°C – Increasing EMAA amount in the laminate enhances repair efficiency									
20 kHz Dukane servo ultrasonic welder	CF/PA6	3	Trigger force 200 N	38 × 38	35	NA	Welding speed 0.2 $mm{\cdot}s^{-1}$	400–1,200	Cylindrical SSW	The effect of preheating on welded joints by USW was investigated. The temperature of preheating was set < T_m while seven different durations were chosen to explore the influence of preheating time; preheating for 30 s	[255]
	Output	– The maximum. shear load was approached by preheating to 200°C and welding energy of 1,000 J = 3,650 N – The 1,000 J was found to be a critical point; increasing the energy will increase the maximum shear load until 1,000 J, then the maximum shear load starts to decrease – The microstructure observation shows that only at low energy there will be interfacial matrix fracture. – More CF involves in the welding layer by expanding the amount of melted material which in consequence increase bonding degree and improve maximum shear load – Welded area increased by increasing the preheating temperature									

(Continued)

Table 2: *Continued*

USW type	CFRP matrix	Parameters							Shape of sonotrode and number of spots	Summary	Ref.
		Welding/ holding time (s)	Welding force/ pressure	Overlap area (mm^2)	Amplitude (μm)	Power (W)	Vibration time (ms)	Energy (J)			
		– Preheating time enhances the welding quality								generates significant softness of welding layer	
SR-2020 multifunction USW 60 kHz	CF/PEEK Output	0.7–1.1	0.3 MPa	10 × 10	25	2,000	NA	NA	Cylindrical SSW	The influence of using ED with thickness of 0.45 mm and welding time on welding strength was investigated, the heat affected zone (HAZ) is high in case of not using ED with high % of crack defects. The ED reduces the peak temperature	[256]
		– Very low strength combined with incomplete fusion defects were found at the interface joint fracture – Cracks and void defects may be caused by too long welding time at the interface of PEEK and CF with LSS < 14.4 MPa – Increasing welding time and using ED will reduce thermal stress between PEEK and CF and will increase the LSS to 28 MPa, and a further increase in welding time may reduce crack defects									
Rinco Dynamic 3000 20 kHz	CF/PPS Output	Holding time 2	0–1.6 MPa	NA	38.1	3,000	NA	NA	Cylindrical SSW	The samples were prepared in sandwich structure	[257]
		– Microhardness was used to further confirm crystallinity									
Rinco Dynamic 3000 20 kHz	CF/PPS Output	0.43	2.2 MPa	25.4 × 12.7	NA	3,000	NA	NA	Cylindrical SSW	A comparison between the effect of welding time and input power effect on welding quality was carried out	[258]
		– USW shows better LSS results than IW and RW – Less damage was observed by the SEM of fracture surface of USW specimens than IW specimens									

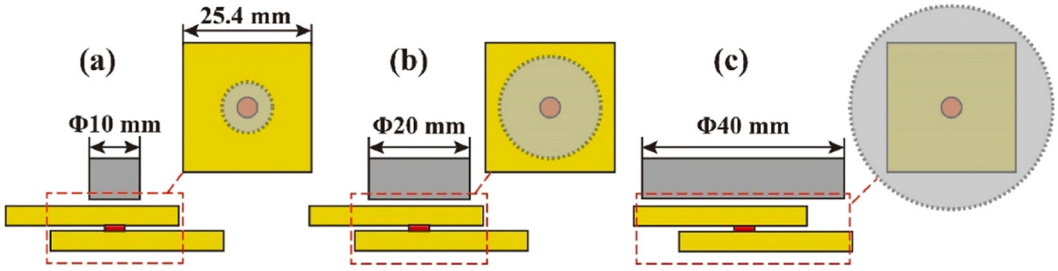

Figure 23: Schematic of SSW joints using three dissimilar Sonotrodes. The grey semi-transparent parts specify the cross-section area of each sonotrode: (a) D = 10 mm, (b) D = 20 mm, and (c) D = 40 mm [231].

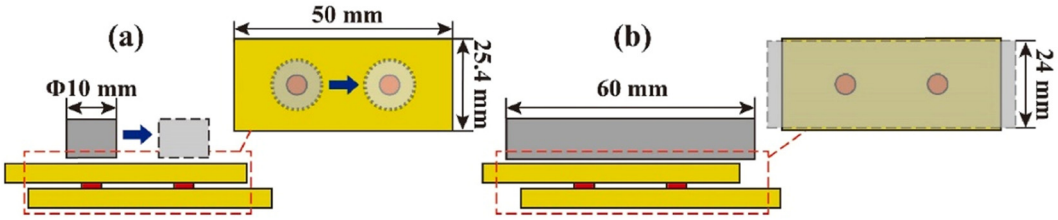

Figure 24: Schematic of DSW joints using two dissimilar sonotrodes. The grey semi-transparent parts specify the cross-section area of each sonotrode: (a) a sequential spot welding with sonotrode D = 10 mm; and (b) an instantaneous spot welding [231].

form the joint without melting the metal material [229,230]. Nonetheless, a tabular classification based on the type of USW machine used in joining polymers is presented in Table 2 without using an interlayer between the two welded specimens.

Furthermore, the welding tool in USW process, known as sonotrode or horn, and it has an impact on the performance of USW processes, welding parameters, and welding quality. However, owing to the high expense of the sonotrode, only a few studies focused on examining the effect of the welding tool. The welding quality and the welding process are affected by the distance between the sonotrode and the interface of the working piece; owing to these joints categorized into two types: (1) Direct ultrasonic (near-field), the distance of a maximum of 6 mm and (2) indirect (far field the distance is greater than 6 mm, which may reduce the amount of energy reaching the interface [175]. Besides, a unique study has investigated the enhancement of changing welding tools on process parameters, overall welded area, LSS, and fracture of CF/PPS [231]. The samples were separated into two groups: single spot welding (SSW) welded the first group samples by using three different sonotrodes with 10, 20, and 40 mm diameters, as shown in Figure 23. The first and second group samples were welded by double spot welding (DSW) with three different sonotrodes 10, 20 and 40 mm diameter as shown in Figure 24 [231]. Furthermore, Yang *et al.* [232] joined CF/PEEK by USW using sonotrodes with 10 and 20 mm diameters with different ranges of spherical radius. Besides, the joint's microstructure, fracture characteristics, and tensile-shear properties were examined. The findings demonstrate that joining with a spherical surface anvil can efficiently concentrate welding energy. As a result, the weld scatter was observed to decrease. The influence of spherical radius on the weld formation and the area of scattered welds are shown in Figure 25. For both large and small sonotrodes, a remarkable quantity of scattered welds was observed on the fracture surface by using a flat anvil, and these results were significantly validated. Figure 25 demonstrates the welding energy and spherical radius enhancement on the joint failure load. A significant variability in the failure load for flat anvils has been revealed, which suggests that the weld quality is quite unsteady. A lower quantity of energy is required to produce over welds, and the energy concentration effect is superior for spherical surface anvils with smaller radii, which implies that the stability time will be shorter for the smaller radius. The spherical surface anvil has increased stability and mechanical qualities compared to the flat anvil [232]. Additionally, the sonotrode displacement and duration directly impacted the weld quality. As a result, an *in situ* inspection approach based on target sonotrode displacement and duration has been developed to assess the weld quality [233].

Moreover, an investigation of the microstructure (fracture morphologies) of short CF/PEEK joined without ED by

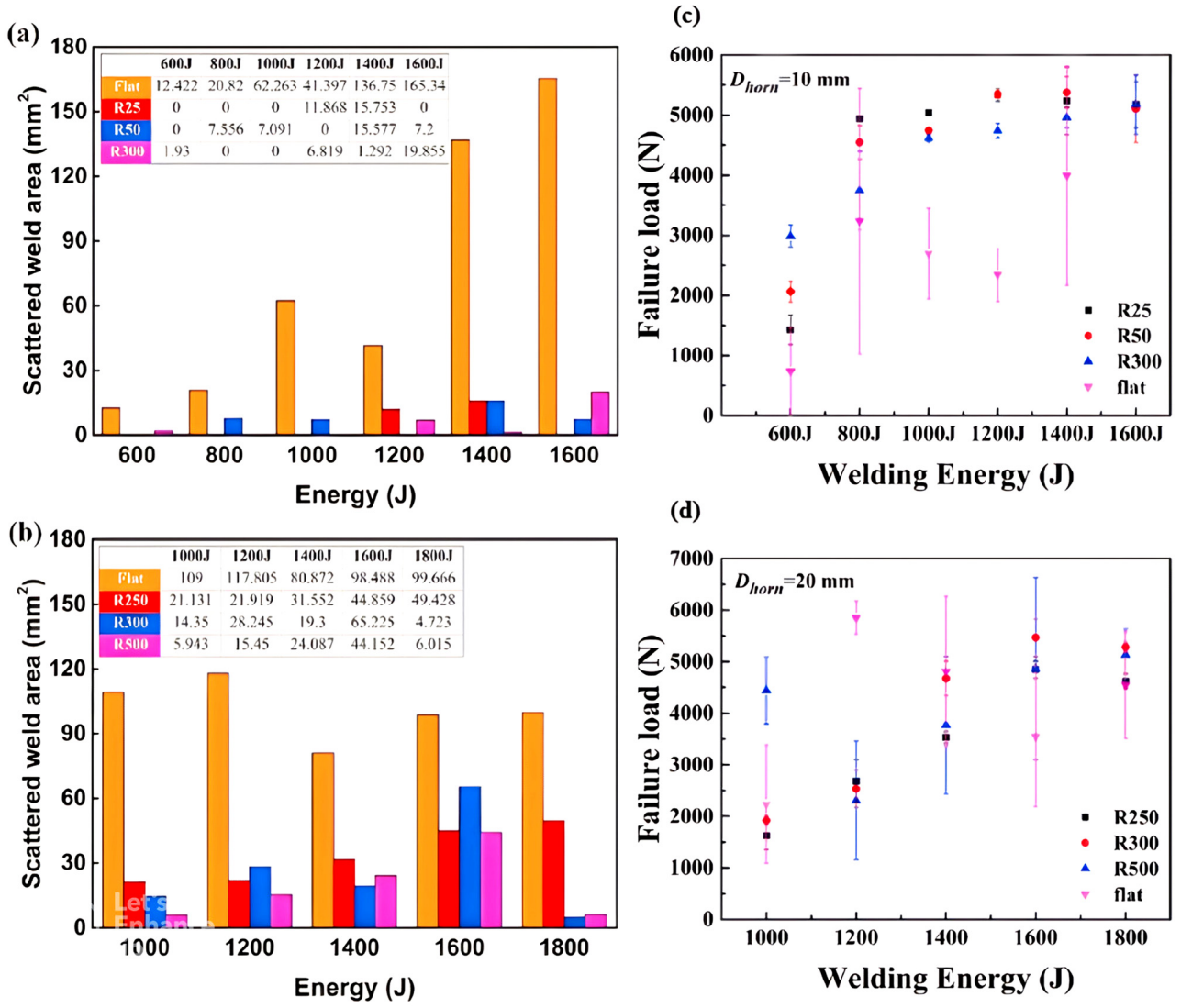

Figure 25: The Measured scattered weld area: (a, c) sonotrode with small diameter 10 mm, (b, d) sonotrode with large diameter 20 mm and the joint failure load at dissimilar welding energies and spherical radii [232].

using different sonotrodes at various welding energies (600–1,600) J, concluded with remarkable results, has been carried [232]. The edge of the sonotrode may cause a stress concentration which caused an approximately annular weld shape and the weld quality was not good. As shown in Figure 26, the fracture morphology is consistent over the whole weld. For a standard weld, the primary fracture mechanisms were adhesive fracture and fiber-matrix debonding. However, as a result of the LSS test and ultimate failure (UF) of CF/PPS joints by USW under different diameter sizes of sonotrode, the ultimate failure load (UFL) was considerably improved by around 86% by using a sonotrode with D = 20 mm, and further improvement has been obtained by using a sonotrode with D = 40 mm. More extraordinarily, the LSS observed reduced by around 22% for sonotrode with D = 20 mm and D = 40 mm for SSW samples. Besides, the averaged LSS achieved by using 20 and 40 mm diameter displayed superficially greater scatter with 13 and 11%, in contrast, sonotorde with 100 mm diameter achieved 3%. Furthermore, the reduction in LSS denotes a decline in the load-carrying efficiency of the SSW joints. This indicates that the total welding quality obtained by utilizing the sonotrode with D = 20 mm and D = 40 mm SSW joint was lower than that welded by using the sonotrode with D = 10 mm counterparts, as shown in Figure 27 [231]. Nevertheless, the sonotrode with D = 40 mm provides more significant energy efficiency due to its additional inspiringly enhanced magnitude, almost 140%, of the spot-welding area. Furthermore, the SEM micrographs have been employed to

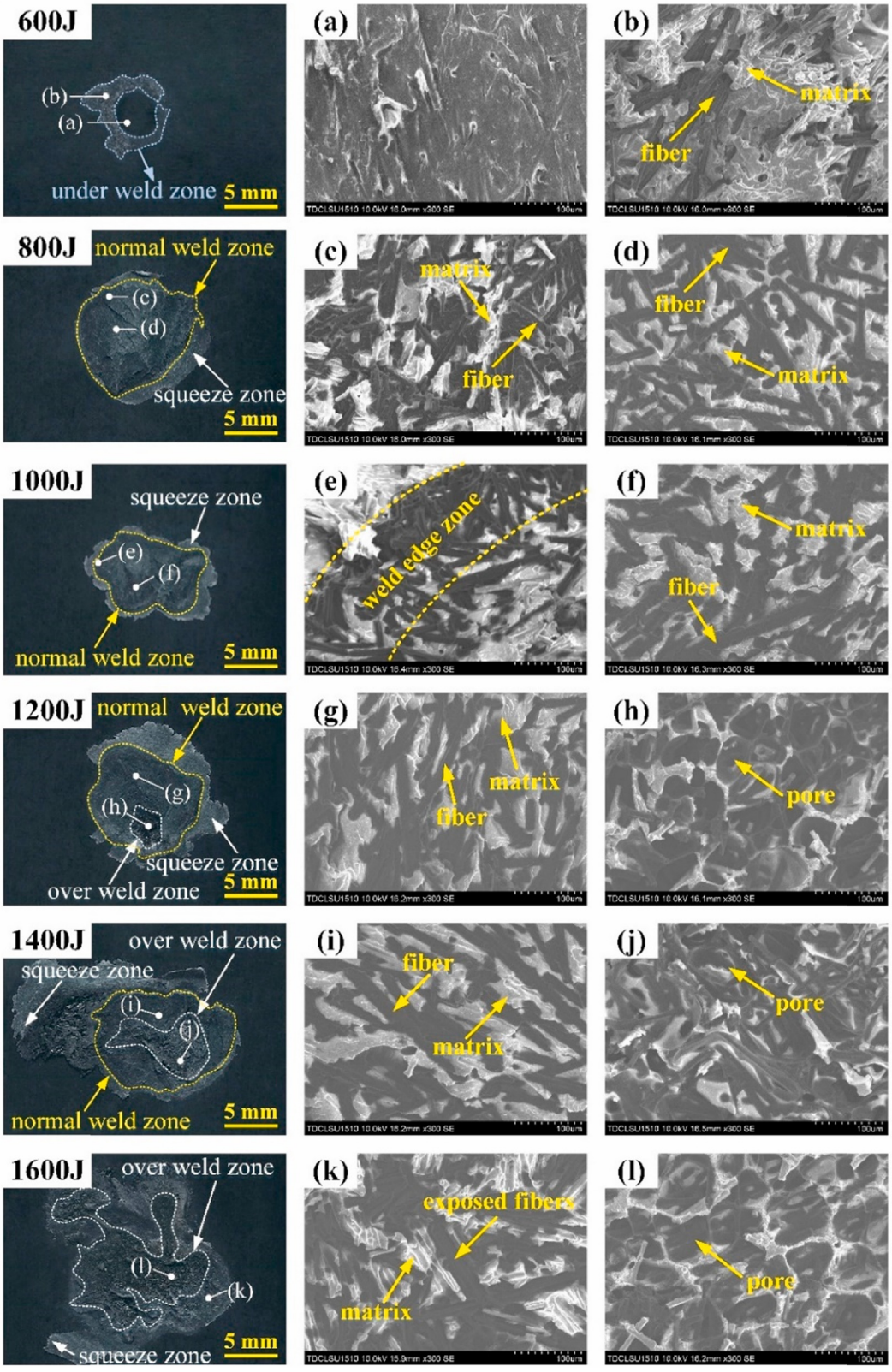

Figure 26: (a) Unweld zone at 600 J, (b) under weld zone at 600 J, (c) and (d) normal weld zone at 800 J, (e) weld edge zone at 1000 J, (f) normal weld zone at 1000 J, (g) normal weld zone at 1200 J, (h) over weld zone at 1200 J, (i) normal weld zone at 1400 J, (j) over weld zone at 1400 J, (k) and (l) over weld zone at 1600 J. [232].

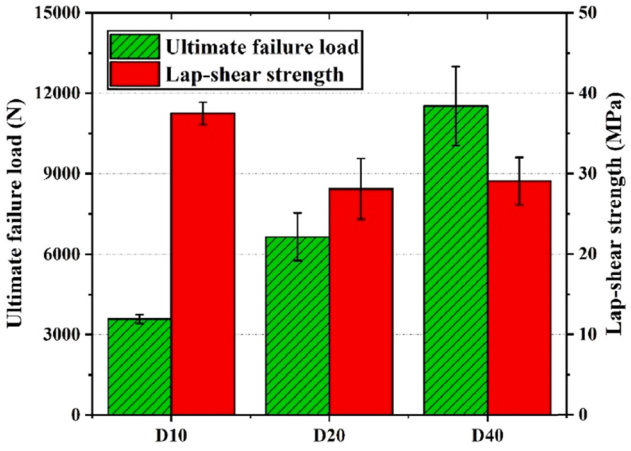

Figure 27: UFL and LLS of the SSW joints formed by diverse sonotrodes at the optimal displacements [231].

examine CF/PPS SSW welded failure modes using different sonotrode sizes to evaluate the welding quality. It was observed that the deep fiber imprints on polymer resins and the bare fiber bundles depend on the fiber matrix featured [231], which indicates that high welding quality was achieved [3]. Figure 28 presents the SEM details of the fracture surface welded by a sonotrode with 20 and 40 mm diameter at 1,500 N, 1,000 $N \cdot s^{-1}$. In Figure 28(a), the fiber was damaged directly and reduced the load-bearing ability of the welded joints. In Figure 28(b), the voids that appeared by using sonotrode with D = 40 mm SSW joints are thought to be one of the features that adequately describe overheated welds as stated by Gao *et al.* and Zhao *et al.* [170,234]. Besides, that considerably reduces the bonding region which could effectively support the load. Jongbloed *et al.* [235] studied the impact of sonotrode with rounded geometry on joining TPCs by USW. It is revealed that significant welding quality can be achieved by using rounded sonotrode, while reducing the required heat at the welding interface since the direct local exposure of the weldment to sonotrode is less.

2.2 Enhancement of spot number in USW (single, double, and multi)

There are three main types of spot joints in USW: SSW, multi-spot welding (MSW), and DSW. The TPCs joined by SSW have similar characteristics of shear-strength joints with single MF of identical size [72]. An example of the difference between the SSW and DSW in the USW process is demonstrated in Figure 29(a) and (b) [170]. However, in the MSW in USW, consecutive welding has the potential to be composite-friendly and has fast-processing viable alternatives to MFs for TPC structure and CFRTP [170]. The main challenge of this type of USW is that each single spot has its unique boundary conditions. Also, the number of spots has an impact on the distribution of vibration among the

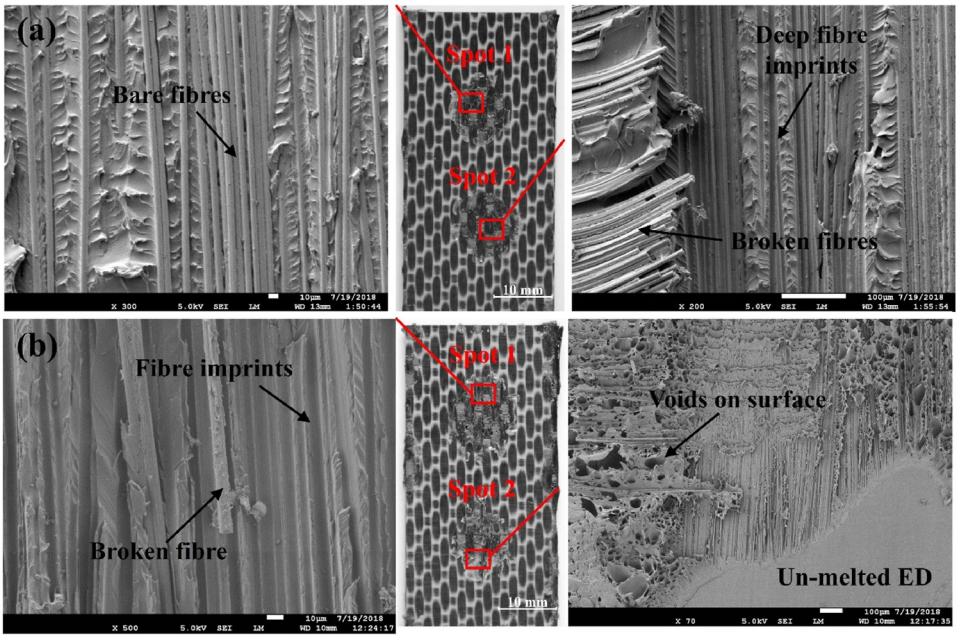

Figure 28: SEM details and fracture surfaces of CF/PPS SSW of (a) sonotrode with D = 20 mm and (b) sonotrode with D = 40 mm welded at the corresponding optimum displacements [231].

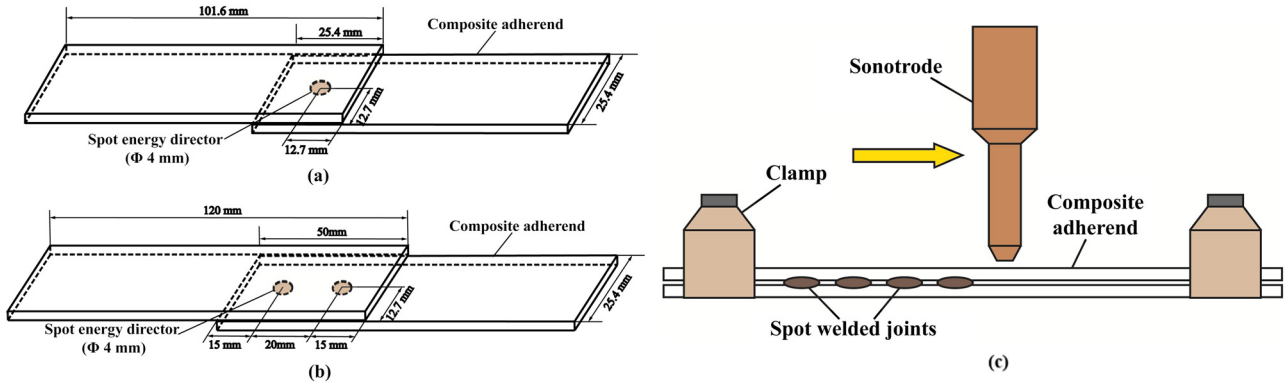

Figure 29: A schematic of an example of welded joints; (a) The single spot, (b) the double spot, and (c) the schematic of multi-spot USW [170].

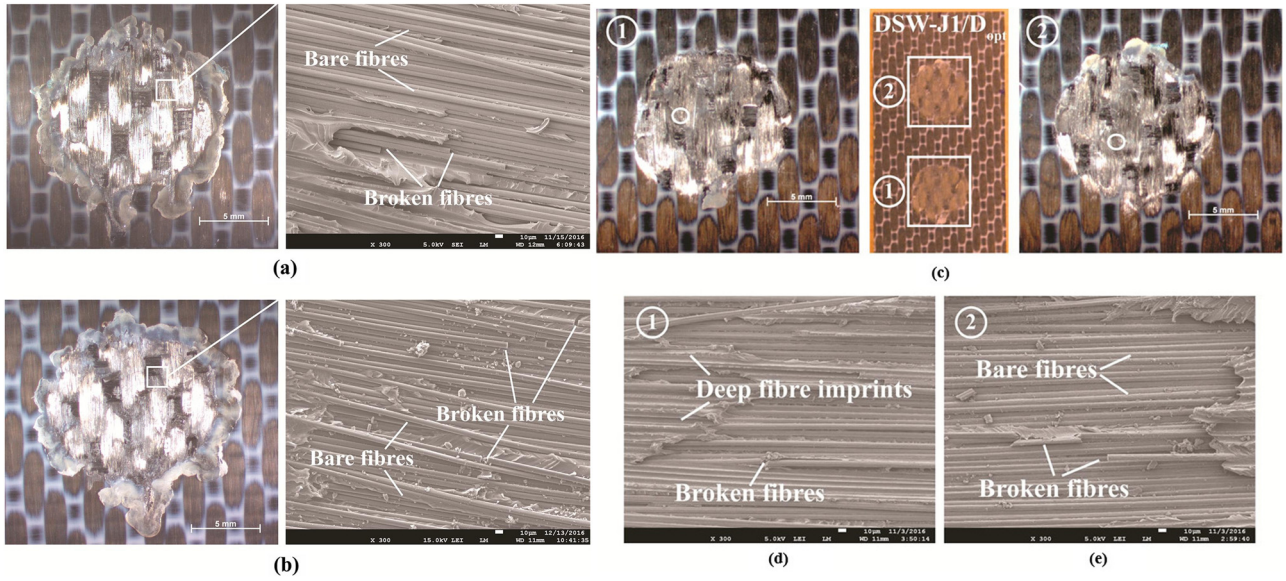

Figure 30: The surface of fracture and the SEM for optimum displacement controlling for SSW and DSW of CF/PPS; (a) the optimal displacement controlled in SSW, (b) the optimal energy controlled, (c) the DSW under optimal displacement controlling, (d) the spot 1 and (e) the spot 2. The scales are 5 mm (for stereo-microscopy) and 10 μm (for SEM) [170].

joining interface. Figure 29(c) depicts a multi-spot USW schematic [170].

Comparison of the fracture surface through SEM of the SSW with specimens joined by the DSW for optimum displacement after the mechanical testing is illustrated in Figure 30. In the SSW joints for both optimum displacement and optimum energy control, bare fiber, deep fiber imprints on the matrix, and torn fibers were detected as the key features on the fracture surface, corresponding to the primary failure mode, which is fiber-matrix debonding [170]. A previous study claimed that the weld qualityhighly affected by the fiber matrix debonding [3]. Furthermore, for DSW, the features of the joints were the same as for SSW: deep fiber imprints, torn fibers, and bare fibers. Moreover, Zhao *et al.* [236] provided a comparison between SSW, DSW and MSW in USW as an efficient substitution of single, double, and multi-MFs. As shown in Figure 31, the LSS has been implemented to obtain the failure and load capacity for each type of joint. After performing the LSS, the samples were examined, and it was determined that all the spot-welded joints had a first-ply failure, as shown in Figure 32. It is noticed that the average welded area in DSW was less in the further examples in the four-row welded joints because of the small spacing between the spots. This can be owing to the contact between melted and unmelted ED during the welding process since it is identical to the double-row welded joints with the least inter-row distance [236]. The study was followed by a further finite element

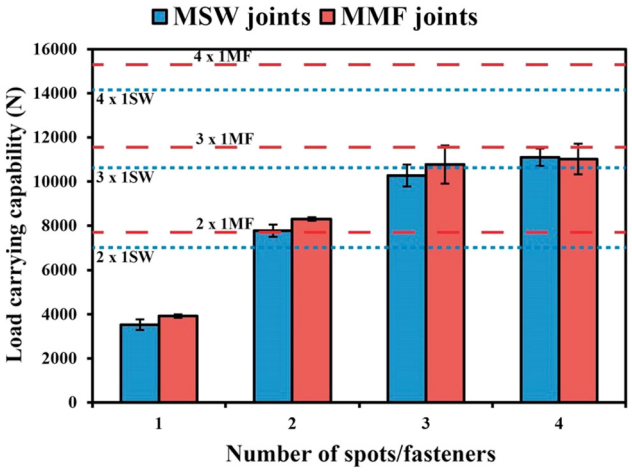

Figure 31: The number of rows that make up the load-bearing capacity of multi-row spot-welded and mechanically fastened junctions with 70 mm overlap length is present in the samples with 2, 3, and 4 rows [236].

(FE) investigation to analyze the mechanical performance of single-lap TPC joints welded together by the USW [237]. Besides, cohesive zone elements were utilized to estimate the welded areas. A comparison among the numerical outcomes and the actual data served as the initial step in validating the provided FE model. The numerical outcomes offer prospective directions for the structural design of TPC joints by USW and are used in airplane construction.

The CF/PA6 joined by adhesive bonding was further repaired by USW and studied by Zhang *et al.* [70]. The fracture microstructures of the adhesive-bonded joints were observed to comprehend the reason for the scatter in joint strength. The fracture surfaces of the examined joints together with different adhesive coverage range at the overlap area are shown in Figure 33, which shows that each joint displayed an adhesive failure mode, demonstrating the weak bond amongst the adhesive and the adherend. Additionally, after curing, the adhesive coverage area transformed from a rectangular form to an irregular form, changing the actual bonding area. As a consequence, the strength of the joints varies. Besides, Figure 34 roves that the weld area increased dramatically as the sonotrode force increased with an oscillation duration of 0.9 s. The expansion in the welded area has considerably improved the joint strength. However, when the joints were subjected to a sonotrode force below 935 N over an oscillation time of 1.2 s, considerable melting and outflow of molten materials were seen at the faying surfaces (Figure 34d), otherwise, the top of the healed joint developed a significant sonotrode indentation.

3 Enhancement of USW parameters and pretreatment process on microstructure characterizations and mechanical behavior

One of the main essential outcomes of any welding process is the welded joint quality and the contract of the welding process; according to this, many studies have investigated the influence of vibrational amplitude [17,65], welding force, welding pressure [259], holding time [259], welding time [259,260], ED shape [3,260], vibration time as well as power [64,238,261]. The USW process parameters have been investigated to find the optimized parameter values [170,262]. In addition, since the USW parameters affect the mechanical properties and microstructure characterization, this section covers the mechanical and microstructure observations. Based on the literature, the welding quality of CFRTP and CFRTS joined by the USW is measured based on the mechanical properties like shear strength, tensile strength, modes of failure, and the morphology of the

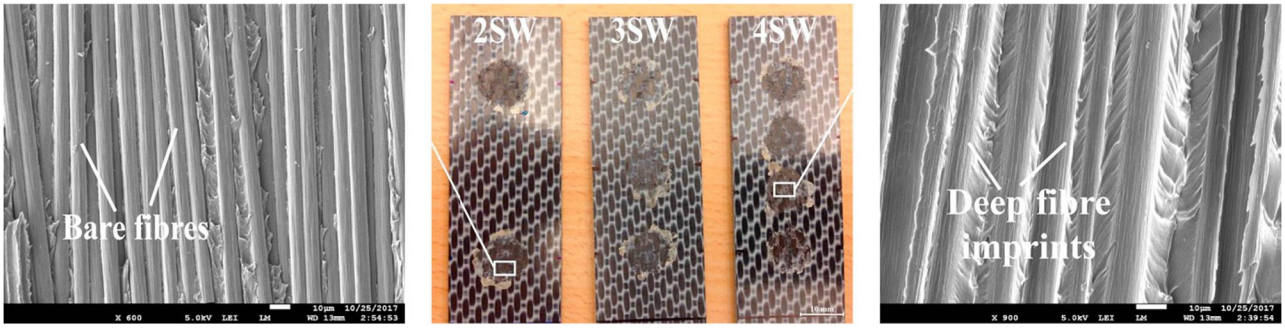

Figure 32: The SEM details of welded CF/PPS show the first-ply failure of fracture surfaces for 2, 3, and 4 SW joints [236].

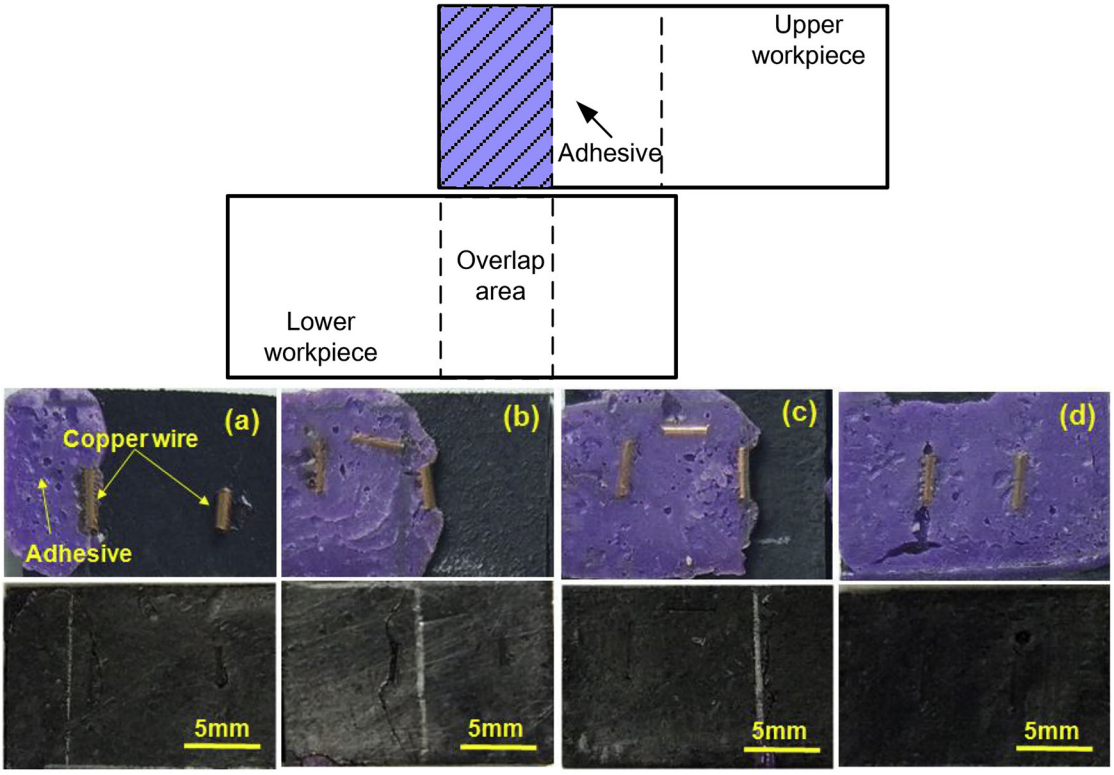

Figure 33: The adhesive effect coverage on the tensile test adhesive-bonded failure modes of 2.3 mm thickness CF/PA6 with 30 wt% fiber: (a) 25%, (b) 50%, (c) 75%, and (d) 100% adhesive coverage [70].

weldment. Moreover, owing to material failure, design failure can be prevented, and the superior material can be guaranteed by studying the mechanical properties. Furthermore, the weld fracture surface can be processed to detect the welding quality [255]. In this context, Müller *et al.* [263] investigated the characterization of welding

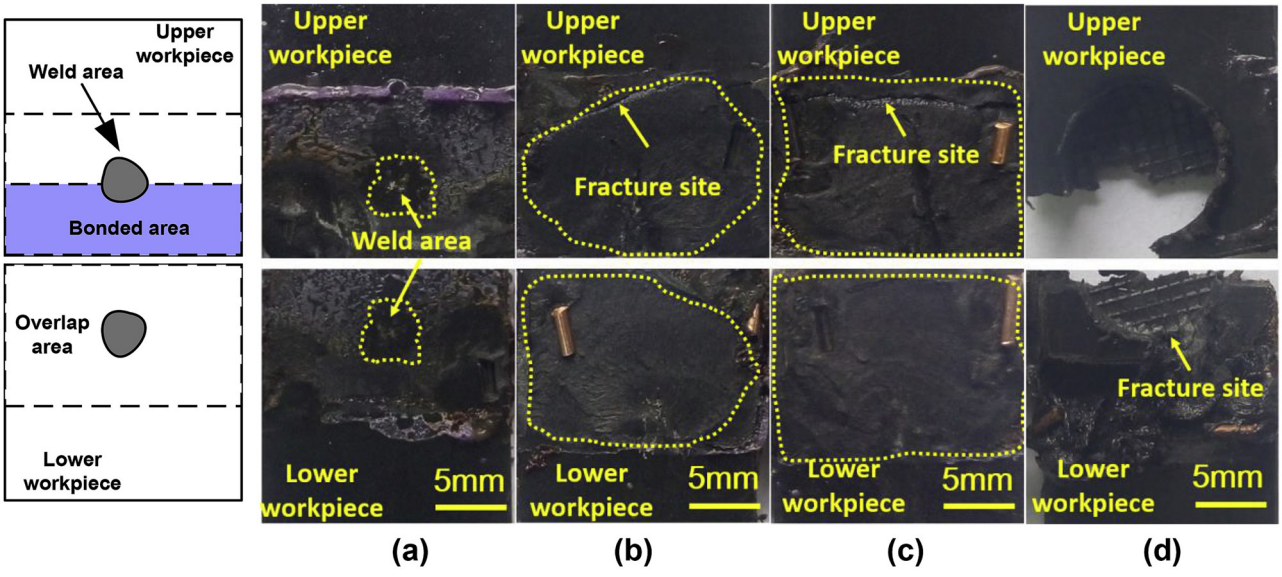

Figure 34: The impact of various process factors used in USW on failure modes of restored adhesive-bonded 2.3 mm thick CF/PA6 composite with an adhesive coverage of 50% at the overlap area, (a–c) welding time of 0.9 s and sonotrode force of (a) 312 N, (b) 623 N, (c) 935 N, and (d) 935 N for 1.2 s.

quality of joined metal by USW through vibrational analysis, and various robust models were developed for various material parameters. Moreover, Gaurav and Singh [264] addressed several parameters that enhanced the fatigue behavior in composite FRP. The factors that trigger this behavior in composites are reinforcement substance fiber alignment or stacking pattern, polymer matrix, fiber content, testing circumstances, and others. Besides, the damaging process developments at the microscopic level and the loading condition factors consist of stress ratio, multiaxial stress, mean stress, and testing frequency. The final welding strength of a joint is controlled by fibers in the welded province, which leads to a decrease in the volume of the melted polymer matrix and impacts the reentanglement of molecular chains in the polymers [240]. However, the LSS is used frequently to test the welded CFRTPCs or CFRTSCs joined by USW, while in case the welded specimens are metallic, the tensile test is used [265–267]. Significantly, the LSS has been used widely for convenience and for evaluating joint shear strength [268].

3.1 Welding energy

By investigating the CF/PEEK joined with SSW USW with respect to modes I and II, the results show that by using constant welding energy, the supreme critical strain energy release rates (GIC and GIIC) were achieved [269]. Likewise, while investigating samples with dissimilar surface roughness, a significant correlation has been noticed between welding energy and welding strength [270]. On the other hand, the adherents' stiffness and thickness considerably impact the amount of required welding energy [64]. Furthermore, it has been indicated that using the welding energy to control parameters is more suitable than using vibration time [64,269]. Zhi *et al.* [271] found that the welding energy affects the weld indentation, joint strength, tensile strength, and welded area. The results of these relationships are presented in Figure 35. In a further investigation, an FE model has been generated to study the stress and welding indentation, and it has been observed that the welding energy directly affects the vibrational stages of the welding process [269]. Besides, Zhang *et al.* [272] found that increasing the welding energy above the optimum value will have the opposite effect on the weld strength and will no more be beneficial. Since designing the welding joint in USW of CFRT is considered to be one of the essential steps, Wang *et al.* [273] explored the microstructure and the fracture characterizations after performing the tensile test for welded CF/PA66. Besides, the obtained results reveal that the structure surface behaves as an ED, which in consequence significantly decreases the dispersion and arbitrariness of the weld dispersal, which emphasizes the weld quality and guarantees more efficient weldment compared with those of unstructured surface.

Furthermore, the LSS has been obtained by two approaches, LSS1 (maximum load over the entire overlap area) and LSS2 (maximum load over the actual welded area), which were measured for cross-ply laminate, and the outcomes show that even when the energy increased over 450 J without using ED, the welding quality was unaffected. Meanwhile, this increase only impacts the welding efficiency. Figure 36 presents the results of welded areas with and without ED under various welding energies [6]. In addition, by measuring the relation between the UFL in the LSS test and the welded area, it is noticeable that in SSW and DSW, increasing the welded area causes a remarkable increase in the UFL and *vice versa* [170].

According to the literature, the fracture surface can be used to forecast the welding quality following the LSS of joined CF/PA6, the partially melted joint bead of the over-welding was examined, whereas the melted material has been ejected [255]. Because the polymer–polymer interface curing of CFRTP for the under weld was the predominant finding in the microstructure analysis, the interfacial matrix fracture has been observed individually, as shown in Figure 37(a). More fibers shift into the weld region as they are welded, which results in more pullout fibers, as presented in Figure 37(b). However, excessive welding caused part of the polymer chains to break into gases, leaving the weldment with significant porosity, as shown in Figure 37(c). Figure 38 shows the supreme shear load with diverse preheating temperatures and welding conditions, and the outcomes without preheating are involved as a baseline. The extreme shear load initially rises with rising welding energy when the preheating state is assumed to be constant.

Nevertheless, at a critical point, it reduces (1,000 J in this case), as presented in Figure 38 [255]. The welded joints go through stages which are under-welded, good-welded, and over-welded by rising the welding energy [274]. However, by studying the influence of welding energy on the microstructure of CF/PA6 with 40 wt%, joined by USW, the microstructure investigation of the welded part shows a close relationship between the mobility of the fiber and matrix inter-diffusion. Furthermore, under welding occurred at low energies (Figure 39) at 200 J. The weld zone is dominated by melted polymer, with hardly any visible fibers. According to Figure 39 at 400 J, when energy rises, the weld region expands, and as polymer chains pass across the welded region, more random fibers are

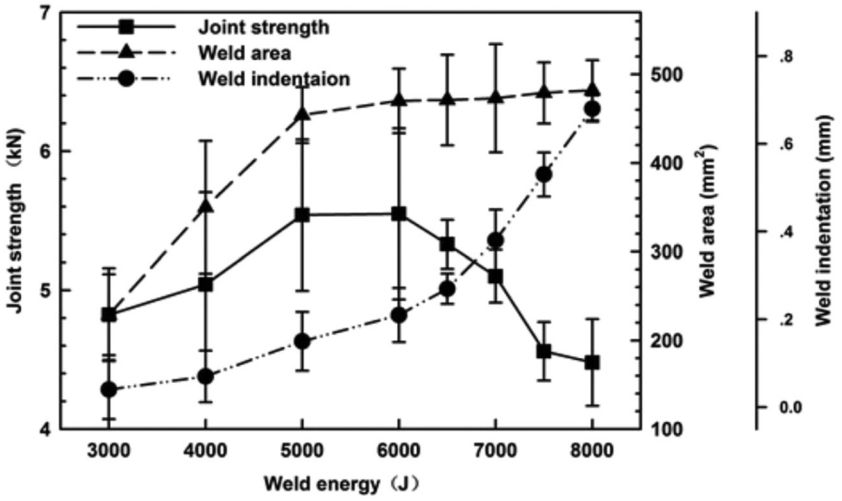

Figure 35: The impact of welding energy on the joint strength, weld indentation, and welded area of the CF/PA66 [271].

observed. Referring to Figure 39 at 600 J, when the joint is over melted with excessive energy, some pores were created that encroach the area amongst the polymer and the fibers, changing the distribution and arrangement of the fibers from the original material [274].

tWeld area and performance features like LSS are two factors that can be utilized to quantify weld quality. Figure 40 depicts the correlation between weld energy, welded area, and welding strength. Three weld quality zones can be established by defining the desired weld strength to three regions: an under weld (region I), a normal weld (region II), and an over weld (region III). Figure 40 demonstrates that when weld energy increases, the weld area asymptotically grows, and LSS has increased before decreasing. Any definition of a "normal-weld" region must include the location of the maximum shear strength. Nevertheless, it is necessary to decide where to position the boundaries of regions II and III [250].

The USW has been utilized to join the TC910 (CF/PA6) with and without implementing the ED by using the controlling mode. Besides, at each welding energy value the welded area and the indentation of the sonotrode were explored. As an outcome, as shown in Figure 41, the twill fiber loads were instantly decreased, followed by a rise to the values mentioned in Figure 41. The same trend can be observed in all different values of welding energy with/without FED. Because, the failure progressively spread from the borders of the joints, identical fracture surfaces were detected with/without FED [6]. By replacing the cross-ply fiber with twill fiber with the PA6-3KT1 (CF/PA6) shows that the maximum load is more significant when using FED. The obtained results of both fibers were similar for LSS and the fracture results were similar to the results that cross-ply fiber identical fracture surfaces obtained were detected whether with/without FED, as shown in Figures 41 and 42 [6].

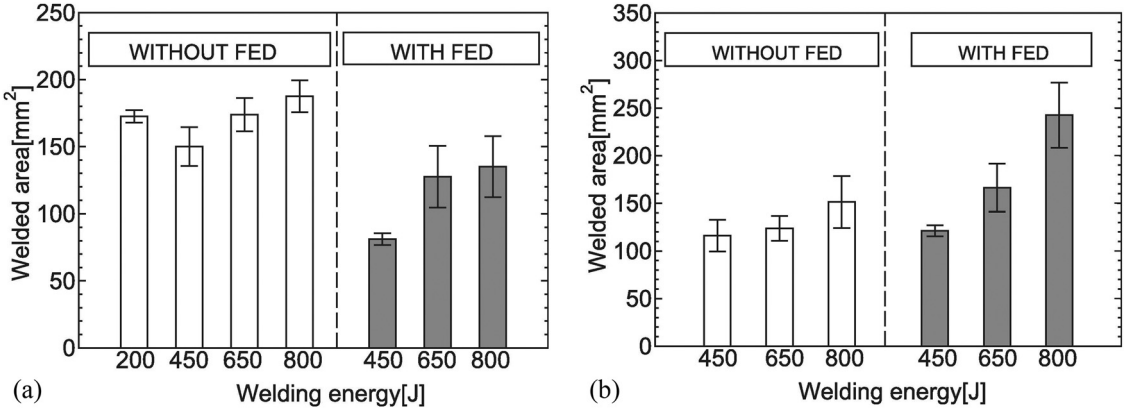

Figure 36: Welded area of (a) cross-ply laminate joints for LSS and (b) twill woven laminate joints for LSS [6].

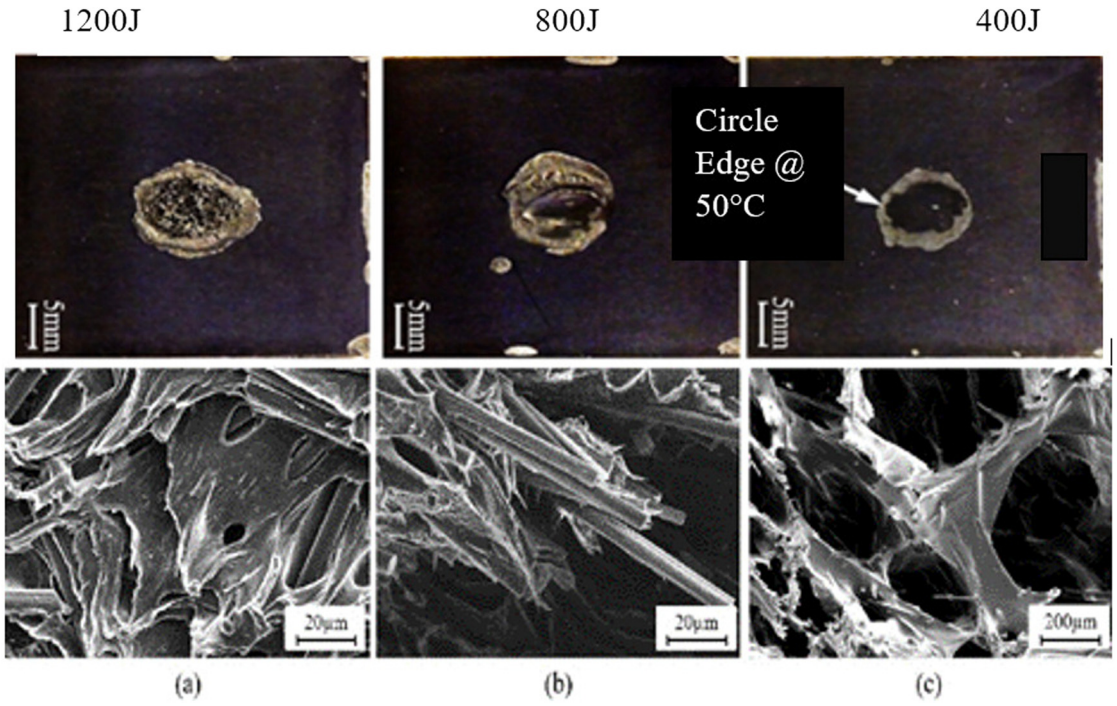

Figure 37: The evaluation of the welded area of CF/PA6 at preheating temperature of 50°C combined with the fracture surfaces at various welded stages; (a) under-welded stage (400 J), (b) good-welded stage (800 J), and (c) over-welded stage (1,200 J) after LSS [255].

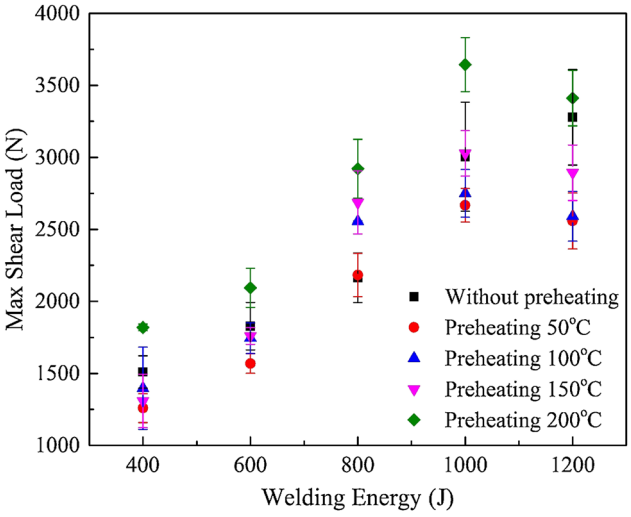

Figure 38: Experimental results of maximum shear load with various preheating temperatures and welding conditions, also the outcomes without preheating are included as a baseline [255].

A recent study found that the shear strength in the welded joint at very high welding energy decreased due to the generation of pores [274]. An FE model following the experimental exploration using ABAQUS was accomplished to apply uniaxial pulling forces to the welded coupons, where a connector comprises two reference points. The CF/PA6 joined by USW under seven various levels of welding energy for examining the assessment of welding attributes without ED and the polymer morphology in the cross-section shown in Figure 43(a). Also, the evaluated fracture surface of the weld area is presented in Figure 43(b). It proves that particular pores were presented in the bonding layer following critical welding energy at 1,000 J. Additionally, Figure 43(c) illustrates the expansion of the pores at 1,600 J of welding energy. It is observed that the pores begin to form within the bonding layer and in the coupon volume, further confirming that overheating during USW is the main reason for the pores to form and not the trapped gas. The bonding effectiveness of the joint decreased because the pores appear in the bonding layer [252]. More information about variations in USW parameters and their enhancements on mechanical properties, welding quality, and welding strength are presented in Tables 2 and 4.

3.2 Welding time

It has been defined that the structure of the welded specimens has a remarkable effect on welding time [269]. By examining the LSS and fracture failure of static welding by USW SSW to examine the similarity between SSW and continuous USW,

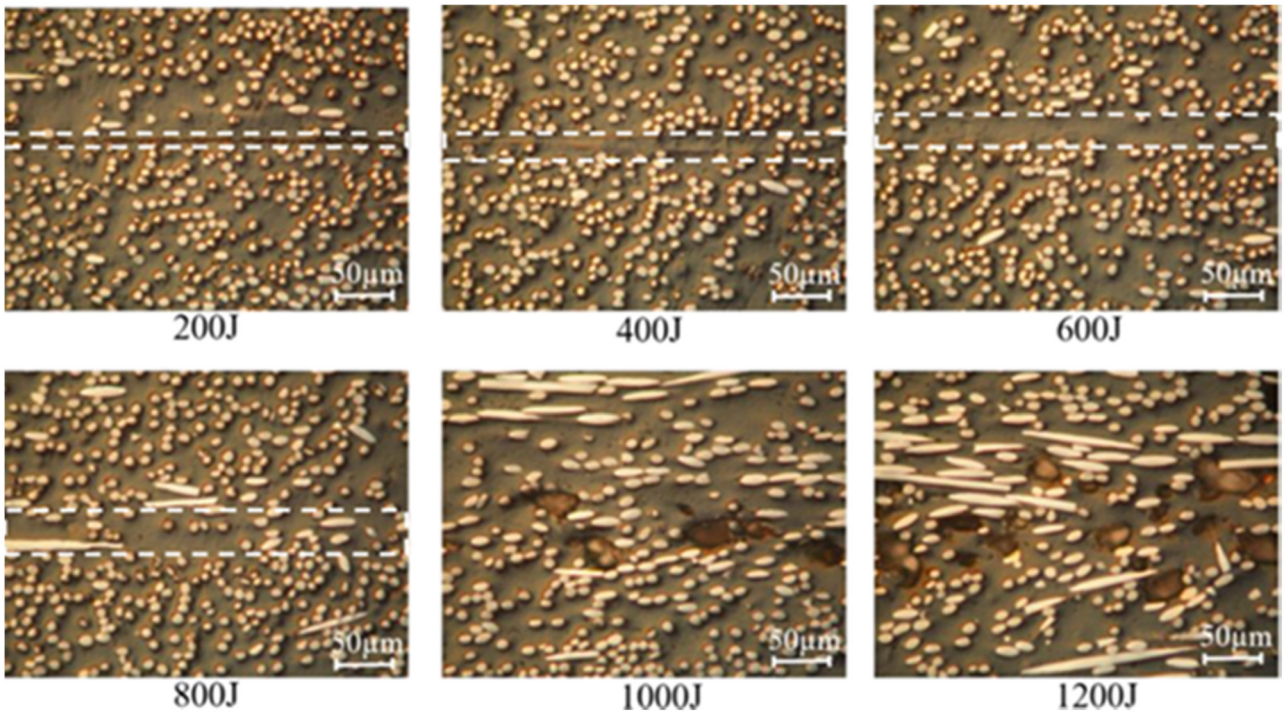

Figure 39: The microstructures cross sectional evolution through the welded area of CF/PA6 [274].

Figure 44 shows the results of LSS values consistent with the SSW process. For 80 µm and 500 N, the strength steadily increased to a high interval, *i.e.*, 36 MPa for a vibration time of 415–565 ms. By maintaining the vibrational amplitude at 80 µm and rising the welding force to 1,500 N, the same strength is obtained in less vibrational time of 260–435 ms [165].

Upon investigating the CF/PEEK and the enhancement of welding time on the welding strength of the joint with and without ED, the results show that gradually rising welding time will increase the welding strength until the welding time reaches its optimum value. However, the welding strength decreased after a further increase in

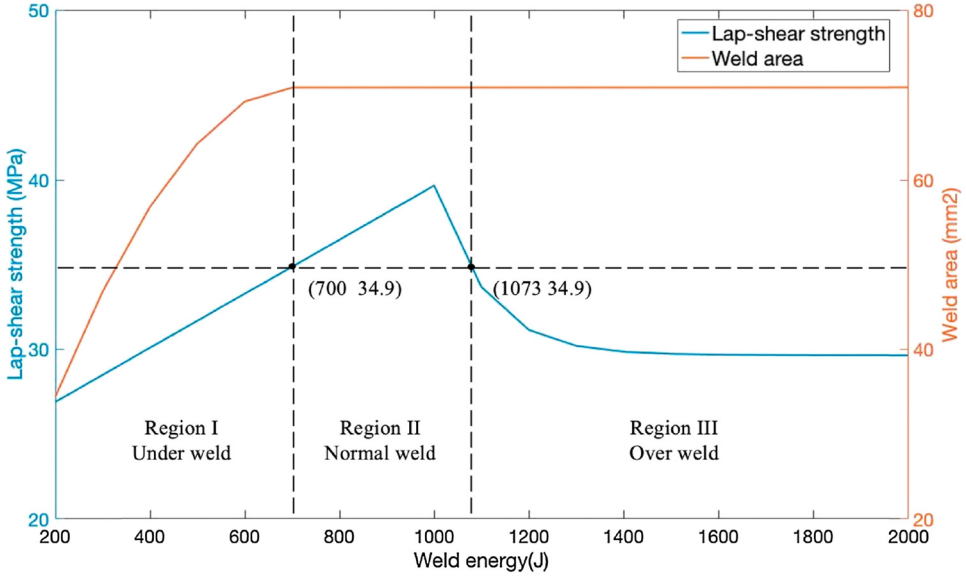

Figure 40: The LSS and weld area variation with weld energy determined by microstructure investigation [250].

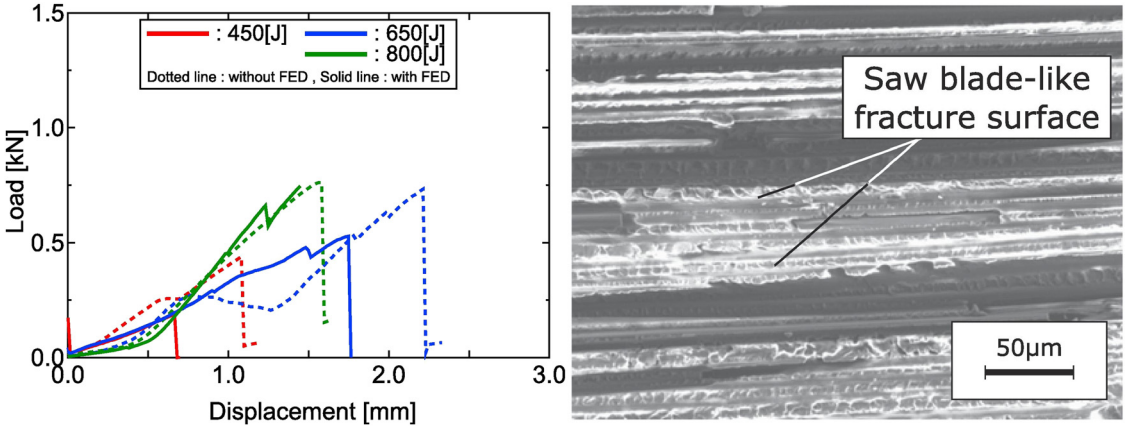

Figure 41: TC910 (CF/PA6) cross-ply fiber load *vs* displacement with/without FED and fracture surface with FED [6].

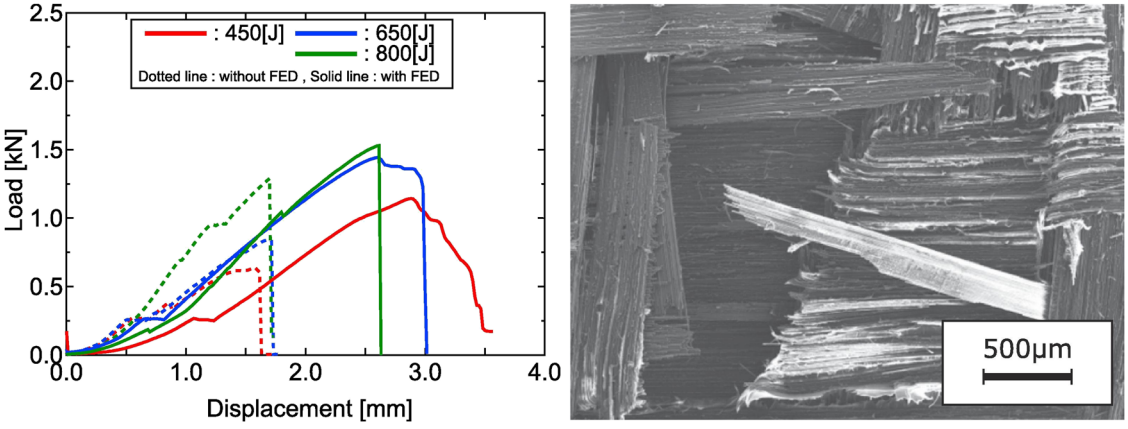

Figure 42: PA6-3KT1 (CF/PA6) twill fiber load *vs* displacement with/without FED and fracture surface with FED [6].

welding time, followed by voids and large cracks [256]. Above all, it has been shown that by studying the relation between welding time and the LSS with and without using the ED, the LSS drops to half of its value without using ED. Figures 45 and 46 demonstrate the joint morphology without ED vibration times of 0.7, 0.8, 0.9, 1.0, and 1.1 s, respectively. An incessant gap at the interface of the joints was noticed because the 0.7 s ultrasonic time was insufficient, and the heat generated in the interface was insufficient to melt the interface entirely, as illustrated in Figure 46(a). The gap length at the interface gradually reduced as the ultrasonic action time extended to 0.8–0.9 s, as illustrated in Figure 46(b) and (c).

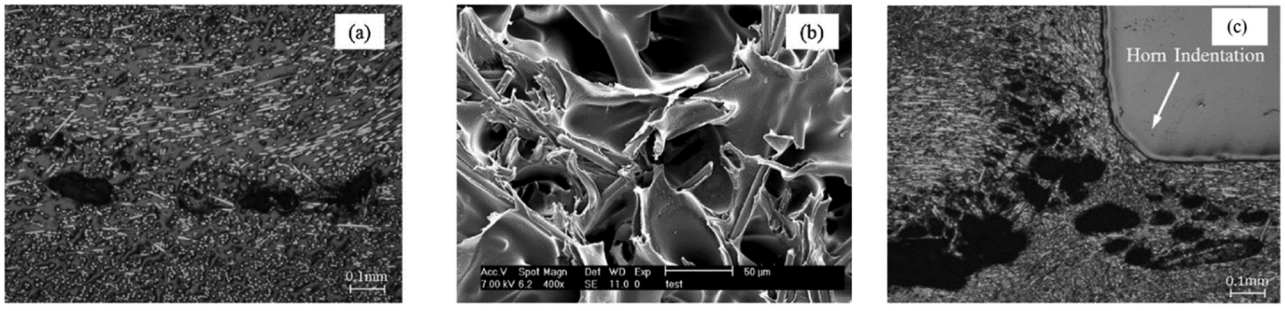

Figure 43: (a) The microstructure cross-sectional area of the weld zone of CF/PA6 at 1,000 J, (b) the resultant fracture surface, and (c) the dispersal of the pores in the welded coupon of CF/PA6 at welding energy of 1,600 J [252].

Table 3: Summary of factors that affect the USW

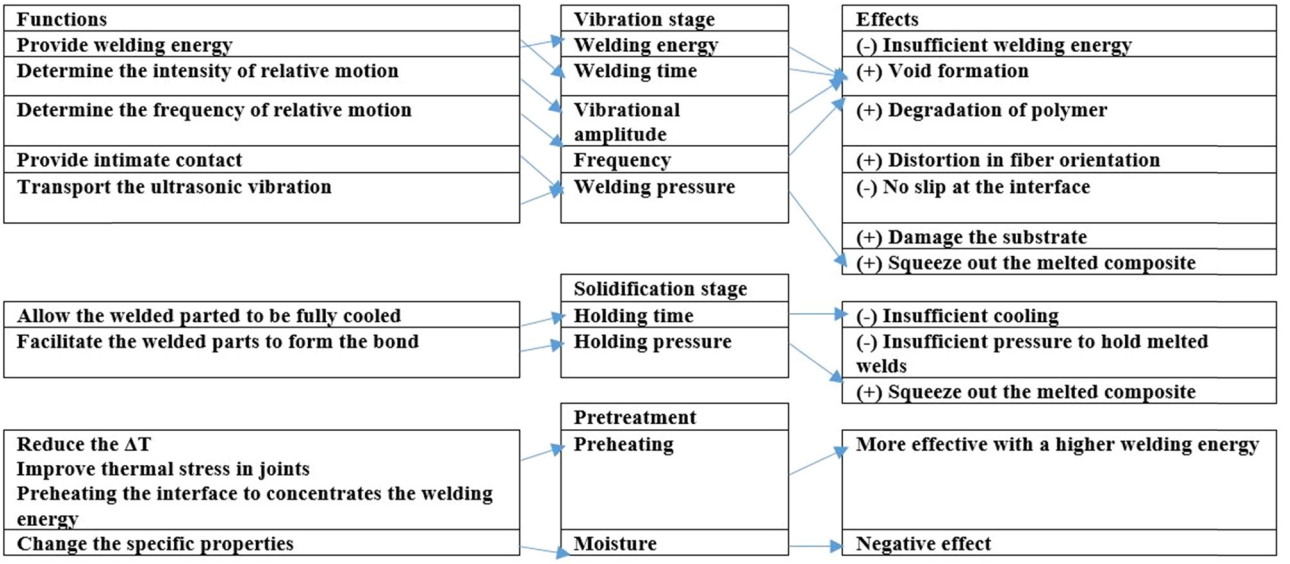

Note: The (+) sign means high value and (−) sign means low value.

Nevertheless, as demonstrated in Figure 46(d) and (e), the excessive ultrasonic duration can also result in cracks and voids at the joint's HAZ. The width size of the HAZ rose from 0.2 to 0.42 mm once the welding time extended from 1.0 to 1.1 s. However, an interface with strong bonding was achieved at 1.1 s ultrasonic action time. Additionally, throughout the HAZ, more substantial voids and cracks were scattered, also the largest porosity area only reached 0.003 mm^2.

The energy dissipation in the TPCs has been enhanced by longer welding time [272], where longer welding time cause to reduce the joints' void formation [275]. However, at an elevated temperature, a degradation in the TPCs and fiber distortion in its orientation may occur due to a very long welding time [276]. Meanwhile, longer holding time is reported to enhance the welded joints' strength by allowing the part to cool down fully [276]. Welding the polyoxymethylene (POM) to PMMA through a coupling layer of PLA in a very short time generated weak friction heat for various welding pressures. Besides, all welded strengths were low at a welding pressure of 0.1 MPa. The highest welding strength was 38 MPa and measured at a welding time of 4 s and a welding pressure of 0.2 MPa. The ideal welding strength at 0.3 MP and 4 s of welding duration was 47 MPa. However, the strengths were first improved and then reduced similarly at 2, 3, and 4 s, as shown in Figure 47(a) [277]. Additionally, after welding PMMA to POM by USW by using the PLA layer, the tensile test was accomplished, and as an outcome, shown in Figure 47(b), the minimal stresses and strains of POM, PMMA, and interposed sheet (IPS), with POM and PMMA recording yield strengths of 61 MPa and 65 MPa, respectively. POM showed ductile performance with an 85% minimal strain, while PMMA displayed brittle features with a 10% nominal strain. Only 43 MPa and 5% were the nominal strength and strain of the IPS, respectively. The rupture surface image of the IPS is shown in Figure 47(c), where it is possible to realize the contact between the transparent PLA and opaque POM. In other words, the sime-crystallinity might be more interesting as compared to the color. However, due to their transparency, the interface of PLA and PMMA was difficult to observe from the photos. There is no evidence of phase separation, which would indicate that PMMA and PLA were also compatible with POM. All of the materials were suitable for welding, and the IPS made of the three polymers successfully joined POM and PMMA [277].

The relation between vibration time and LSS of joined CF/PPS similar welded by USW with triangular ED has been tested. The results indicate that the LSS as a function of the vibrational period increased until the optimum value of vibrational time, as shown in Figure 48. Also, at an approximation vibrational time equal to 217 ms the LSS reached around 30 MPa, and by increasing the vibration time to 520 ± 58 ms, the LSS increased as well to 37.1 ± 1.3 MPa. It is worth mentioning that the required vibration time to reach the extreme strength by using triangular ED is lower than the required vibrational time when using FED [278]. The numbers in the graph designate the stage in the welding process in which the specimens for mechanical investigation were achieved.

Table 4: Classification of CFRP joined by USW based on type of USW machine with using ED or an interlayer

USW Type	CFRTP	Interlayer material	Parameters						Shape of sonotrode and number of spots	Summary	Ref.
			Power (W)	Welding time (s)	Frequency (kHz)	Overlap area (mm^2)	Amplitude (μm)	Force and pressure			
20 kHz Rinco Dynamic 3000 ultrasonic welder	CF/PEI	PEI	3,000	NA	20	12.7 × 25.4	51.8–86.2	300,500 and 1,500 N	Cylindrical SSW	A neat of PEI film has been used as an ED between two composite layers. After USW, a metaphysical model was developed by the FE to study the phenomena during heating phase and the machine accuracy and welding quality	[321]
	Output	– The numerical solution approved that the apparatus efficiency = 13% – Numerical solution confirmed the predicted degree of adhesion – NS. Confirmed that the first heating phase due to the interfacial friction – At high temperature, the dissipation of bulk viscoelastic in the interface is predominant – At the transition temperature of glass, a dramatic increase in dissipated power was noticed at the interface									
Electrical motion 20 Ultrasonic welder Rinco ultrasonic	CF/PEEK	PEI	NA	1	20	NA	32	3,000 N	Cylindrical SSW	The PEI as an ED has been used to avoid PEEK matrix melting	[336]
	Output	– Optimum Condition 1 at 500 N, 1 s, 32 μm – Optimum Condition 2 at 1,000 N, 0.6 s, 32 μm – The temperature profile in both cases are dissimilar but the fracture surface in both is the same – Low LSS was observed by PEI-based fracture, where higher mechanical strength has been observed by the PEEK-based fracture – The diffusion of PEI and PEEK during welding specimen caused a gradient of attentiveness at the interface – Maximum LSS = 47 MPa – LSS increased with time								The physical changes were evaluated followed by investigation of parameters effects on single LSS and fracture surface Operating high-quality welding by controlling process parameters and the mechanical strength with the temperature generated during welding By using similar parameters in USW, the mechanical strength and interfacial fracture will also be similar	
KZH-2026 multifunction USW machine	CF/PA6	Henkel 5089 Ep-Ethyl-4-methylimidazole	2,600	2	20	12.5	25	312, 623, 935 N	Cylindrical SSW	A repairing test was done by ultrasonic pulse using adhesive-bonded in lap-shear CF/	[70]

(Continued)

Table 4: *Continued*

USW Type	CFRTP	Interlayer material	Parameters						Shape of sonotrode and number of spots	Summary	Ref.
			Power (W)	Welding time (s)	Frequency (kHz)	Overlap area (mm^2)	Amplitude (μm)	Force and pressure			
		(2,4-EMI) and Hydroxyethyl								PA6 with 30 wt%, the process was done under different set of parameters (force, oscillation time). The transient temperature was measured and the impact of the repaired process on the strength of joint was investigated	
	Output	– The optimal force is 623 N and oscillation time is 1.2 s – The joint strength rises with the increase in the adhesive coverage displacement in all percentages of adhesive coverage until a critical value and then it starts to decrease – By studying the relationship between increasing oscillation time and joint strength, a variation was found in the three different caseloads under 50% adhesive coverage – The maximum value of joint strength recorded 11 MPa on applying 312 N									
20 kHz micro-processor controlled ultrasonic welder	CF/PEKK	Arkema PEKK 7002 polymer film	6,200	NA	20	12.7 × 25.4	86.3	1,000 N 3.1 MPa	Rectangular SSW	Study the enhancement of fiber orientation in the plies close to the weld line on the USW, taking into consideration heat generation, transformation, and the impact on edge defects	[337]
	Output	– There were no edge defects at 90° while the edge defects were noticed at 0° – Shorter heating time, uniformed heat distribution was noticed at 90° caused by the heating conductivity along fibers 5.94 $W·(mK)^{-1}$ – Maximum LSS at 0° = 37.4 MPa – Maximum LSS at 90° = 25.2 MPa – Samples with 90° plies failure occurs at 45° ply								The ED covered almost all intended welding area	
Rinco Dynamic 3000 microprocessor-controlled ultrasonic welder	CF/PEEK -HEXPLY 913 unidirectional CF/Ep	PEEK as ED (neat layer), PEEK coating on CF/Ep	1,500, 2,100	NA	NA	12.7 × 25.4	72–120	300, 1,500 N, 4.7 MPa	Rectangular SSW	Preventing degradation of CFRTP welded by USW at high temperature by using very short heating time, the fractographic and FTIR analyses have been used and the displacement-	[190]

(Continued)

Table 4: *Continued*

USW Type	CFRTP	Interlayer material	Parameters						Shape of sonotrode and number of spots	Summary	Ref.
			Power (W)	Welding time (s)	Frequency (kHz)	Overlap area (mm^2)	Amplitude (μm)	Force and pressure			
										controlled welding has been used	
	Output	– In optimum welding, heating time can be decreased by increasing amplitude and welding force – Average short heating time is 460 ms was achieved at 1,500 N, 4.7 MPa, 90 μm, 2,100 W, and 0.10 mm optimum displacement (short heating time condition) – Increase the average heating time to 830 ms at 300 N, 0.9 MPa, 72 μm, and 1,500 W (long heating time condition) – Both long/short heating time results in preventing thermal degradation with fast process								No. of samples in each welded joint type ≥5 The coating layer was used only in one type of welding It is necessary to keep the heating time low in second to avoid thermal degradation The thin coating layer of PEEK works as heat shield by using the ultra-fast USW	
Ultrasonic TWTP	PLA/POM IPS	PLA (as IPS)	NA	1–5	28	NA	30	0.1–0.4 MPa	TWTP	Welding of dissimilar material was achieved by IPS material, outstanding plasticity property was observed, and the welding time and pressure have high impact on welding strength. Owing to ultrasonic TWTP, low mechanical strength of the matrix and IPS restricted the welded strength	[279]
	Output	The yield strength (YS) of PLA = 58 MPa, POM = 61 MPa, and PLA/POM = 52 MPa – The strength of PLA/POM composite is 10% less than the strength of pure PLA matrix or pure POM matrix – PLA shows brittle behavior with 10% strain after YS – A ductile behavior for POM was observed with 85% strain after YS – PLA/POM composites show a nominal strain of 250%						Thermodynamic properties were studied			
Ultrasonic TWTP	PMMA/POM	PLA FGM as (IPS)	NA	1–4	28	NA	30	0.1–0.4 MPa	TWTP	The TWTP process was used to join the	[277]

(Continued)

Table 4: *Continued*

USW Type	CFRTP	Interlayer material	Parameters						Shape of sonotrode and number of spots	Summary	Ref.
			Power (W)	Welding time (s)	Frequency (kHz)	Overlap area (mm^2)	Amplitude (μm)	Force and pressure			
										immiscible TPCs without adhesive, and the third phase FGM of IPS was prepared. Microstructure, mechanical, and thermal properties were investigated	
	Output	– The YS of POM = 61 MPa, with strain = 85%; ductile behavior – The YS of PMMA = 65 MPa with strain = 10%; brittle behavior – The YS of PLA = 43 MPa with strain = 5% – The transparent property of PMMA and PLA makes the observation of interface difficult; while *vice versa* for POM and PLA – The maximum welded strength was recorded at a pressure value of 0.3 MPa at four different welding times and the maximum overall welding strength was approximately 50 MPa at 0.3 MPa and 4 s. From the DTA-TG test, there is a noticeable variation in between PMMA, POM PLA, and IPS values of the heat-flow/temperature curve – The peak surface temp. is 140°C (welded interfaces)								47 MPa was recorded as the peak of welding strength, which is only 80% of tensile strength of POM. The welded structures were divided into four parts	
HiQ DIALOG SpeedControl ultrasonic welder	CF/PEEK CF/Ep	PEI	NA	NA Solidification 4	NA	12.7 × 25.4	86	1,200 N	Rectangular SSW	Investigate the sensitivity of heating time at different heating time. ED was added to avoid heating. The microstructure observations were correlated to weld strength. Displacement control welding was used. 250 specimens were assessed and results were compared with the PEEK-PEEK configuration	[338]
	Output	– CF/PEEK to CF/PEEK welded is less sensitive to heating time than dissimilar composite welded joints									

(Continued)

Table 4: *Continued*

USW Type	CFRTP	Interlayer material	Parameters						Shape of sonotrode and number of spots	Summary	Ref.
			Power (W)	Welding time (s)	Frequency (kHz)	Overlap area (mm^2)	Amplitude (μm)	Force and pressure			
		– High peel stresses in Ep-PEEK may result by reducing the thickness of the weld line, and at the same time, it increases the LSS until a specific value, and then it starts to decrease – The maximum LSS for Ep-PEEK250 = 39.1 ± 1.3 MPa – Ep-PEEK250 threshold LSS 35.2 MPa – The maximum LSS for Ep-PEEK175 = 38.7 ± 2.5 MPa – Ep-PEEK175 threshold LSS is 35.2 MPa – By rising the displacement, the required heating time increases – Welding process sensitivity was not affected by decreasing the thickness of the coupling layer								An FE model was developed by using ABAQUS software	
Rinco Dynamic 3000 ultrasonic welder	CF/PEI-CF/Ep	Neat PEI film and PEI as ED&	0–3,000	4	NA	12.7 × 25.4	86.2	1,500 N	Cylindrical SSW	The potential of a coupling layer of PEI to promote heat generation was investigated, as findings overheating in CF/PEI adherend were observed in case of no loose ED or coupling layer	[261]
	Output	– Regarding the mentioned parameters the heating time was very short – A spherical TPCs particles were observed in the Ep resin with D = 1–10 μm – The glassy PEI partially dissolved by the diffusion of Ep monomers and *vice versa* until the gelation point of Ep resin – Limited miscibility cause phase separation – At 500 and 700 J, the welding strength is the same – A porosity at the welded line was observed at 600 J – The rich region with PEI is the welded line and it is between the fiber bundles of CF/Ep and CF/PEI adherents – Maximum LSS found in reference ED which is approximately 37.5 MPa – Minimum LSS found in ED-less-60 and is equal to 17.3 MPa – Full welded overlaps were observed in the reference ED samples – Great size of unwelded area and degradation cause low LSS								A high-strength weld was found in CF/Ep and CF/PEI welding As overall, this study investigates 4 different types of joints Hence the same amount of time and load were used for solidification. Both displacement and energy dissipated were used as a controller The CF/Ep with PEI layer-PEI ED-CF/PEI was	

(Continued)

Table 4: *Continued*

USW Type	CFRTP	Interlayer material	Parameters						Shape of sonotrode and number of spots	Summary	Ref.
			Power (W)	Welding time (s)	Frequency (kHz)	Overlap area (mm^2)	Amplitude (μm)	Force and pressure			
										set as a reference welded case	
USW machine with AWC-6 microprocessor controller	CF/Ep-CF/Elium	Elium (ELP ELF)	NA	3	20	25.4 × 25.4	48.75	5 bar	Square SSW	The feasibility of using USW to weld carbon/Elium to carbon/Ep by using two different joint configurations (ELF & ELP) as a coupling layer; results were equated with Elium samples as a baseline weld. Two different amounts of ELP were used to examine the effect of volume	[284]
	Output	– The LSS significantly increased by 95% by adding 0.31 $mg \cdot mm^{-3}$ of ELP – A partially cohesive failure mode was observed with using ELP – The failure in Ep laminate was adhesive without using the coupling layer – Maximum LSS for CF/Ep without coupling layer = 5.02 MPa – Maximum LSS with co-cured ELF to Ep = 3.12 MPa – LSS significantly improved by welding with the ELP and reached 9.83 MPa – By studying the load vs displacement the maximum load is above 4 N and achieved by using ELP 0.2 g per welded area								Using the ELP was found to enhance the LSS and welding quality while it is the opposite in case of using ELF where it resulted in poor bonding strength	
HiQ DIALOG Speed Control ultrasonic welder	CF/Ep-CF/PEEK	PEI	5,000	4	NA	25.4 × 12.7	60 and 86	400–1,200	Rectangular SSW	Investigate the sensitivity of USW for welding dissimilar composites and study how varying the process parameters enhance the welding strength and quality. The ED made of PEEK film was used to enhance the local heat generation	[282]

(Continued)

Table 4: *Continued*

USW Type	CFRTP	Interlayer material	Parameters						Shape of sonotrode and number of spots	Summary	Ref.
			Power (W)	Welding time (s)	Frequency (kHz)	Overlap area (mm^2)	Amplitude (μm)	Force and pressure			
	Output	– The heating time increased by reducing either the amplitude or welding force. – Decreasing load or amplitude leads to increase maximum temperature between coupling layer and CF/Ep adherend – Even at high strength, a thermal degradation was observed (local signs) in CF/Ep adherend – Maximum LSS = 40.2 ± 2 found at 800 N and 86 μm corresponds to heating time 471 ± 12–543 ± 17 ms – Around 0.24 mm resulted as unwelded areas which equal to (6% and 10% of the overlap in the 1200/70 and 1200/60 configurations, respectively, similar to the 1200/86 configuration) – A limited failure in CF/Ep adherend presented by reducing the amplitude – The infamous effect of thermal expansion of welding stack at low welding force cause variations in the original constant displacement – A severe drop in LSS caused by decreasing force or amplitude – Decreasing the welding force has significant influence on LSS *vs* displacement curves								For each configuration, three welded specimens were used The design of experiment was applied by using ANOVA	

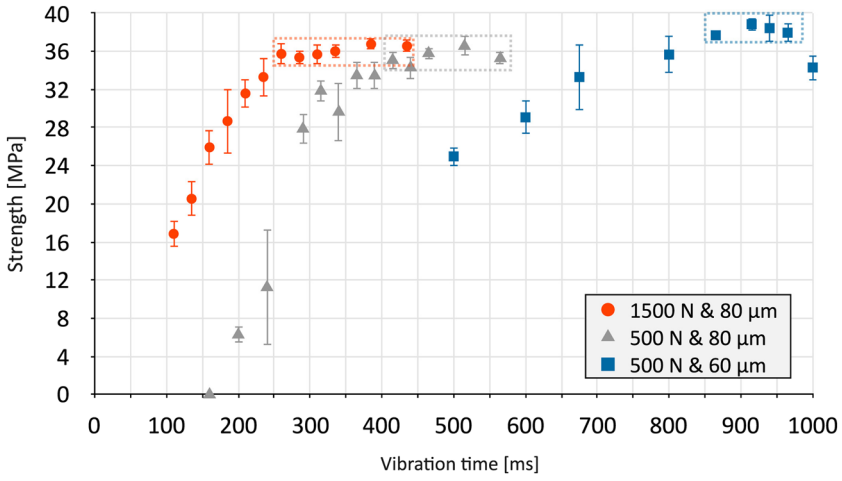

Figure 44: Average LSS OF SSW at different welding/vibration times at various welding forces and welding amplitudes. The bars denote plus and minus [165].

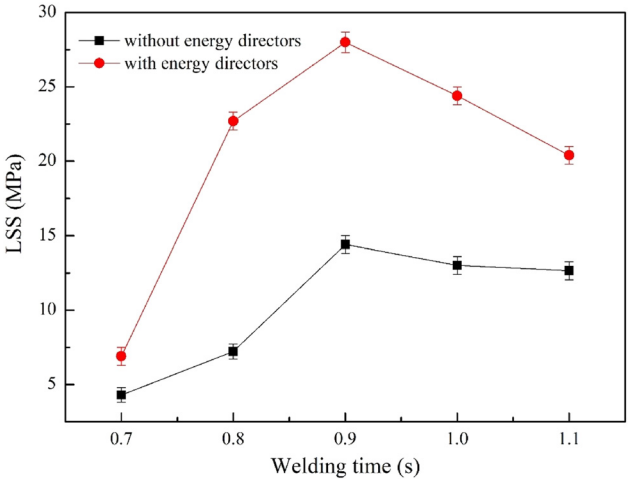

Figure 45: LSS of samples with and without ED [256].

Considering the welded interface of POM to PLA joined by USW as a microstructure observation through the polarizing microscope at 4 s welding time and 0.2 MPa welding pressure, as presented in Figure 49 [279]. There are differences in the crystalline forms of PLA and POM; the crystalline form of PLA is smaller than that of POM. However, the POM crystalline is identical to the IPS crystalline. Additionally, the two sides of the interfaces melt and produce molecular inter-diffusion due to IPS ultrasonic vibrations. According to Figure 49(a), the pressure employed during welding causes the melted polymers to force out of the interfaces. As a result, if the welding pressure was significantly high, some of the melted IPS polymers were forced out of the interfaces, breaking the IPS and stopping the friction among the two weld matrixes. The IPS thickness was altered to be between 40 and 50 µm, as shown in Figure 49(b). The IPS was separated into two shapes, particularly along the interfacial direction, as shown in Figure 49(c) and (d). The crystalline forms of PLA are more substantial for the weld line on the PLA side referred to as the mixed layer of PLA and IPS. This inter-diffusion layer surrounds the weld for PLA and IPS molecules. The crystalline morphologies were comparable, and the interface is fuzzy for the POM and IPS weld lines, as shown in Figure 49(d). In contrast to the other blend layer, the POM and IPS blend cannot be easily noticed by the polarized microscopy [279]. Furthermore, the relation between joint strength and welding time for the similar joined CF/PA66 without ED with 30 wt% CF has been examined, and the microstructure characterization was defined [127]. It has been observed that the pores found in the areas between the fusion zone, the HAZ, and the severe weld indentation on the surface of the upper workpieces reduced the loading capacity of the USW joints and led to the early fracture of the welded carbon/nylon 66 composite. The balance between the beneficial impacts of the weld area and the detrimental effects of the weld indentation and porosity at the fusion zone determined the strengths of the ultrasonic welds. Figure 50 presents the impact of the sonotrode pressure and the welding time on joint strength. Meanwhile, Figure 51 shows the microstructure observation [234]. Zhi *et al.* [243] studied the impact of welding time on peak load and welded area; both values show a linear increase until welding time reaches 2 s. After that, both values remained constant. This outcome is accurate in case that circular conventional USW and hollow fixture USW (HFUSW) were utilized. Additionally, if the square conventional USW and HFUSW were used instead, the peak load and welding area would increase to the optimum welding

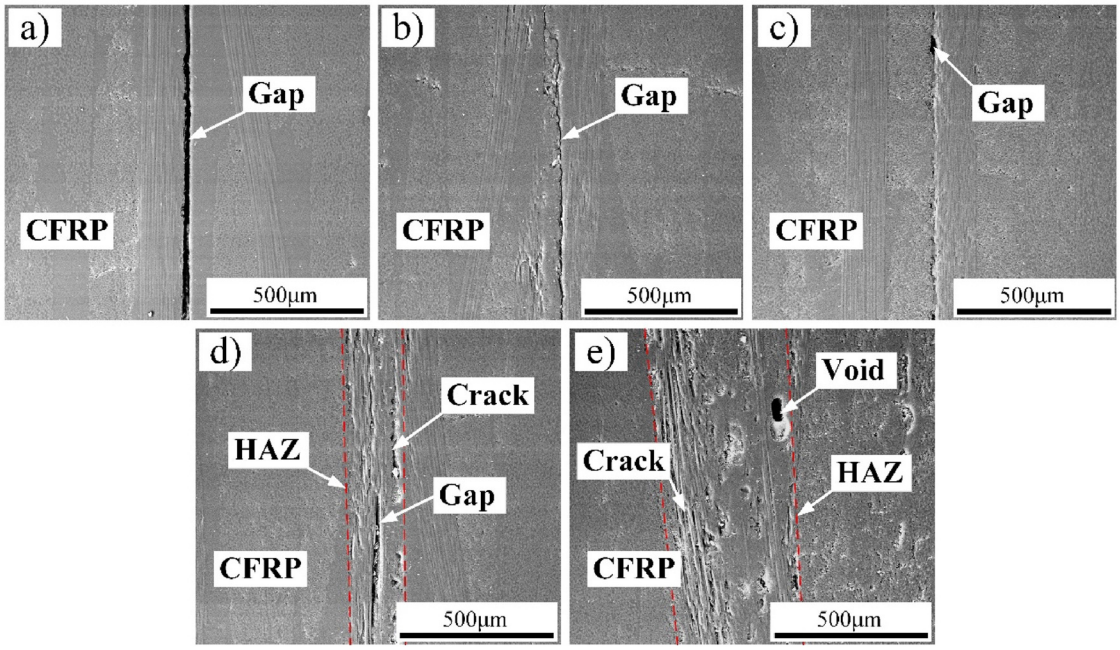

Figure 46: Morphology of the welded CF/PEEK without implementing ED at various vibrational time: (a) 0.7 s, (b) 0.8 s, (c) 0.9 s, (d) 1.0 s, and (e) 1.1 s [256].

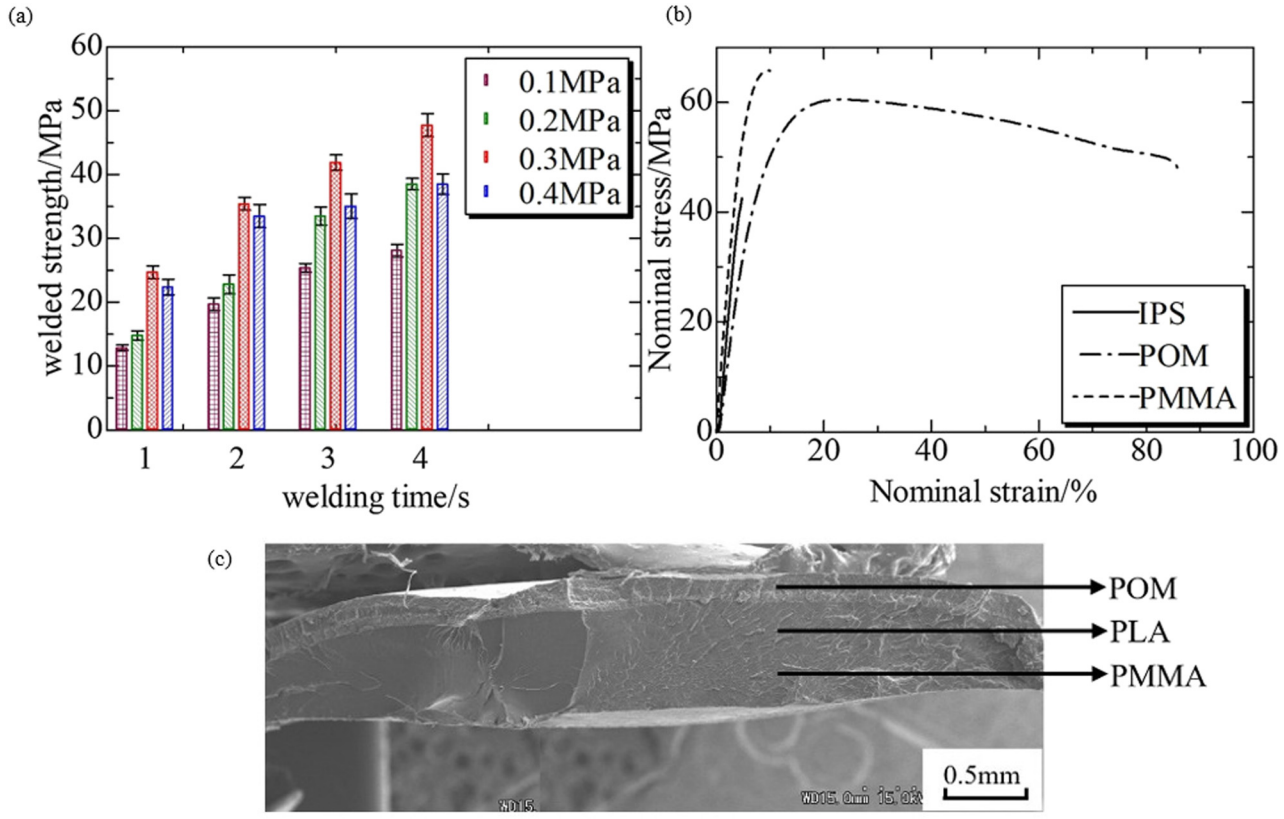

Figure 47: (a) The welding strength at different welding pressures and various welding times; (b) nominal stress *vs* nominal strain for PMMA, POM, and IPS; and (c) the SEM images of the IPS fracture surface after the tensile test [277].

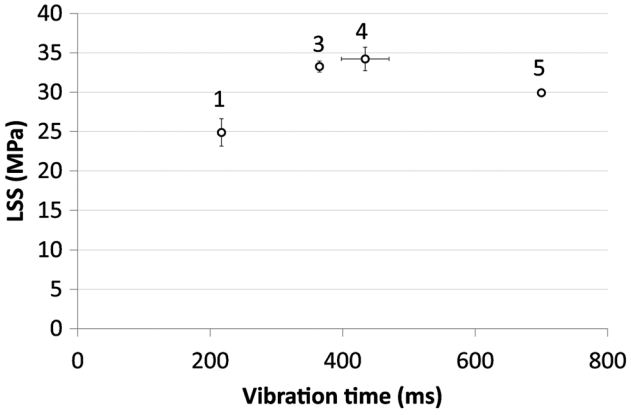

Figure 48: The LSS as a function of vibrational time [278].

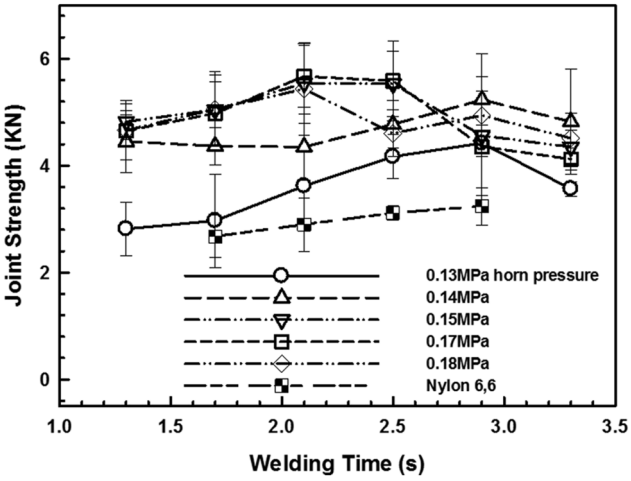

Figure 50: The observation effect of sonotrode pressure and welding time on the strength of the CF/PA66 without ED [234].

time, which is almost 1.75 s, followed by a decrease in both values. Furthermore, Alexenko *et al.* [280] joined PEI/CF by USW without using ED at various welding time. The obtained results show that by rising the welding time from 0.4 to 0.8 s, has no significant changes in LSS were it reached 42 and 48 MPa, respectively, although the microstructure of the fusion zone has been noticed to fundamentally change. Besides, the experimental test was followed with numerical simulation, which shows that the thickness of prepreg and the ratio of PEI/CF did not cause a significant impact on the tensile strength stress–strain diagram.

However, Calabrese *et al.* [281] performed LSS to explore the welding strength of CF/Ep joints by USW through optimizing process parameters, especially welding time and sonotrode pressure. Meanwhile, the welding process was accomplished by including electrospun veils which consist of either nylon or polyether into the outer layers of the laminated composite. A remarkable impact of the TPCs interlayer was achieved, although by implementing the

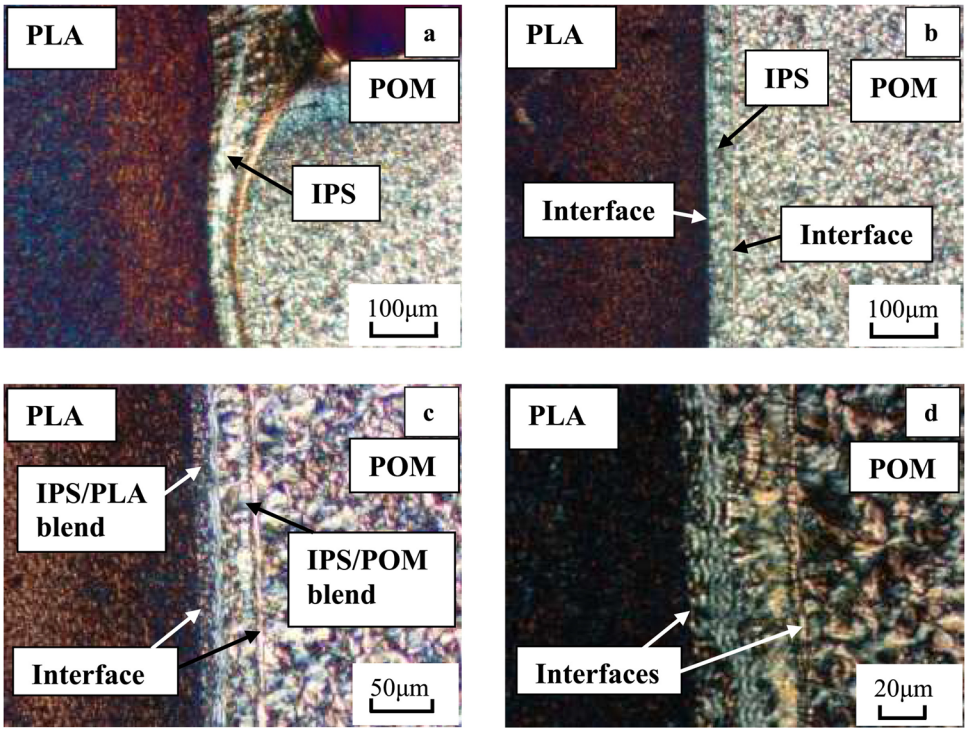

Figure 49: Polarizing microscopy images of the welded interfaces of POM/PLA joints [279].

nylon, greater mechanical strength was obtained. Additionally, this type of joints has promising application in sports automotive, in which the reliable and rapid welding part is fundamental. More information about variations in USW parameters and their enhancements on mechanical properties, welding quality, and welding strength are presented in Tables 2 and 4.

3.3 Welding force and pressure

In a displacement-controlled USW of complete overlaps, a plateau in displacement has been obtained due to employing a constant welding force, where it occurred just before the optimum stage [64,65,238]. In contrast, some studies hold the welding force constant [72].

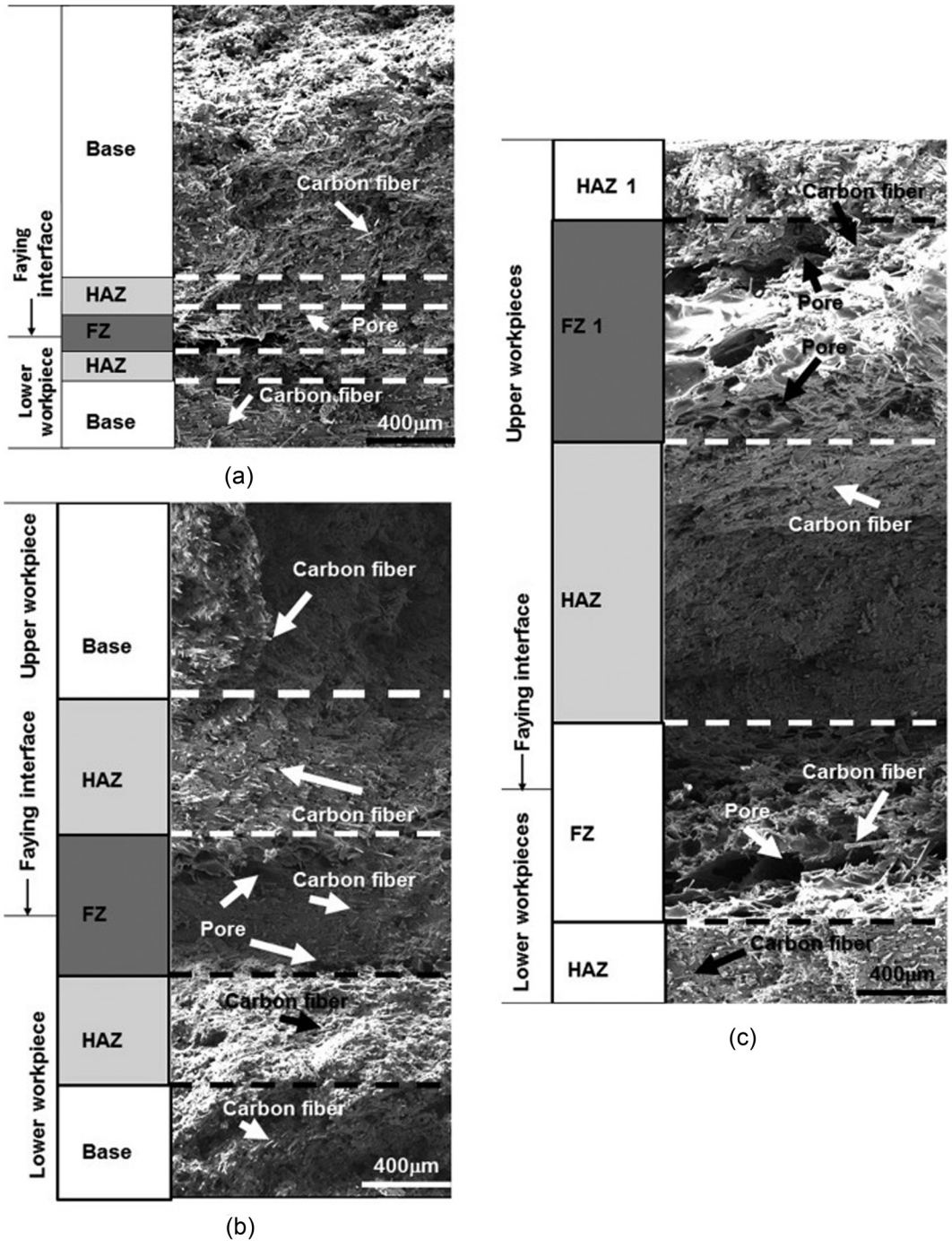

Figure 51: The observation of the effect of welding time (a) 1.7 s, (b) 2.1 s, and (c) 2.5 s on the microstructure of the CF/PA66 without ED [234].

However, it has been proven that varying the welding force and vibrational amplitude affects the vibrational time and dissipated power significantly [65]. Furthermore, increasing welding force or vibrational amplitude leads to greater dissipated power combined with more significant and quicker heating rates at the welding interface consequently, the vibrational time decreases for a travel value [64]. Overall, the combination of high vibrational amplitude and force limits the supreme size of the welded area due to increased power in a short welding time [65]. A further investigation studied the relationship between different travel, welding force, and amplitude and their impact on the LSS presented in Figure 52 [64].

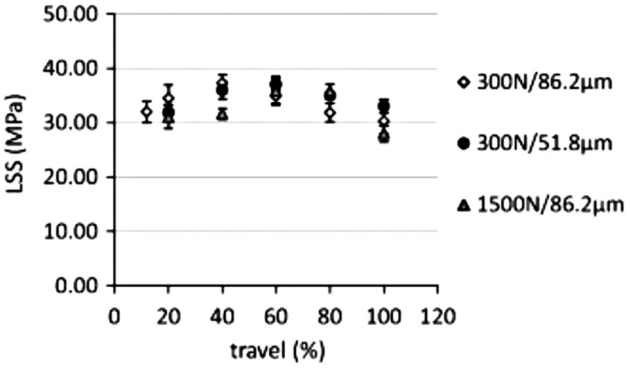

Figure 52: Average LSS *vs* travel for the different sets of amplitude and force [64].

The USW technique has been used to create a dissimilar joint of CF/PEEK-CF/Ep by implementing a coupling layer of PEI. The relation between welding force and vibration into the other welding process parameters and welding quality was examined. The obtained outcomes reveal that reducing the vibrational amplitude or the welding force will rise the essential heating time which is required to achieve the optimal welding strength, since the heat generation rates reduced. Besides, the reduction in amplitude or welding force increases the exposed temperature of CF/Ep in the welding process. Nevertheless, during the welding circumstances which produced the highest welding strength, local symptoms of thermal degradation were discovered in the CF/Ep adherend. Nevertheless, these changes were not substantial enough to be shown as impacting the welded joints' maximum LSS. Figure 53 demonstrates the impact of sonotrode displacement on the LSS for arrangements welded at various welding force. As indicated in Figure 53, reducing welding forces caused the process to move toward minor displacement values. This change had a substantial impact on the 400/86 setup. Meanwhile, the reduction in LSS in the 1,200/86 configuration was less noticeable than the values recorded in 800/86 and 400/86 at the maximum points. Hence, the maximum points are 0.28 mm displacement for 800/86 and 0.18 mm for 400/86. Furthermore, Figure 54 presents the concerning variations in the welding force in 1,200/86 and 400/86 and the impact of reducing welding force on the generated temperature at the welding interface. The generated temperature improved at a similar step, and the 800/86 configuration temperature improved expressively [282]. Nonetheless, that study shows that both ED as well as the coupling layer expert a squeeze flow, as verified through the reduction in thickness and a slightly wavy edge among both the polymers as shown in Figure 55 which presents the cross-section micrographs. Since the heat generation rates were identical at all conditions, and the temperature curves were overlapping until almost 250 ms into the welding process Figure 54 [282].

Koutras *et al.* [245] examined the degree of crystallinity at the welding interface of USW CF/PPS joints by exploring the effect of welding amplitude and force. The results prove that the cooling rates at the center of the overlap of the joints dropped from 41 to 16.9°C·s^{-1} with moderately low welding force of 300 N and vibrational amplitude of 51.8 µm, contrary to great welding force of 1,000 N and vibrational amplitude of 86.2 µm. The decelerate heat generation below 300 N and 51.8 µm was attributed to the lower cooling rates. In addition, at lower welding force of 300 N and vibrational amplitude of 51.8 µm increased the crystallinity to moderate levels and the crystal perfection. However, great welding force of 1,000 N and vibrational amplitude of 86.2 µm primarily formed amorphous PPS and imperfect crystals. Besides, reduction in cooling rates and longer melting time with lower welding force and vibrational amplitude, which favored the circumstances for strain-induced crystallization to take place, were guaranteed. Moreover, the combined static (welding force) and dynamic (vibration amplitude) strains throughout the USW process led to the cyclic strain, ε_0. In addition, it can be assumed that only the dynamic strain will significantly affect heat generation because it is numerous orders of magnitude lower than the static strain [283].

By studying the factors that affect joint strength, Liu *et al.* [259] reported that the welding pressure is less crucial than other parameters on welding strength. However, Zhang *et al.* [272] testified that the significant welding pressure cause to have acceptable interfacial contact for joining which accordingly reduce the welding strength significantly. Another investigation reported that a drop in the overall strength was detected when increasing the welding pressure significantly, which destroys the TPC substrates and crowds out the molten matrix from the contact area, which becomes delicate [276]. Nevertheless, the

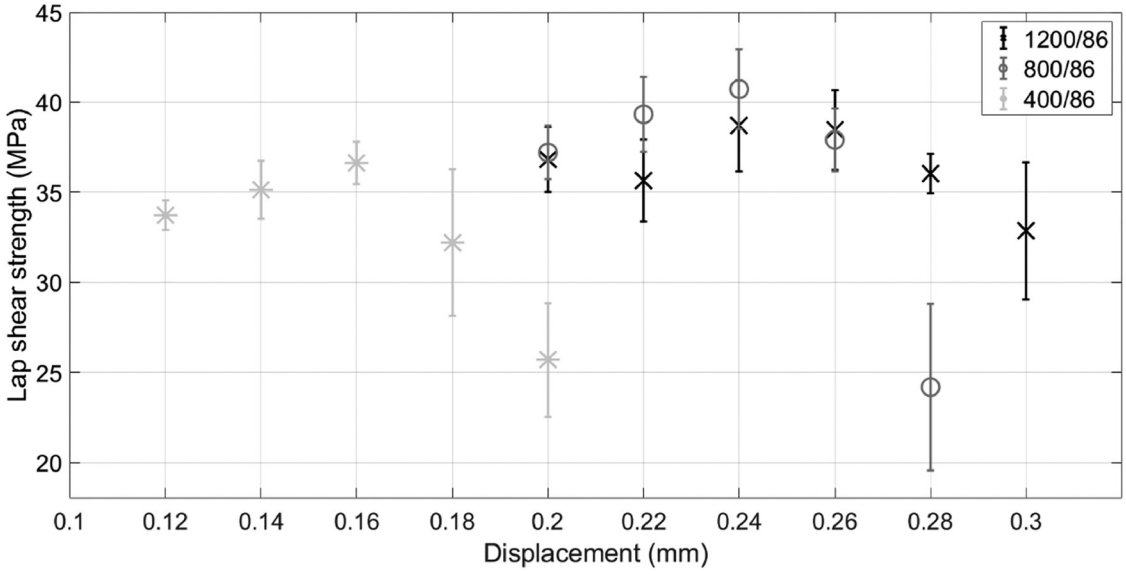

Figure 53: The impact of sonotrode displacement on the LSS evolution in the 1,200/86, 800/86, and 400/86 configurations [282].

holding time of pressure has no effect on the welding efficiency of high-stiffness material [12].

In addition to the parameters mentioned earlier, travel replaces vibrational time with the displacement of the sonotrode, which is considered one of the parameters of the vibrational phase. In travel, as a function in a range of 0%–100%, the thickness of ED will decrease, though the complete melt and maximum squeeze of ED occurred before reaching 100% travel. Figure 56 presents a comparison by SEM of welded CF/PEI between different percentages of travels: 20, 40, 60, and 80% [64]. At a travel of 20%, it is observed that there is a deep fiber imprint on the post-welded ED, and there were no patches of intact ED. Besides, at 40% of travel, broken fiber bundles were observed on the fracture surface. Furthermore, it is noticeable that there were resin flashes and kinking of the uppermost layers of the lower substrate at the edge of the overlap, combined with porosity at 60 and 80% travel. Likewise, at short travels, significant patches of intact ED and shallow fiber imprints on the post-welded ED were observed [64].

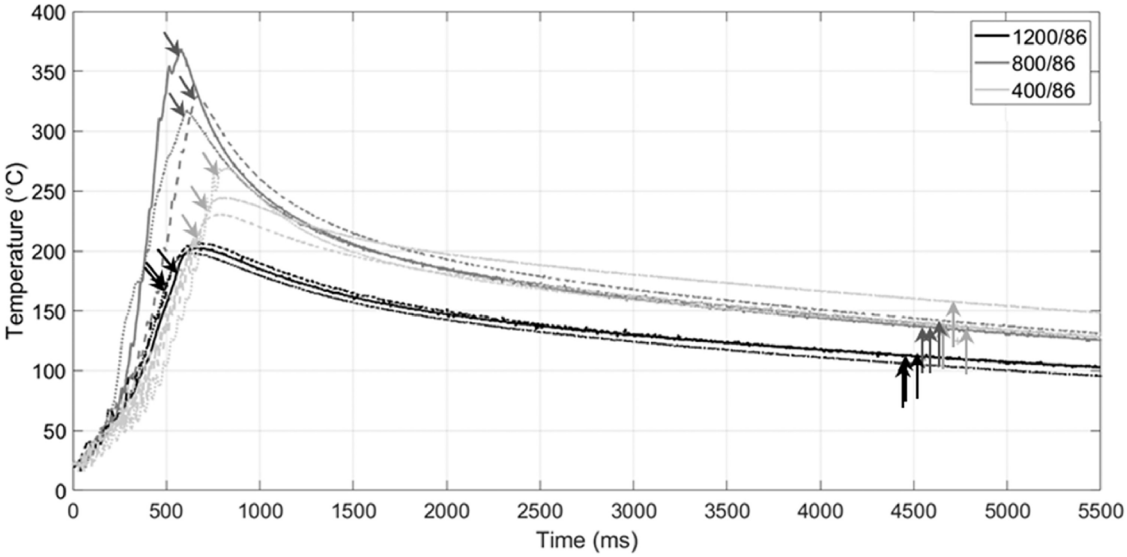

Figure 54: The enhancement of reducing force on temperature progress at the interface between the PEI coupling layer and CF/Ep adherend (0.28 mm displacement in the 1,200/86 and 800/86 cases, up to 0.18 mm in the 400/86 case). The diagonal arrows specify the end of the vibration. While, the vertical arrows specify the end of the USW welding process [282].

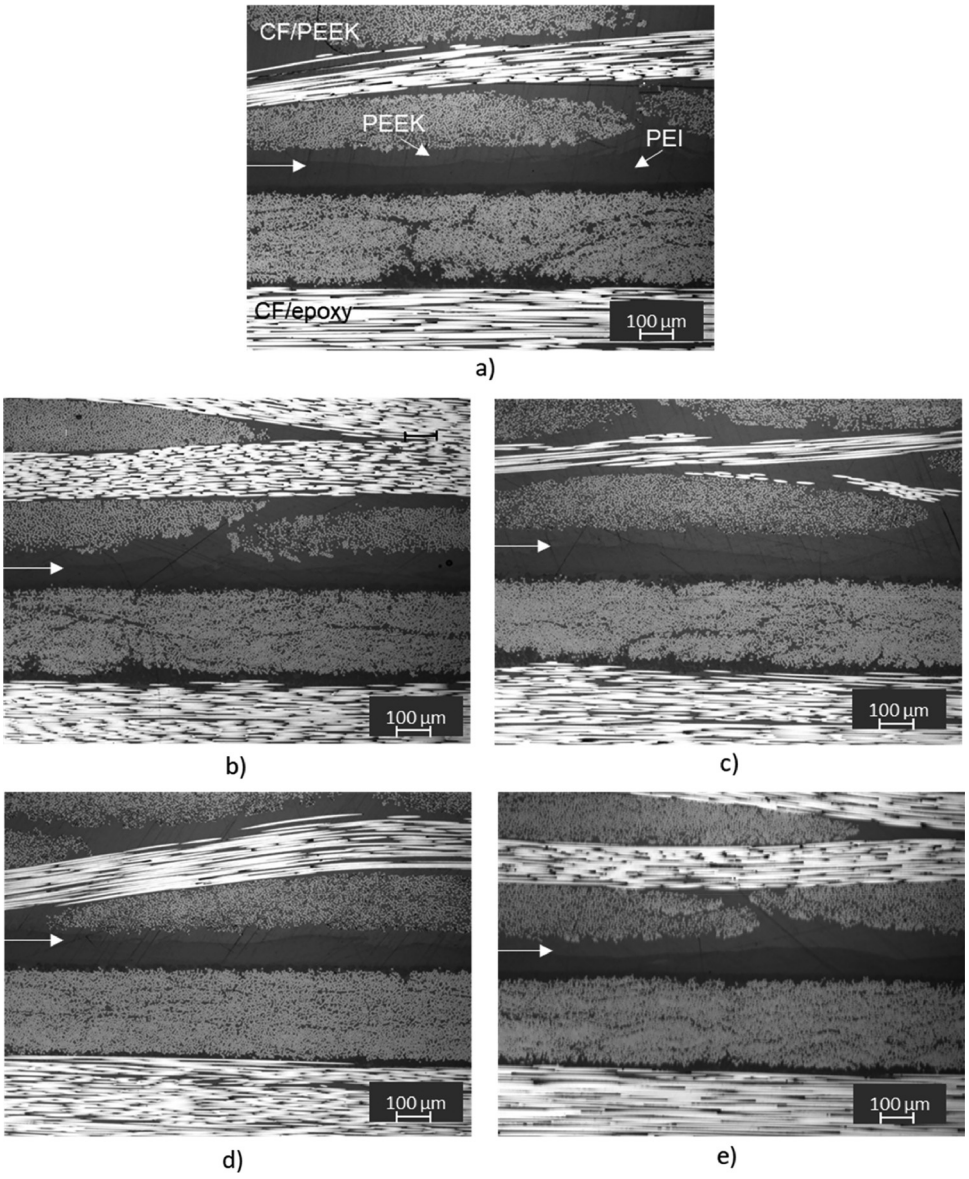

Figure 55: The cross-sectional micrographs of illustrative samples of CF/PEEK with PEI ED at diverse force/amplitude patterns and diverse displacement caused in supreme LSS. The displacements values are (a) at 0.24 mm, (b) at 0.24 mm, (c) at 0.16 mm, (d) at 0.24 mm, and (e) at 0.24 mm. The arrows specify the resin-rich weld line [282].

For the purpose of examining the fatigue behavior of the carbon/Elium®, a stress ratio (R) = 0.1 was adjusted at elevated temperature and 5 Hz, while considering the optimum value of LSS. Figure 57 presents the results of LSS and the S–N curve for several cycles of failure for both adhesive and the welded formation [63]. Figure 58 shows the microstructure after mechanical failure with the naked eye and SEM test formation [63].

Additionally, Figure 59 displays maximum LSS values and load–displacement curves for various welded setups of weldment CF/Elium®-CF/Ep; with the absence of a coupling layer, a carbon/Ep laminate shows a supreme LSS of 5.02 MPa at a welding condition of 3 s and 5 bars of weld pressure. The weaker link between the adherents, which led to the pure adhesive failure, is the reason for the reduction in the welding strength. Besides, Elium® composite welded to Ep composites with co-cured Elium® film (ELF) has revealed significantly lower LSS readings of 3.16 MPa. The failure modes justify the drastic reduction in bonding strength. The film was entirely de-bonded from the Elium® particle (ELP) rather than being cohesive or between adherents; the failure occurred between the ELF and the ELP adherend [284].

However, based on the observation from this review, the shortage in results obtained by investigating the impact

of welding force on welding strength and quality may be due to the reason stated in literature studies. More information about variations in USW parameters and their enhancements on mechanical properties, welding quality, and welding strength are presented in Tables 2 and 4.

3.4 Vibrational amplitude

The impact of vibrational amplitude and welding force on CF/PPS welded by USW has been studied. The results show that a reduction in the cooling rate was caused by setting the low vibrational amplitude and welding force, which leads to slowing down the heat generation. As a result, a substantial HAZ is generated [245]. Moreover, a considerably high welding strength may result by employing high vibrational amplitude, which produced further energy on the weldment, leading to increased strength [285]. Additionally, it has been revealed that the deformation of fibers at the fracture surface decreases with the reduction in the amount of vibrational plausible amplitude [64].

By investigating the fracture surface through SEM after the DLS of CF/PEEK joined with USW by using spot ED, a post visual examination of the welded specimens revealed that the fracture surfaces contained a circular welded junction on the overlap. As illustrated in Figure 60(a), there was no additional damage visible, and the remaining overlap was undamaged. Besides, the SEM investigation confirmed intralaminar failure in light of the excellent bond produced by the welding technique. Such failure mechanism is illustrated in Figure 60(b) and (c) by tearing the outermost laminate ply's fiber bundles and debonding the fiber matrix. Figure 60(d) shows a further magnification of (c) to provide a more explicit observation of the separation of the fibers from the TPC resin, which denotes the debonding of the fiber matrix [72].

The exploration of crystallinity on the interface of ultrasonically welded CF/PPS joints has been reported by examining the vibration amplitude and welding force effects on the level of crystallinity on the welding interface. The outcomes show that the USW process parameters significantly influenced the degree of PPS's crystallinity and crystal perfection. Besides, low welding force of 300 N and vibrational amplitude of 51.8 µm increased the crystallinity to an adequate level along with the crystal perfection. However, great welding force of 1,000 N and vibrational amplitude of 86.2 µm primarily formed amorphous PPS and defective crystals. In addition, from the DSC thermograms and the WAXD diffractogram, it was evident that a semi-crystalline structure was achieved in the PPS, even if the crystal perfection and crystallinity degree were not as

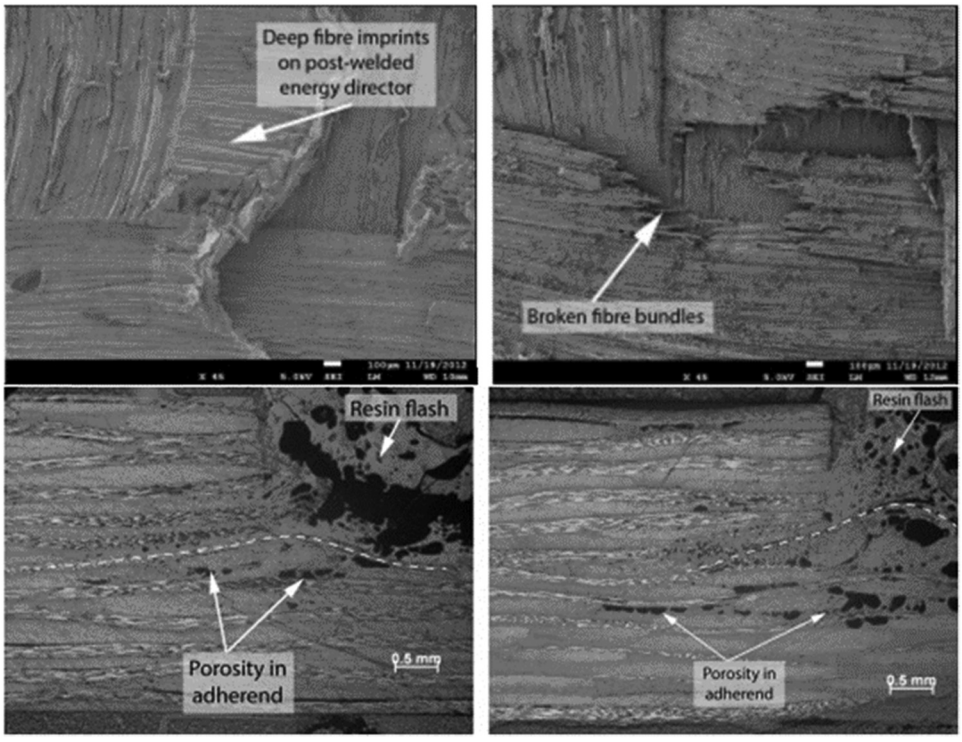

Figure 56: SEM detail of CF/PEI joint at 300 N; 86.2 µm; and 20, 40, 60, and 80% travel [64].

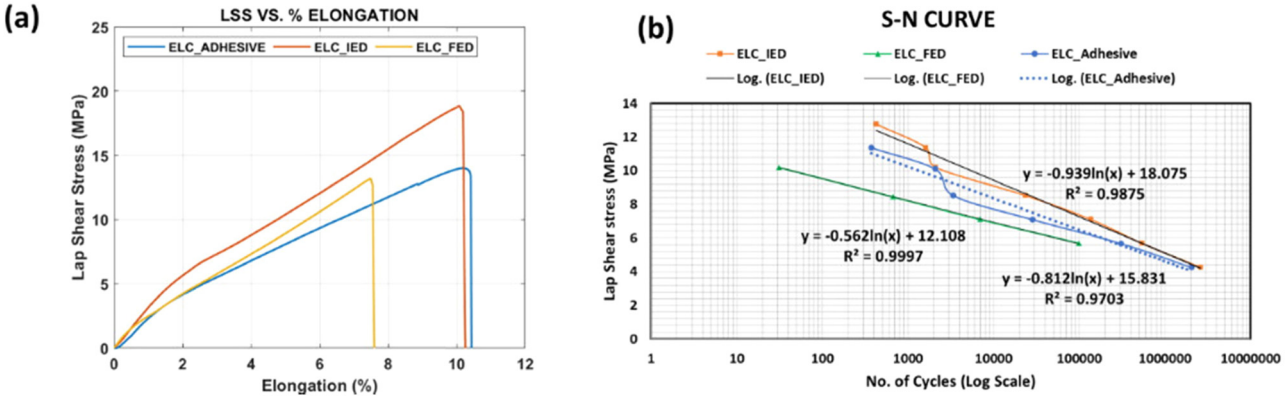

Figure 57: Adhesive and welded formation results: (a) LSS *vs* elongation and (b) fatigue test results [63].

great as in the original conditions of the PPS EDs (*i.e.*, before USW) Figure 61 shows the impact of USW process parameters on the crystallinity of the PPS ED [245].

The microstructure of CF/PA6 welded by USW without ED using a servo-driven welder has been examined. Besides, the SEM results before and after the welding process are presented in Figure 62. The cross-section of a weldment while being welded under standard conditions using a servo-driven welder is illustrated. Intimate contact between the two surfaces exists after the two workpieces proximity to joint, as shown in Figure 62(a). The fibers were still securely encircled by the matrix during that time because the components at the interface had not yet started to melt. The polymer chains spread over the interface as the temperature rises, and the surface becomes less smooth (shown in the yellow box). As the joint was created under the ultrasonic, as depicted in Figure 62(b), the visible interface among the workpieces vanished, and more fibers were exposed as the interface material melts [248]. In addition, this welding process was run at various conditions of process parameters; the relation between parameters and the weld characteristics using a servo-driven welder is presented in Figure 62(c). Furthermore, research focused on studying the welding quality of CF/Ep to CF/PEEK joined by USW with and without a coupling layer of joining PEEK, taking into consideration two welding parameters, which

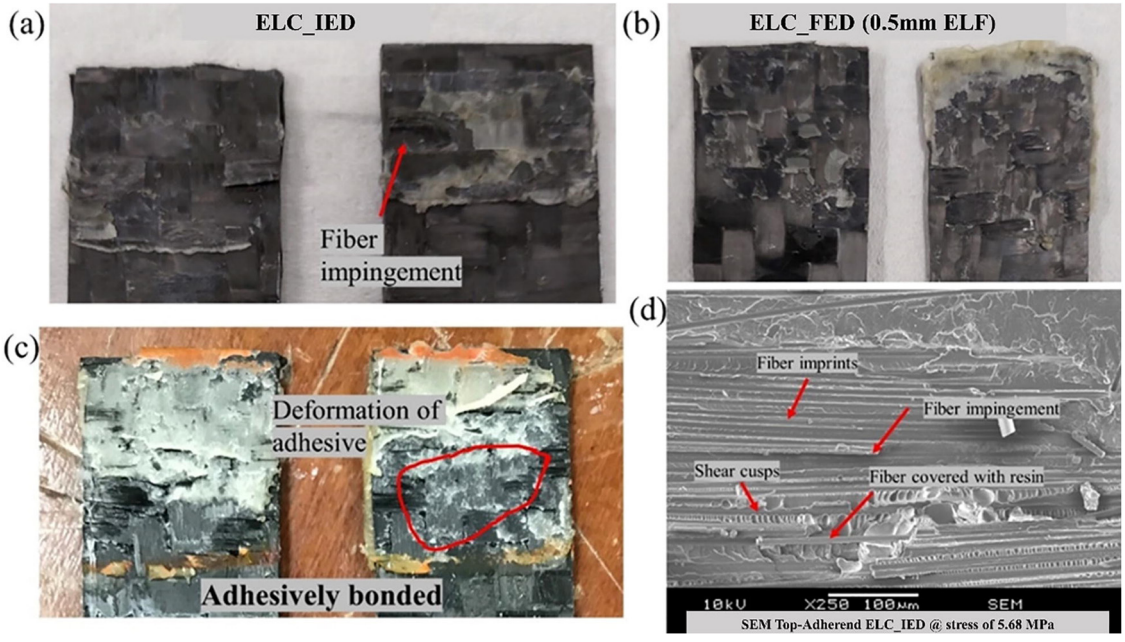

Figure 58: The adherends failure at 5.68 MPa: (a) ELC_IED, (b) ELC_FED, (c) adhesively bonded (SAF 30 5), and (d) the SEM of ELC_IED top adherend [63].

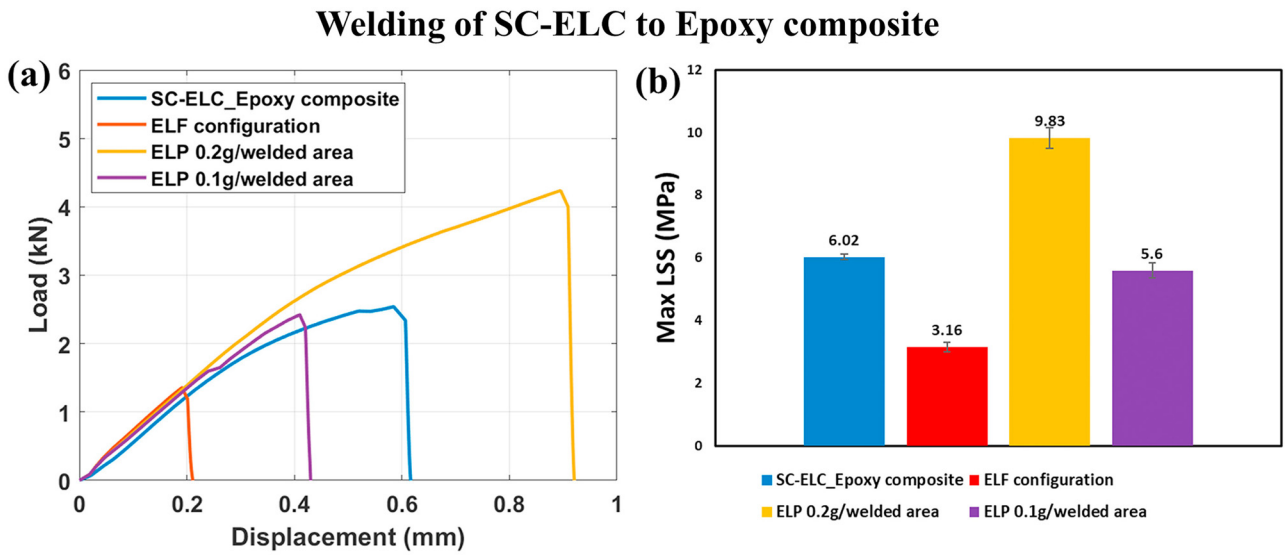

Figure 59: (a) Load *vs* displacement and (b) the maximum LSS of all the welded configurations [284].

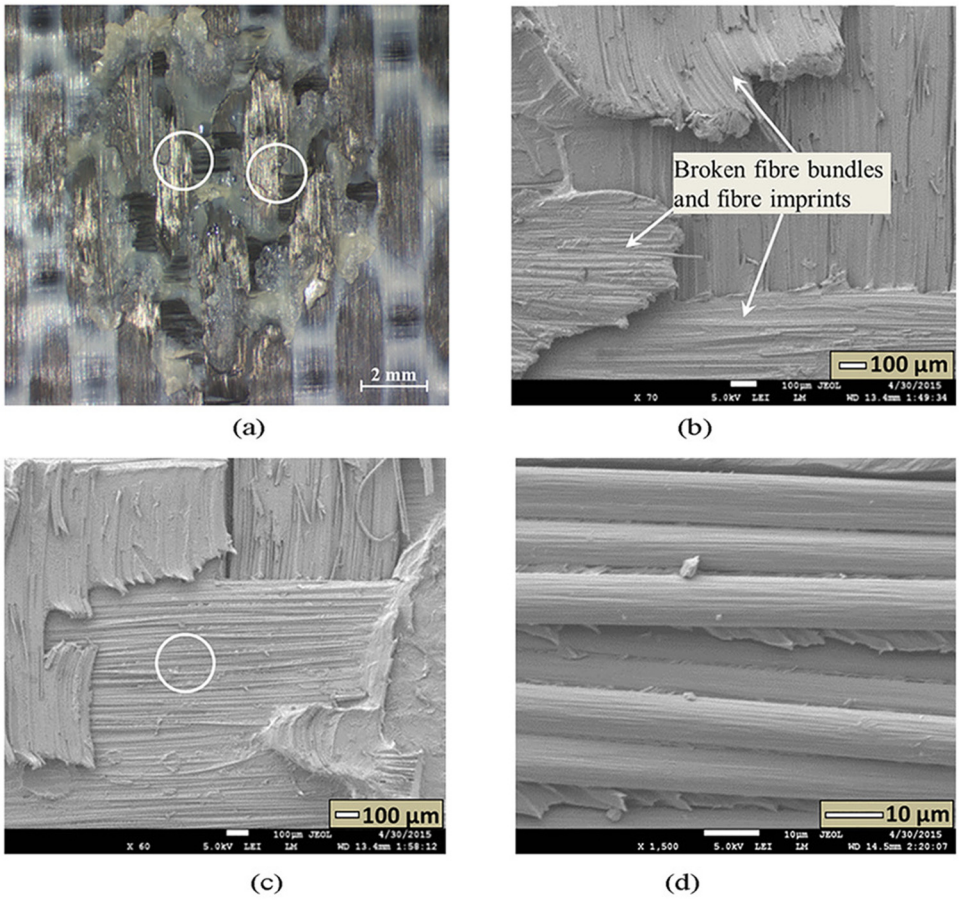

Figure 60: The fracture surface of CF/PEEK at (a) optical and SEM detail, (b–d) for USW spot welding after DLS tests. Welding parameters: 600 J energy, 1,500 N welding force, and 60.8 µm peak-to-peak amplitude [72].

are vibrational amplitude and welding force, was carried out. The results show that these combination of parameters have an impact on preventing the thermal degradation of Ep resin owing to the short heating time [190]. In the case of TPCs/TSCs welding, a delay in the degradation in TSC adherents may be caused by a very short heating time. The heat which generates adhesion was caused by the reduction in heat transformation from TPC coating to TSCs. Brito *et al.* [247] found that the peak load increased linearly with the increase in amplitude in joining the CF/PA66 under the effect of moisture on the USW. However, by studying the effect of increasing moisture absorption with increasing amplitude, the welded area and peak load were decreased. According to the authors, the vibrational amplitude may be affected by using misaligned adherents as well as other USW process parameters. However, Villegas [65] stated that the magnitude and the duration of power consumption were affected by the vibration amplitude during all USW process stages; either low/high welding force was utilized.

Three welding samples per alignment, up to 0.28 mm, have been examined by Tsiangou *et al.* [282], to determine the impact of reducing amplitude on temperature at the interface amongst the PEI coupling layer and CF/Ep adherend. The variation in temperature at the interface in between the CF/Ep adherend and the PEI coupling layer, in welding setups with various welding forces and vibrational amplitudes is shown in Figure 63. The temperature raised at an almost identical pace in the 1,200/86 and 1,200/70 configurations regardless of variations in the vibrational amplitude. The temperature generally rose more slowly in the 1,200/60 setup than in the other two configurations. In contrast, the maximum average temperature value was recorded at 800/86 equal to 339 ± 27°C. In addition, it should be noted that the most extraordinary temperatures were mainly attained just after the vibrations were turned off, which is compatible with the theory that the temperatures were caused by heat conduction through the PEI coupling layer. Furthermore, Wang *et al.* [286] considered the enhancement of welding amplitudes on CF/PEI joint properties, and the temperature measurement field has been analyzed. Acceptable welding quality has been obtained at the optimum amplitude value. However, the PEI resin of the joints' interface melts significantly when the amplitude increases excessively. More information about variations in USW parameters and their enhancements on mechanical properties, welding quality, and welding strength are presented in Tables 2 and 4.

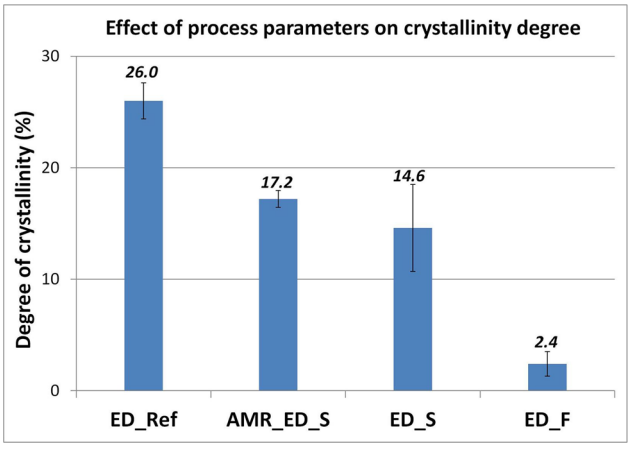

Figure 61: The standard DSC measurement of the calculated crystallinity degree of PPS ED films. The ED film with moderate crystallinity processed by low vibration amplitude and low welding force. But predominantly amorphous ED films were produced by the high vibration amplitude and high welding force [245].

3.5 Impact of pretreatment process (heating time and heat treatment)

The preheating process enhances welding quality and joint quality. Besides, it has an extraordinary benefit whereby preheating for a longer time causes the maximum shear load followed by the reduction due to the porosity generated by the over-welded welding layer [255]. Furthermore, the decomposition in the CFRTP can be eliminated, and the temperature gradient can be reduced by the preheating process for the inter-substrates [239]. Likewise, the fatigue performance and the thermal stress in the joint produced by welding were improved by performing a preheating process before joining with USW [287]. Hargou *et al.* [254] performed a fractographic study of the laminates of the CF/Ep/mendable polymer, EMMA joined by USW. The results indicate that the EMAA changed from solid to porous filaments, as shown in Figure 64(a). Besides, the shown porosity indicates that the raised temperature in the welding of laminates was sufficient to start the condensation reaction between both the Ep and EMAA phases, which leads to the development of gas-filled pores inside the filaments. However, USW produced substantially fewer and smaller pores compared to oven heating in the EMAA (Figure 64(b)). The reason for this discrepancy was that there was a shorter accessible time through welding for the reaction process to generate volatiles, which permeate from the Ep-EMAA interface (where the reaction happens) into the filaments, where it is essential to condense the volatiles to produce the pores.

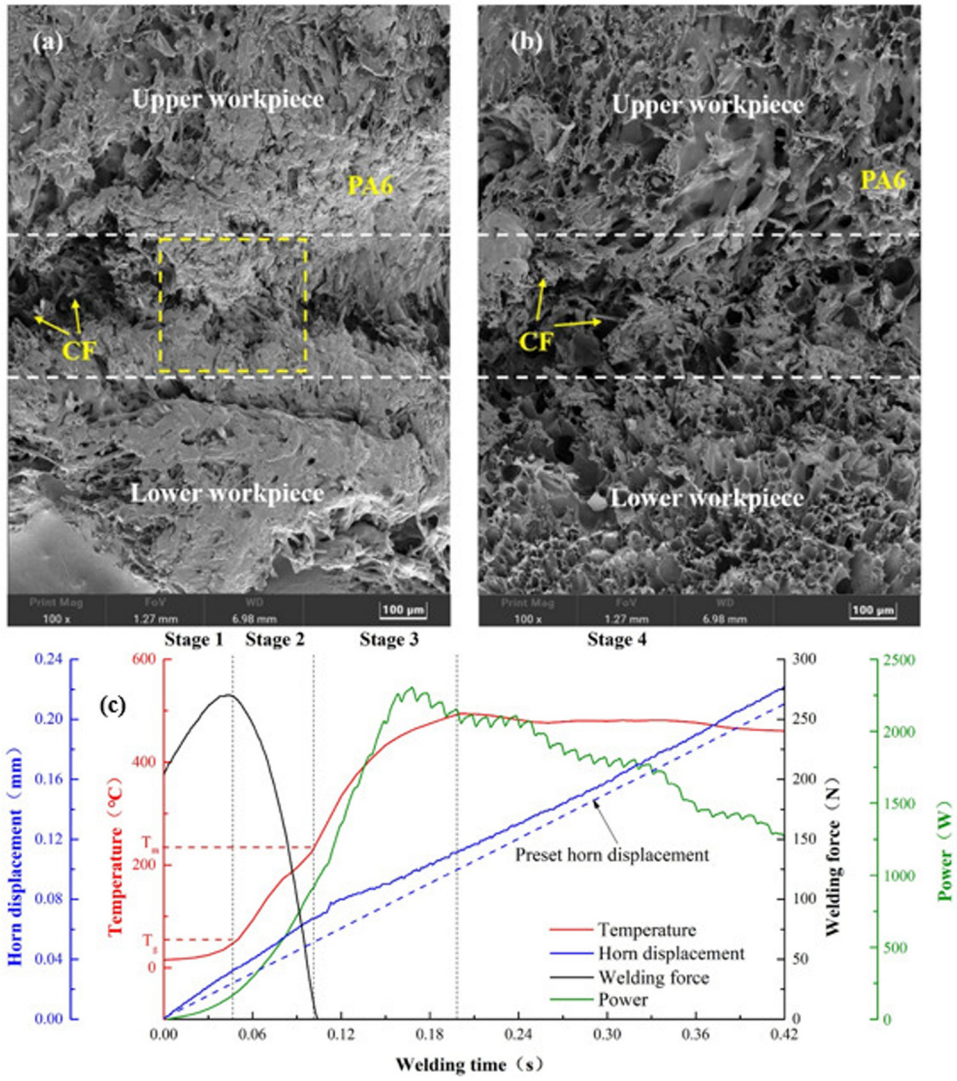

Figure 62: SEM of CF/PA6 of the weldment cross-section under servo-driven welder: (a) The initial unmelted interface, (b) the welded joint, and (c) under typical circumstances with the following characteristics: 600 J of welding energy, 90% of the maximum amplitude, 0.5 mm·s^{-1} of plunging speed, and 200 N of trigger force. Positive displacement value indicates that the sonotrode is moving downward [248].

As a significant part of the relationship between viscoelasticity and temperature, the preheating treatment directly affects the USW parameters. Consequently, it enhances a superior microstructure characterization and mechanical properties such as tensile test and failure. The preheated CF/PA66 has been investigated, and the impact of various preheating temperatures on the welded area and peak load of the joints in various welding times under 0.15 MPa was inspected and illustrated in Figure 65. As the welding time changed, the preheated and as-welded (*i.e.*, non-preheated) welds both followed a similar pattern. In particular, the welding area first increased and then began to plateau, whereas the peak load first improved with the welding time and then reduced. It anticipated that as the preheating temperature increased, the ideal welding time for the joint with the highest ultimate tensile strength dropped. For workpieces prepared at different temperatures of 25, 75, 125, and 175°C, the ideal welding time was found to be 2.1, 2.1, 1.5, and 1.3 s, respectively [239]. In addition, various preheating temperatures were employed to evaluate the fracture surfaces of the broken workpieces CF/PA66 joined by USW. The outcomes are displayed in Figure 66. The macrostructure and microstructure of the cracked workpiece surface heated to 25 and 125°C were identically compacted. In contrast, some pores were dispersed throughout the workpieces, which were heated to 75 and 175°C. Besides, it has been revealed that the occurrence of porosity in the workpiece reduces the mechanical

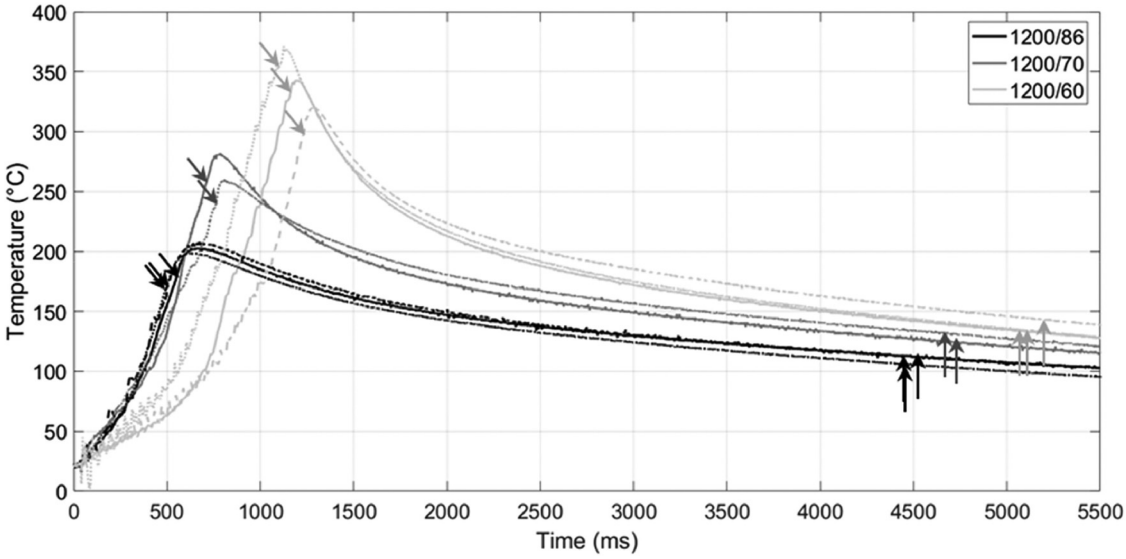

Figure 63: The variation in temperature at the interface in between the CF/Ep adherend and PEI coupling layer affected by the reduction in amplitude (three welding samples per configuration, up to 0.28 mm in all cases). The vibration's end is indicated by diagonal arrows. the end of the vibration is indicated by vertical arrows as the end of the welding process [282].

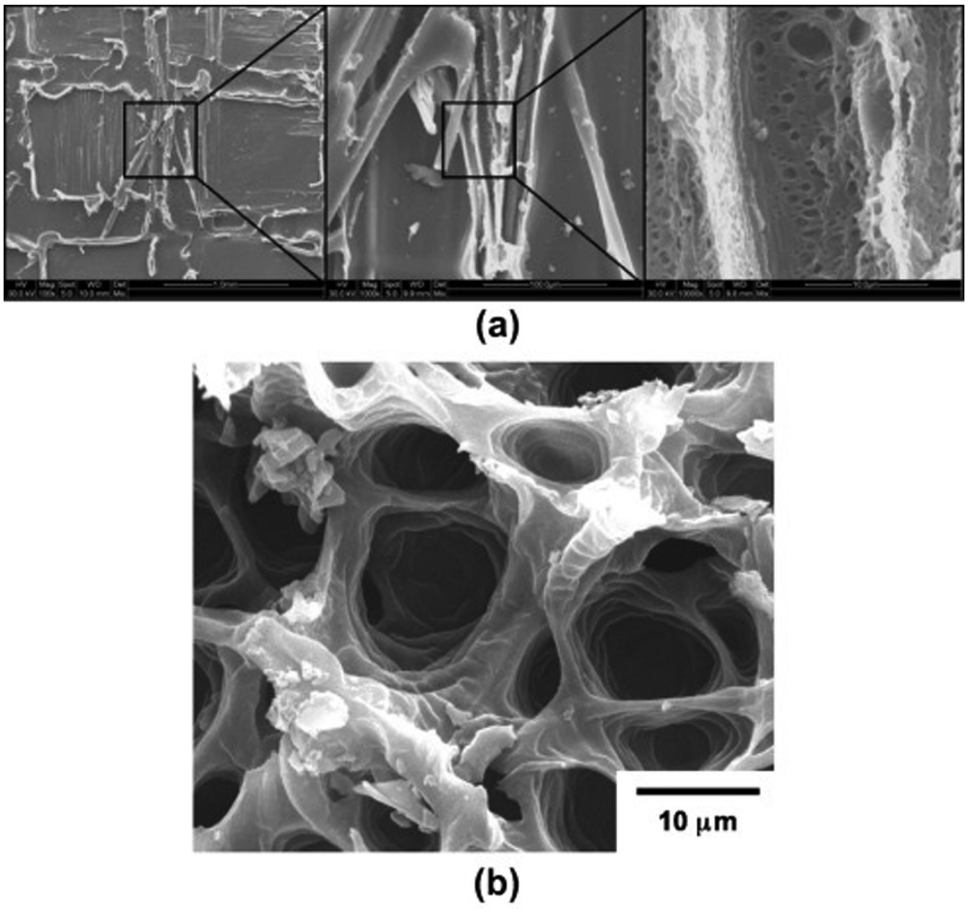

Figure 64: (a) Various magnifications of the delamination fracture surface of a mendable laminate (from left to right: 100× – 1,000× – 10,000×). An EMAA filament is visible in the magnified region, and the porosity is shown clearly (Right side) caused by volatile formation. (b) Porous structure in the EMAA phase following the curing by oven heating [254].

properties of CF/PA66. As a result, joints with preheating temperatures of 75 and 175°C obtained relatively lower tensile strengths than workpieces with no pores. These properties might be associated with the joints' temperature history during welding [239]. Moreover, small voids were noticed in the faying interfaces of the workpieces preheated to 25 and 125°C. However, for those treated at 75 and 175°C, the small voids expanded into huge pores marked as porous regions. Many techniques assist in reducing and eliminating the fracture toughness. For instance, the annealing heat treatment process for CFRPPS tapes to CFRPP laminates has been shown to substantially reduce the welded interface's fracture toughness [288].

In a recent study by Qu *et al.* [289], the uttermost appropriate composite post-treatment method routed between the ultrasonic-assisted reinforcement and annealing methodology has been determined. The study's primary objective was to enhance crystallinity, prevent and decrease the inescapable voids within the printing procedure, and improve its general mechanical characteristics. Furthermore, increasing the crystallinity may decrease the PEEK fracture toughness [290]. Besides, it has been presented that the fracture toughness of PEEK increased by a drop in crystallinity [291,292]. The tensile test has been performed to explore the moisture impact on the mechanical properties of CF/PA66 joined by USW [239]. The welded interface between the two welded workpieces was examined for dry and wet specimens to compare the moisture effect. It has been revealed that in the tensile test results, the quantity of voids in the weld joint decreased the loading capacity when the water absorption reached a specific point (*i.e.*, above 1.7 wt%). Moisture absorption damaged the weld microstructure together with the composites' mechanical qualities. As an outcome, the joints created using specimens that absorbed a partially small amount of moisture exhibited workpiece breaking, while the junctions created using specimens that ingested a considerable amount of moisture fractured during the tensile test due to the degraded weld joint.

On the other hand, the microstructure at the faying interface became loose, and the mechanical characteristics declined, even though the weld area of the wet joint fell less than the peak load with the increased water absorption. Consequently, the change in the weld area was independent of peak load [239]. Li *et al.* [293] explored the enhancement of quantum heating on the USW for joining polymers with double-vibrator parameter. Furthermore, Barkley *et al.* [294] explored the correspondence of interfacial and surface temperature through disparity spot USW for joining TPCs. More information about variations in USW parameters and their enhancements on mechanical properties, welding quality, and welding strength are presented in Tables 2 and 4.

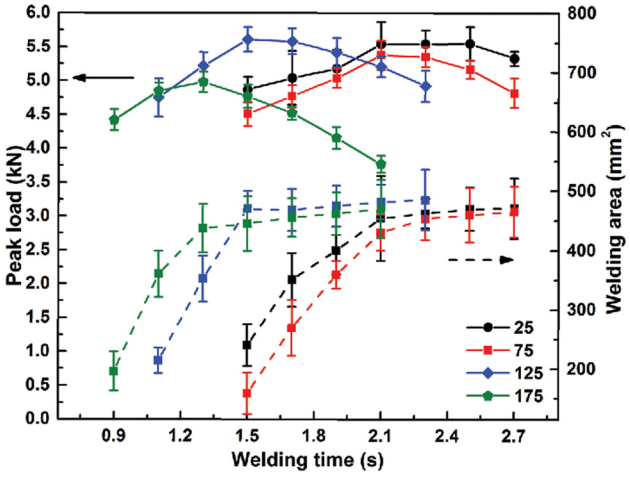

Figure 65: The relationship between welding time on peak load and joints welded area of fabricated preheated workpieces under different temperatures [239].

3.6 General contribution of process parameter in USW

From the literature, many factors play a key role in controlling the welding quality of USW such as preheated or pretreatment methods and process parameters during both vibration and solidification stages. The impact of these factors is given concisely in Table 3 [37].

By studying the welding quality of CF/PA6 welded by USW without ED utilizing a servo-driven welder, the process parameters were found to have a direct relation with bonding efficiency and the overall welded area. Figure 67 illustrates the connection between the welding area and bonding effectiveness. It is observed that the strongest bond is produced when the welding region is near the sonotrode contact area. At vibration amplitude of 50–70% and minor amount of welding energy (*i.e.*, 200 J), materials were insufficiently melted when the welding area is small compared with the contact area. The increase in welding force brought on by great trigger force of 1,000 N and plunging speed of 1.2 and 1.5 mm·s^{-1} would squeeze roughly some molten materials out of the weld region. Besides, when the welding area is larger than the contact area, it results in reducing the bonding effectiveness. Additionally, the welding time and the quantity of melted materials are influenced mainly by amplitude. However, only the first three stages and fewer melted components were visible at

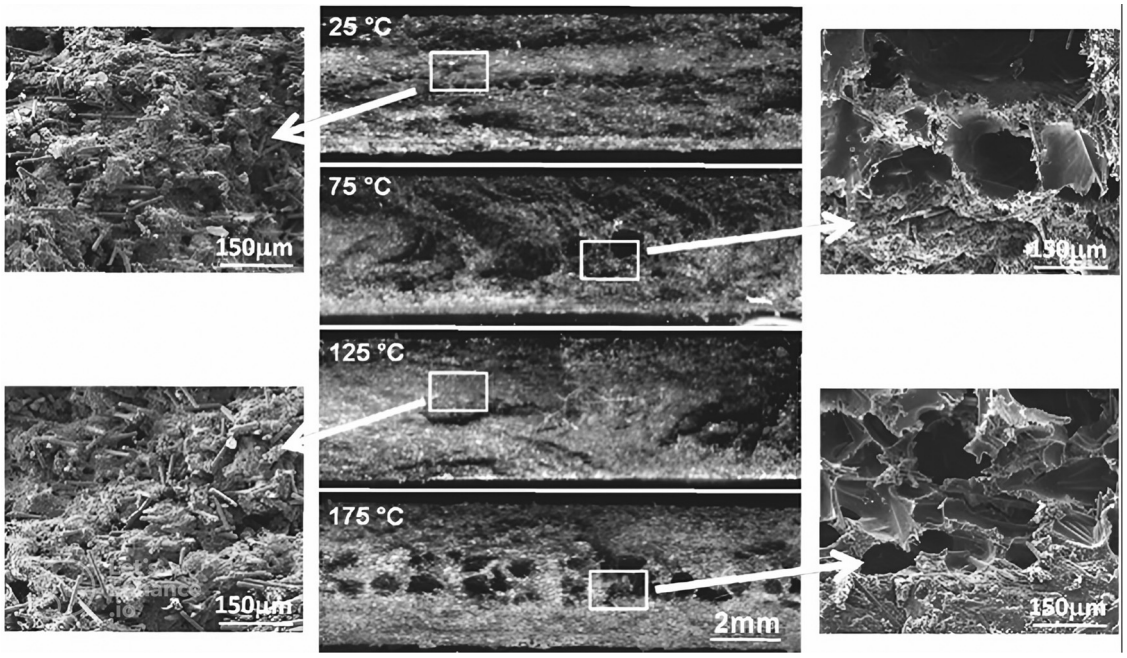

Figure 66: Morphology of CF/PA66 of the fractured surface for upper work pieces with various preheating temperatures after the fatigue test [239].

low energy and vibration amplitudes, resulting in a relatively limited weld area. In comparison, great energy can melt additional materials. However, because welding takes a long time, excessive melted materials might be squeezed out [248].

Welding process factors, weld characteristics, and joint behavior are essential to evaluate the weld quality and are all related. The degree to which a weldment satisfies its practical necessities is the definition of weld quality. Weld attributes are a weldment's visible traits, while weld performance is a weldment's internal qualities. The weld quality can be circuitously defined by weld qualities and joint behavior, such as weld area, the morphology of the weld zone, and extreme LSS, founded on the relationship of the previous four sets of variables [250]. Figure 68 shows the correlation between weld quality, characteristics, and joint performance. Overall, the ideal heating time and the optimum frequency in USW were found to be 3–4 s and 20–40 kHz, respectively, in large-scale consideration [295]. An increase in welding strength was reported due to high vibrational frequency, which also increases material vibration [296,297]. Moreover, it is anticipated that USW will always have a very high instantaneous strain rate due to the nature of the process, which involves a very high strain due to the high vibrational frequency. It has been established that a substantial strain rate affects the crystallization of the polymer [298–301], as a further enhancement of the strain rate.

4 Improvement of USW process by ED and interlayer

The heat generated in the overlapped welded area is a difficulty caused by the high-frequency stress; this heat is due to vibrational energy. The ED works as heat dissipation, where it molds to initiate melting [302]. It is possible to use a tie layer (an interlayer made of substrate material) instead of ED in the USW [303,304]. The ED consists of resin protrusions on the welding surfaces, and it is artificial [64]. Table 4 presents a tabular classification based on the type of USW machine used to join different types of CFRP with an interlayer between the two welded specimens. However, the ED is usually made of TPCs such as PEI, PE, PEEK, or PSS. Besides, it is generated in different shapes. For example, previous studies presented a beneficial influence of the PPS film and its composite crystallinity on the tensile characteristics [305,306]. Although interpreting the difficulty of introducing ED, as in USW, on sheet components (between the two specimens to be welded) is considered one of the main limitations of fiber-reinforced material [73]. However, this process is compatible with adding polymer-coated material in dissimilar welding [307]. Figure 69 shows a graphical diagram of contact initiation and propagation for USW with/without ED [240]. Furthermore, Singh Rana *et al.* [308] utilized the USW to join specimens made of sustainable polymers and design by printed molded by implementing EDs with various geometries.

Moreover, it has been shown that there are some difficulties in the USW process in the absence of ED or interlayer in between the specimen [30]. The ED usually has incredibly higher viscoelastic heating and tremendous strain during the welding process than the bulk material; the reason is owing to the small cross-section of ED [309]. Furthermore, the stability of welding quality depends on ED [309]. The ED, used in TPCs welded by USW, is made of traditional molded matrix resin on the consolidated adherents in a second production step [269,310]. Meanwhile, the geometry of ED is one of the critical factors that may affect the USW technique besides vibration amplitude and welding time [259]. Linear ridges with semi-circular, rectangular, and triangular cross sections are the shapes of ED due to plastics industry procedures [311]. Nonetheless, Khatri *et al.* [312] investigated the efficiency and welding quality of joining PEEK fabricated by AM with CF/PEEK and joined by USW by implementing various shapes of ED. It has been observed that the circular ED obtained greater failure forces associated with mesh-shaped counterparts ED.

Furthermore, the welding process and its results are highly affected by the orientation of the ED, and its shape [12]. The ED surface is usually made of resin protrusions which helps to perform the weld, and the welding quality is directly influenced by the shape and size of ED as well as the morphology of these resin protrusions [3]. In addition, it has been revealed that by increasing the geometry complexity of ED and it is surface to have an optimum ED design, well cause to enhance welding quality [313]. Koyanagi *et al.* [314] investigated CFRP joined by USW using an ED associated with a numerical model. An ED made of poly-vinyl-butyral (PVB)/graphite nanoplatelets film has recently been produced and employed to join CF/Ep by USW by Cilento *et al.* [315]. Besides, a modern ED made of stainless steel mesh has been utilized in USW for joining CF/PA66, and the enhancement of ED mesh size on the welding quality has been investigated [316]. Moreover, it has been observed that a smaller wire diameter of the mesh ED and great wire spacing lead to good welding quality. Li *et al.* [316] explored the CF/PA66 joined by USW by implementing an ED made of stainless steel with mesh geometry, as illustrated in Figure 70. Besides, it revealed that a higher amount of pore defects in the joint were obtained by small wire spacing. However, a wire which has a great diameter causes the absence of fusion defects. Also, the energy concentration effect was reduced by a large mesh area. Moreover, it has been revealed that the damage in the fusion zone can be reduced to minimal and eliminate thermal degradation by implementing various types of PEI ED [317].

Korycki *et al.* [318] examined the effect of ED thickness on joint quality and thermal diffusion during USW of CF/PEEK. The PA6 film has been employed as an ED to join cold rolled steel with CFRTP by USW [319]. Also, the authors addressed the effects of preheating temperature and welding energy on the joint characterizations (microstructure and mechanical). The heating of FED was excited by the surface friction, which results in time variation to melt the ED [8]. A fragile weld line identical to the thickness of resin-rich regions within the adherents in TPC/TPC welding has been observed because the most molted ED is squeezed out of the overlap welding [64]. The adhesion and displacement of ED and FED during USW were investigated [320,321]. Furthermore, to attenuate the upshot of adverse fiber location at the interface, it has been recommended to

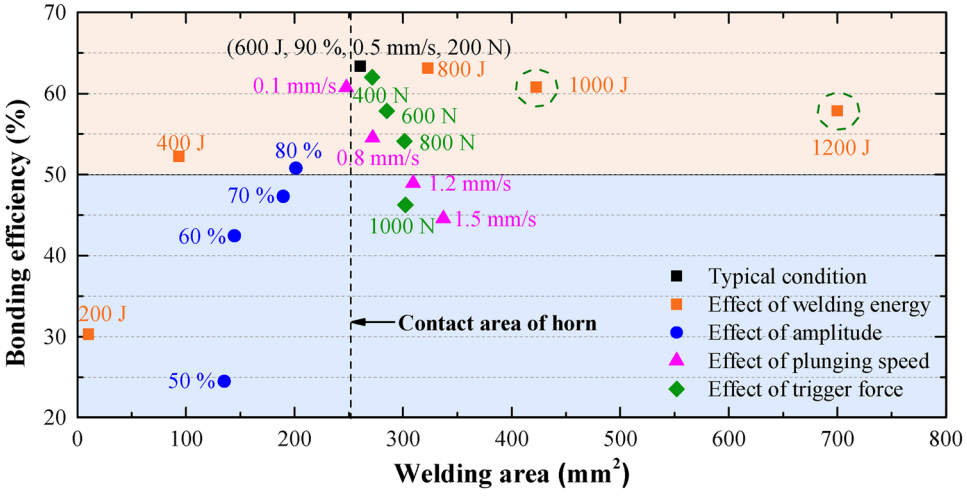

Figure 67: The relation between bonding efficiency with welding area and process parameters effects [248].

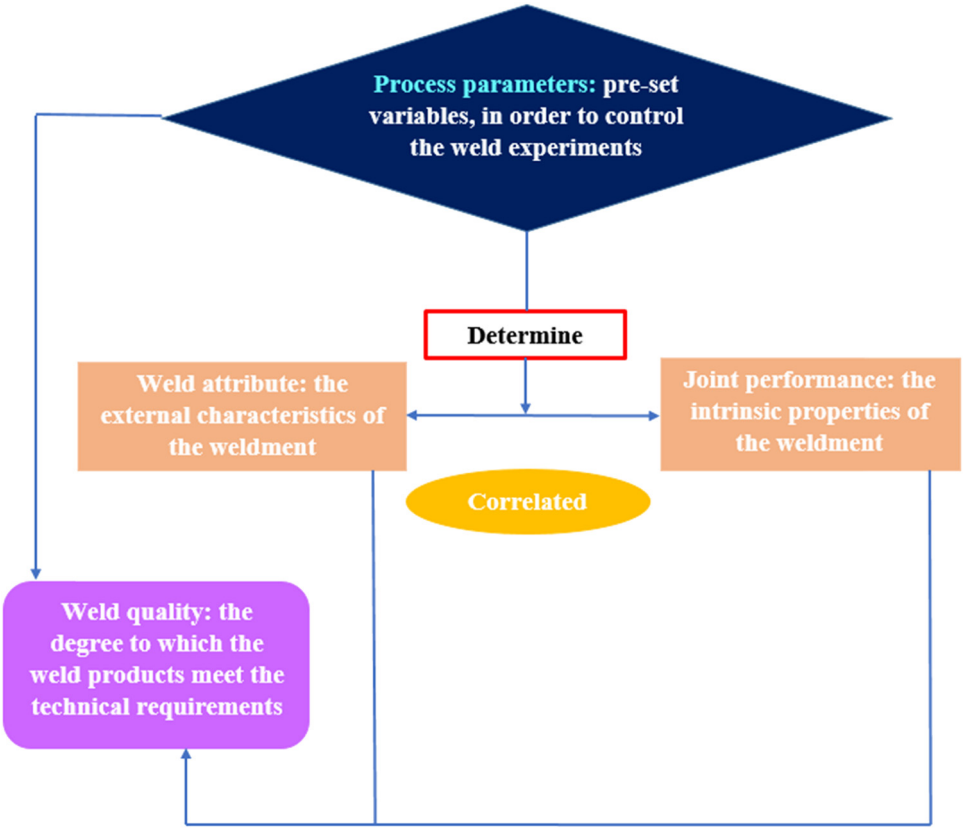

Figure 68: Relationship between welding quality, welding characteristics, and joint performance.

utilize an ED made of TPCs, which emphasizes the material weldability [302]. On the other hand, the ED may have some weaknesses, like limited reduction in fiber [234,252,322], although it provides good weldability and welding quality with using ED. Figure 71 presents a schematic of welded layers with an FED [244]. The impact of using ED made of PVB NCs for joining TSCs by USW has been investigated by Cilento *et al.* [323].

Furthermore, a joint was performed with using ED, where the ED has melted and performed the joint in between the two pieces, after the ED melts, solidifies and cools down. The ED melts due to the generated friction heat by the effect of ultrasonic vibration [172]. In addition, the reason for melting the ED without distortion in the micro-grooves is that the ultrasonic amplitude and applied force were lower than that needed for ultrasonic hot embossing. Nonetheless, Wang *et al.* [324] investigated the weldability of CF/PA6 as well as PA6 joined through a servo-driven USW with/without using ED. For the purpose of examining the impact of the ED on welding process parameters in joining CF/PPS and joining CF/PA6, the qualitative examination of displacement during the joining process is presented in Figure 72. When the triangular ED melts, the sonotrode descends rapidly. When the material melts at the faying surface of the triangle, it descends slowly. Also, in the CF/PA6 30 wt.% welded without using ED, it was detected that the power increases grow abruptly and then remains stable with minor variations [37]. Furthermore, incase of applying two differnet types of ED as 4T ED and FED to join CF/PPS similar vibration time, welding energy, LSS and maximum dissipated power were obtained. Also the obtained results of FED were similar to triangular ridges moulded on one slack stripe of neat resin and triangular ridges moulded on the surface of the bottom adherend. Besides, the sonotrode displacement was analysed, it was shown that the sonotrode hold its initial position before starting its gradually descending [260]. However, since ED is not used for USW of CFRTP, the sonotrode descends linearly vertically at a constant speed.

An investigation on a unique zero-flow welding method for continuous USW of TPC plates has been carried out. The suggested method produced robust welds before the squeezing flow starts at the welded interface. The outcomes demonstrate the viability and point to the possibility of rapid high-strength welding between TPC plates. In addition, the relation between LSS and welding speed for 60, 80, and 100 mm·s^{-1} has been examined. The outcomes show that, overall, the LSS values at 60 mm·s^{-1} are greater than

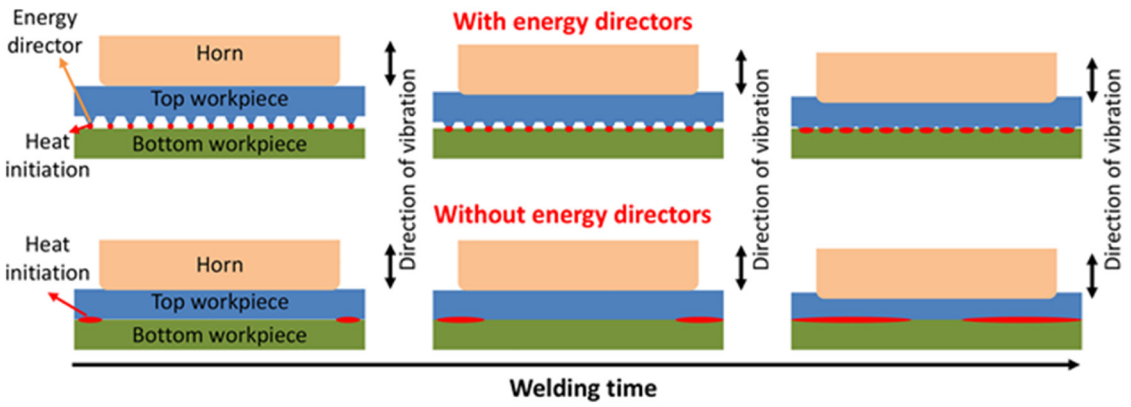

Figure 69: The heat generation and propagation flow in USW toward welding with/without ED [240].

those at 80 and 100 mm·s^{-1} [325]. For investigating the mechanical properties of CF/PEEK joined by USW through implementing a spot ED, a double LSS was performed, and the outcomes were likened with MFs results; the fiber-matrix debonding failure for the welded specimen causes naked fiber bundles and resin-rich pockets to become evident on the uppermost ply of the adherend. However, the first ply is the only part of the adherend with this intralaminar damage, while the remainder of the layers were unaffected. In contrast, matrix cracking and delamination severely destroy the laminate structure of the MFs joint. The part's upper side deforms due to the Hi-Lok® fastener head penetrating it. A full description of the through-the-thickness damage is given by the cross-section micrographs of the welded samples, as illustrated in Figure 73 [72].

Tao *et al.* [256] compared the morphology observation of a weldment processed with and without ED by using FED and noticed a considerable reduction in the HAZ width at identical welding time and in the number of cracks, which is due to the melting of the ED absorbing a particular amount of heat and decreasing the impact of heat on the matrix. Accordingly, using FED increases the joints' strength with rising the PEEK resin gratified, and improves the attentiveness of ultrasonic energy at the interface. Besides, the ED directly affects the fracture surface, as shown in Figure 74.

Some variations were noticed by comparing the micrograph results of the fracture surface of cross-ply laminate with and without FED. Figure 75 presents the fracture surface of cross-ply with FED after the LSS; fibers are observed in Figure 75(a), the fiber bundle is parallel to each other, and the fracture is considered narrower without FED, and the absence of fractured fibers (Figure 75(b)–(d)). A slip in the fracture surface caused by the pull-out of the fibers at the edge of the free-edge side at point D of the welding area was observed. Moreover, at point E, there is a flat fracture surface. However, at point F the fracture befell at the edges of the grip side and the middle of the welded area, this fracture mode is similar to the fracture caused without FED [6]. Additionally, an FE model was developed to examine the fracture mechanism of cross-ply laminate with and without the FED. Where the CF/PEI joined as a similar welding with FED, the heating phenomena and thermal degradation were examined. The analysis of the fracture surface during ideal welding indicated matrix degradation symptoms, resulting in less consistent quality.

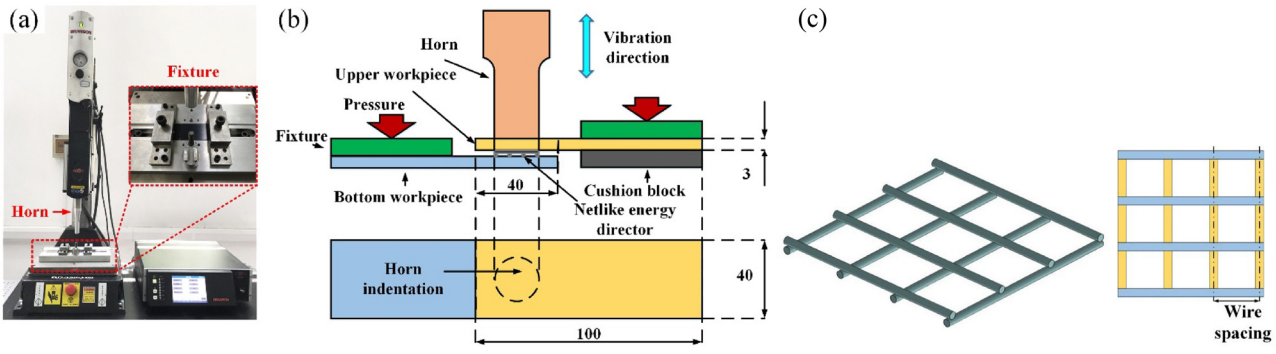

Figure 70: (a) 2000XD USW machine, (b) the welding process schematic, and (c) the stainless steel mesh ED [316].

Moreover, it is probably caused by a higher heat generation rate in the substrates and ED and higher temperatures close to the ED melting temperature [238].

A further investigation studied the CF/PEI similar welding using a different configuration of ED by changing the orientation parallel to the plates, perpendicular to the plate, and two EDs parallel to the plate [3]. Besides, triangular EDs were molded into laminated composite surfaces using a hot platen press. LSS samples were created to examine the effects of numerous ED configurations and the EDs' orientation concerning the load. It is revealed that several transverse EDs were significantly effectively filling the overlap area once they melted, resulting in minimal damage to the fiber at the welding. The effect of changing ED geometry and the configurations on the welding quality were studied. As a finding, the multiple EDs improved the overlap welded area without hindering the resin flow. As well as, by using multi-EDs, a remarkable reduction in fiber distribution in the outer layers of the weldment was observed. However, the parallel ED configuration provided more welded area scatters than the transverse EDs [3]. Furthermore, the high number of scatters makes studying the ED configurations on mechanical properties more difficult. Nevertheless, Wang *et al.* [326] employed the genetic algorithm and neural network to optimize the process parameters and predict the weld strength, including welding time and pressure of USW that were implemented to join CF/PEI. Moreover, Villegas and Palardy [278] explored whether using triangle ED in USW instead of FED may significantly shorten the required heating time to reach supreme weld strength. The significant finding was that, in the particular scenario, the triangle ED did heat up, melt, and collapse almost twice more quickly than the FED, and this difference was substantial. However, the integrated triangle ED did not require significantly longer heating time to reach the optimum weld strength compared to FED. However, a published review found that many studies joined the TPCs to the TSCs by using an interlayer made of TPC films as an interlayer or coupling layer [37]. Furthermore, the PEI has been used as an interlayer to couple different matrix's of CFRTP based on its unique characteristics under the co-curing process [193–195]. The porosity produced by resin sublimation created in C/Ep adherents after welding is concluded by comparing a study that used 50 μm thickness of PEI interlayer *vs* another study that used 250 μm [192]. Nevertheless, when using PEEK as a coupling layer for dissimilar joints by USW, it is usually not soluble in uncured Ep systems owing to the high chemical resistance [5,94,190]. Additionally, Wang *et al.* [327] explored the enhancement of welding time on the welding quality of CFPEEK, by using an ED which was manufactured by implementing the ultrasonic embossing. The obtained outcomes show that using the ultrasonic embossing helps on concentrating the welding energy which decreases the dispersion and randomness of the weld distribution as well as enhances the failure load by 30% compared with joining without using ED. Furthermore, Rubino *et al.* [328] developed a TPCs hybrid interlayer to join GFRP by USW. Figure 76 represents the graphic demonstration of the manufacturing route and the USW set-up. Meanwhile, Tian *et al.* [329] explored the effect of pre-pressing ring on the welding quality of USW in joining short CF/PA6 composite.

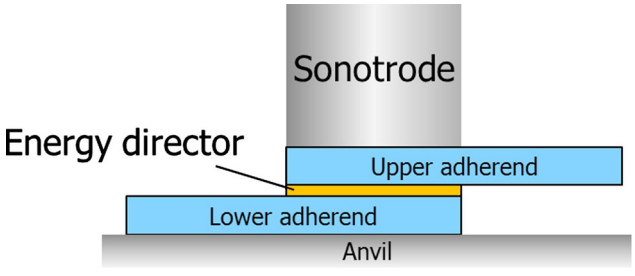

Figure 71: Principle of USW TPCs with an FED [244].

Generally, the size, geometry, and the number of implemented ED have a direct impact on welding, since the ED affects the resin flow and heat generation [256]. Besides, the welding strength was found to be influenced by the ED much more than vibrational time and welding force [330]. Some of the most effected properties by ED are illustrated in Figure 77. However, apart from the mentioned and discussed studies, the literature is rich with further investigations which focused on overcoming the drawback of the traditional EDs for enhancing the welding quality. For instance, Jongbloed *et al.* [331] developed a compliant mesh ED made of woven polymer to enhance the uniformity of the weld. The obtained results reveal that the developed mesh ED enhances the LSS and the weld uniformity. Furthermore, Brito [332] recorded the best welding results by the combination of increasing welding force with implementing a discontinuous ED film. However, the impact of ED is varied as long as the material of specimens to be welded is varying. For instance, in some cases, the triangular ED can achieve more favorable results than FED in welding polyethylene [333]. Moreover, recently Bose *et al.* [334] implemented the developed methodology of water-submerged USW (S-USW) with three various types of ED to join CF/PA. This methodology enhances the welding strength as well as mitigates the material degradation that may be caused by the rapid heating which occurs during the traditional USW process. Besides, the obtained results by using the S-USW with a semi-circular ED

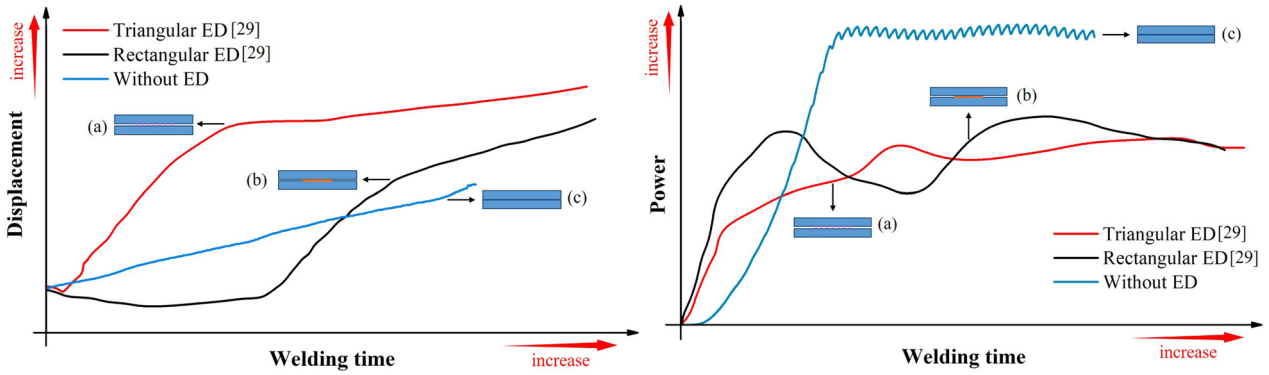

Figure 72: The variation displacement and power during USW for diverse surface settings: (a) CF/PPS with using triangular ED (vibrational amplitude = 86.2 μm, holding force = 500 N); (b) CF/PPS with using rectangular ED (vibrational amplitude = 86.2 μm, holding force = 500 N); (c) CF/PA6 without using ED (vibrational amplitude = 36 μm, holding force = 200 N [37].

recorded 16.4 MPa as welding strength, while it reached 14.3 MPa and 14.69 by using the traditional USW with triangular and rectangular Eds, respectively. In a further investigation accomplished by the same authors, Bose *et al.* [335] implemented the S-USW to join PVC/PVC and PP/PP. The obtained results show that the LSS of PP/PP and PVC/PVC increased by 21 and 39%, respectively compared with the results obtained using traditional USW.

5 Challenges

The main throwback of USW is that it is still limited in assemblies with considerable overlap area [238]. Likewise, one of the most remarkable challenges of USW is that for each new welded spot, a new set of boundary conditions must be reset [170]. Implementing the USW process is till limited since there is no significant quantitative evaluation methodology for defining the bonding strength [339]. Joining assemblies with huge overlaps by USW is still defied and limited [238]. The ultrasonic amplitude in the USW is inhomogeneous as usual over the sonotrode area, which makes the unfilled molten polymer more challenging on large areas near micro-cavities. Furthermore, the energy output of piezo stacking, driven in resonance for achieving high amplitude in the USW, controls the sonotrode; this significantly controls the overall contact area processed in one step [172]. In the case of joining TPCs either in similar/dissimilar joint USW, a dimness in the

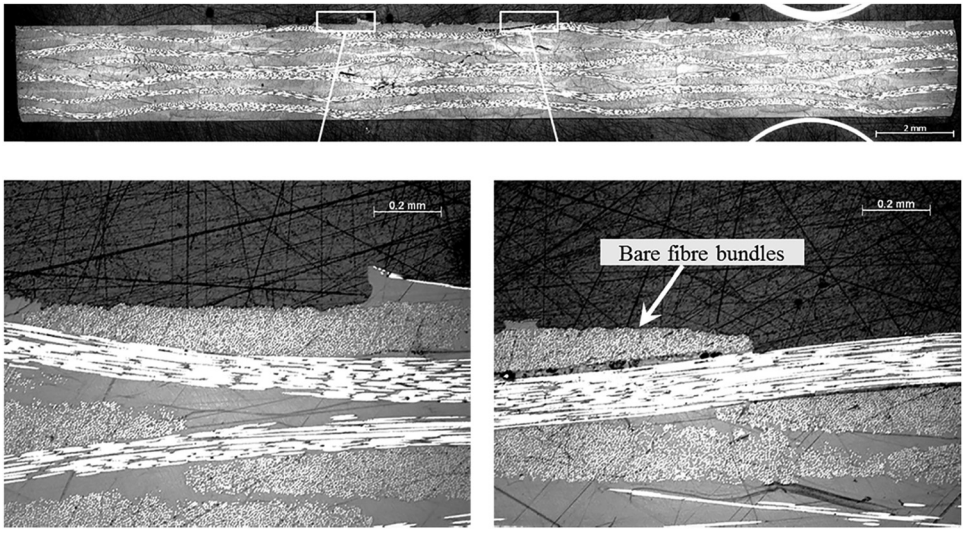

Figure 73: The micrographic cross-sections of spot-welded joint of CF/PEEK after DLS tests. The scale bar for 2 mm is presented in the top figure. The below images are the magnification of the parts in the white boxes of the top one [72].

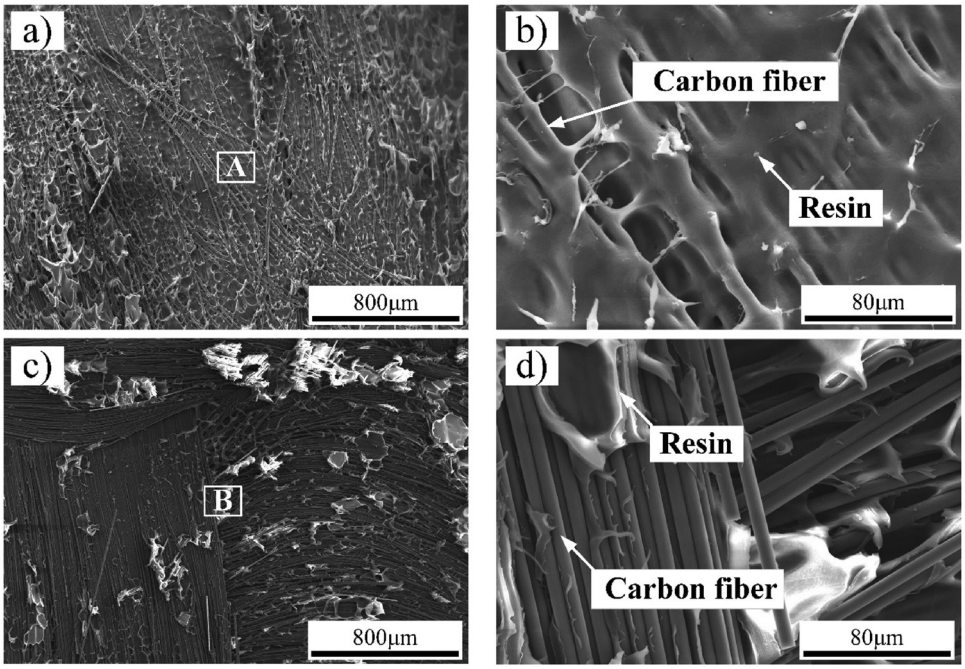

Figure 74: The fractured surface morphology of (a) CF/PEEK joint without using ED at 0.9 s, (b) region A with high magnification, (c) the joint with FED at 0.9 s, and (d) region B with high magnification [256].

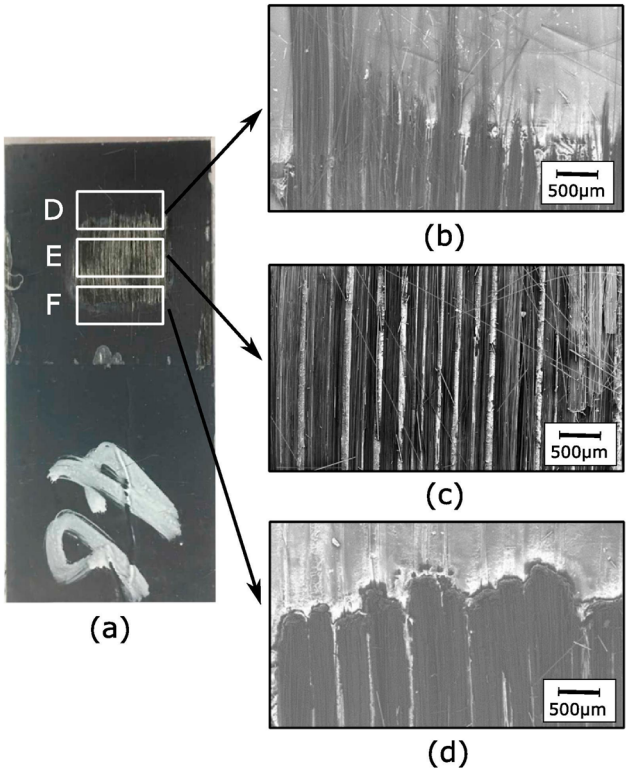

Figure 75: The fracture surfaces of cross-ply laminate joint of CF/PA6 with implementing FED after LSS [6].

composite structures' assembly, which tends to fail first, may present. This means the damage must be detected to prevent local degradation and evade a catastrophic failure [77]. Although owing to great heat generation at the interface throughout the USW process, the thermal degradation of the thermoset substrate is a severe dilemma to be determined [37]. Besides, damage growth occurs in the interface between the weldment components that are joined by SSW of USW [340]. Moreover, the physical mechanisms of the USW are still under debate, subsequently predicting the optimum sets of process parameters that led to optimum welding quality and welding strength remains a challenge [341]. Besides, determining the optimum amount of the reinforced wt% to be added to the polymer matrix which effects the welding strength is challenging, for instance, by increasing the GF above 20 wt% in PP matrix the welding strength was reduced [342]. Additionally, Tirband *et al.* [343] enhanced the welding quality of GF/PMMA and GF/PP, respectively, by using the laser surface treatment approach where the obtained results show a superior interaction between the coupling layer and the treated surface parts were achieved. In addition, avoiding the trapped air and restricting the melted polymer flow during the USW process are challenges that can be avoided by implementing an optimum ED design [344]. However, finding the

optimum ED for each specific USW is an essential concern. Furthermore, increasing the energy may cause a slight reduction in the LSS [345]. Moreover, the necessity of higher fiber content for sufficient energy focusing in the ED is a considerable challenge in USW for acousto-ultrasonic composite transducers, by comprising a piezoceramics materials in reinforced polymer matrix [346]. Likewise, finding the optimum welding temperature is essential since increasing the temperature reduces the required welding time, in contrast the molecular diffusion rate limits the welding process at high temperature [347]. However, it has been reported that the ultrasonic vibration treatment as a post-processing approach can improve the joint strength in applications that require medium to high welding strength at optimum process parameters [348]. Apart from the mentioned advantages and disadvantages in Figure 4, Figure 78 presents further advantages and limitations of USW process.

In order to improve robustness and reliability and to develop continuous welding of complex and more significant parts, there is an essential need to develop a consistent FE models with the up-clambering of using USW in industrialization [325]. Some studies developed an FE model to study different mechanical properties such as stress distribution and stress-strain, although FE analysis of CFRTP is still considered slightly limited. In addition, mathematical modeling and numerical examination remain deficient [22]. Nonetheless, by investigating the thermal coupling during USW process by developing FEM by Zhang and Li [349], it was found that the main reason for bond formation in USW is the severe restricted plastic deformation. Furthermore, the accurate and realistic mock of the vibration and heating performance of TPCs in the USW process was allied with excessive difficulties. In certain, the solution by essential frequency and temperature that dependes on mechanical stiffness and damping behavior in the high-vibrational frequency range are inefficiently, which cause to have limited numerical expectation of the weldability in the progress of USW technique [350]. Additionally, there is an essential demand for optimum specimen's geometries as well as further progresses in the assessment routine to enhance the analyzable temperature range combined with the quality of the generated material. The developed model based on reverse engineering approach is shown in Figure 79.

Moreover, Yang *et al.* [351] examined the contact performance and the temperature characterization in USW of CF/PA66 by developing a mathematical modeling as shown in Figure 80, through implementing the harmonic balance methodology. The obtained results show that in NL contact and heat generation there was a certain separation between the specimens and the friction heat generated in the earlier welding stage, while in viscoelastic heating, no significant separation was recorded. Besides, increasing welding time and vibrational amplitude produced a remarkable increase in the temperature of the welding surface. However, by analyzing the spatial and temporal temperature enhancement during the USW of FRTP numerically as shown in Figure 81, the obtained results show that there is an essential need to focus more on the viscoelastic heating since it increases the polymer matrix temperature to the decomposition temperature [352].

To investigate the welding quality by using the vibrational signal, Zhu *et al.* [353] employed variational mode decomposition and Hilbert-Huang transform (HHT) to acquire the HHT spectrum, where a support vector machine (SVM) model has been developed and trained by using the Bayesian optimization (BO) algorithm as shown in Figure 82 to define the optimal parameters for weld quality categorization and recognition. The outcomes reveal significant performance, accomplishing 95.35% accuracy rate. This designates that there is remarkable

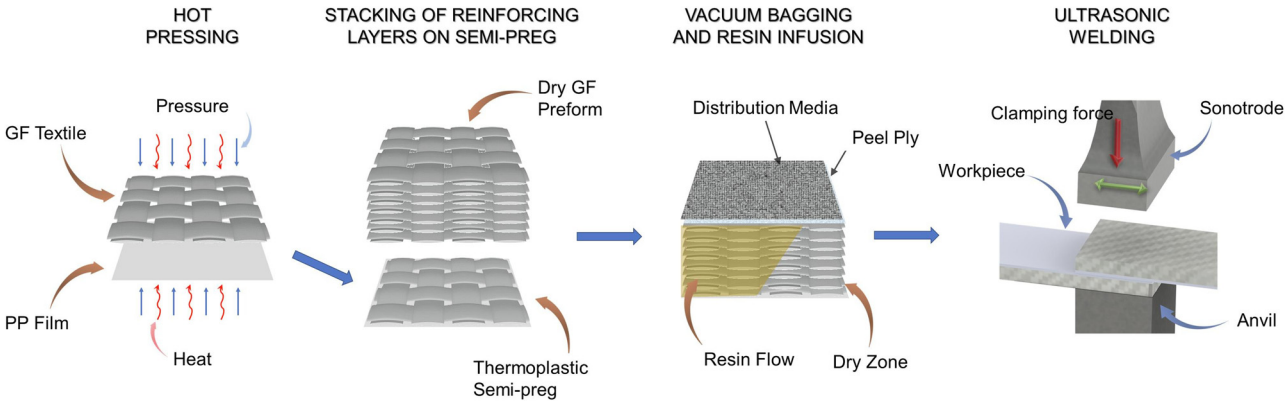

Figure 76: The schematic of the procesing route of manufacturing process of TPs/TSs hybrid composite to USW of the fabricated laminates [328].

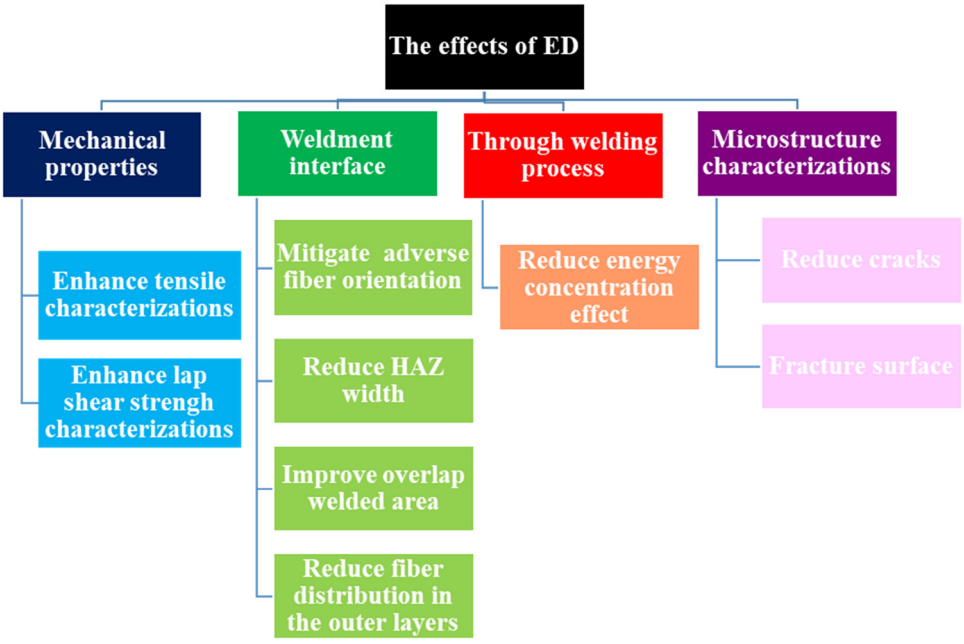

Figure 77: The properties most affected by the ED.

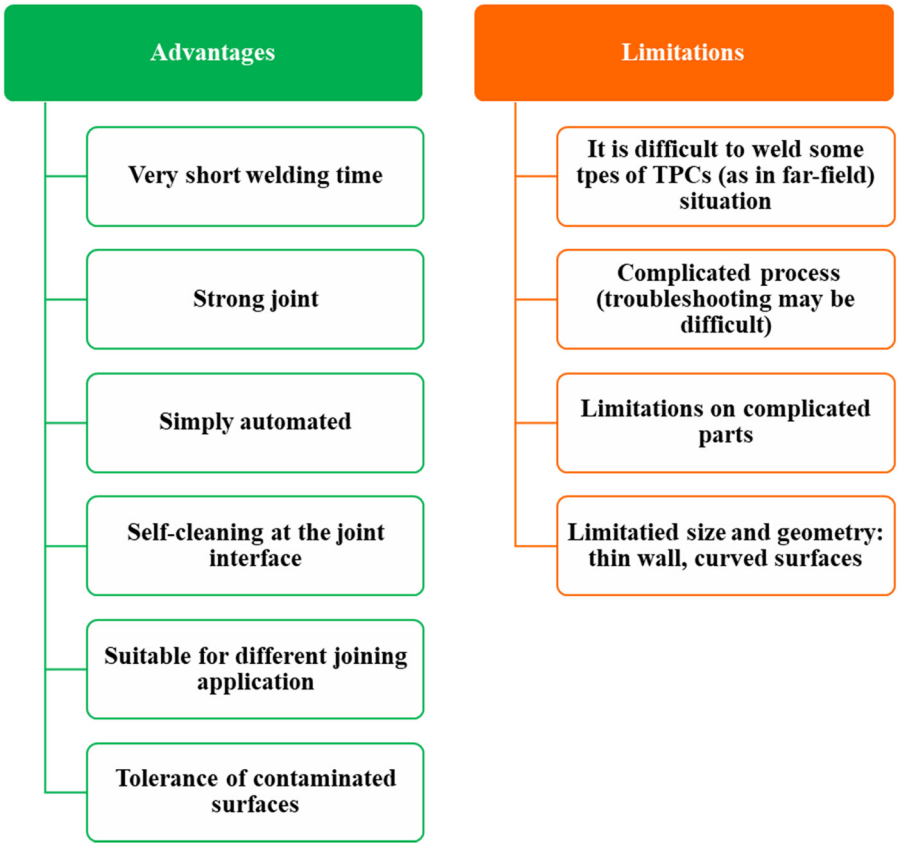

Figure 78: Further advantages and limitations of USW process.

potential for virtual detection of CFRTP welding quality through ultrasonic vibration signals.

Furthermore, despite the overall advantages of polymers, such as mechanical properties and lightweight, they also have some drawbacks. For instance, the major drawback is that it is not simple eco-friendly, where researchers and organizations have expressed tremendous concern about the development of non-recyclable plastics in the environment by developing plastic that is recyclable or biodegradable.

For recyclability purpose, utilizing biodegradable polymers have several environmental benefits such as reducing carbon dioxide emissions regeneration of raw material, and biodegradation [354]. Some of the commercial polymers such as PA6, PA66 were found to be biodegradable and were proved under the SEM, FTIR, and EDS analysis [355]. However, the PA66 can be replaced by the bio-based polyamide 56 (PA56) [356]. Besides, the PBS is also completely biodegradable [357]. Moreover, polyesters such as PET can be replaced by natural polymers such as polysaccharides (wood, pectin's chitosan, and gum) and animal and plant proteins (collagen, soya, gluten, gelatin, casein, and whey). Besides, the PLA can be produced by both natural resource (rice, corn, sugar beets, *etc.*) and chemical resource. In contrast, PEEK is an example of non-biodegradable and is unfeasible to recycling [358]. Nonetheless the biodegradation process is enhanced by numerous factors such as the morphology structure of the polymer, the molecular weight as well as the chemical treatment process [359]. In addition, the key features of biodegradable polymers are, the potentially undesirable mechanical qualities, the high rate of decomposition and their primarily hydrophilic nature. Meanwhile those features can be enhanced by mixing natural and synthetic polymers [360,361].

6 Discussion

Diverse types of joining techniques can be employed to join similar and dissimilar CFRPs. One of the best-developed techniques is the USW. The joining occurs due to the heat generated by the vibrational amplitude and ultrasonic wave. The heat is generated between the interface layer, and it reaches these points by the welding tool known as horn/sonotrode. Usually, an ED, interlayer, or coupling layer, is used between the two layers (adherend) and must have a melting temperature inferior than the melting temperature of the polymer matrixes. The parts that need to be joined are exposed to an ultrasonic vibration. Remarkably, viscoelastic heating is the most significant of the various heating mechanisms in the USW. The friction of the plastic molecules rubbing against one another is to blame. As more deformation is produced, more heat will be generated.

Moreover, USW welding machines are similar, with some differences, such as frequency value or range and the geometry of the sonotrode. The USW machines for joining polymers have two main classifications which are continuous welding and the spot welding which are further classified as single, double, and multi. However, only a few studies investigate the impact of sonotrode geometry on enhancing the welding process parameters and

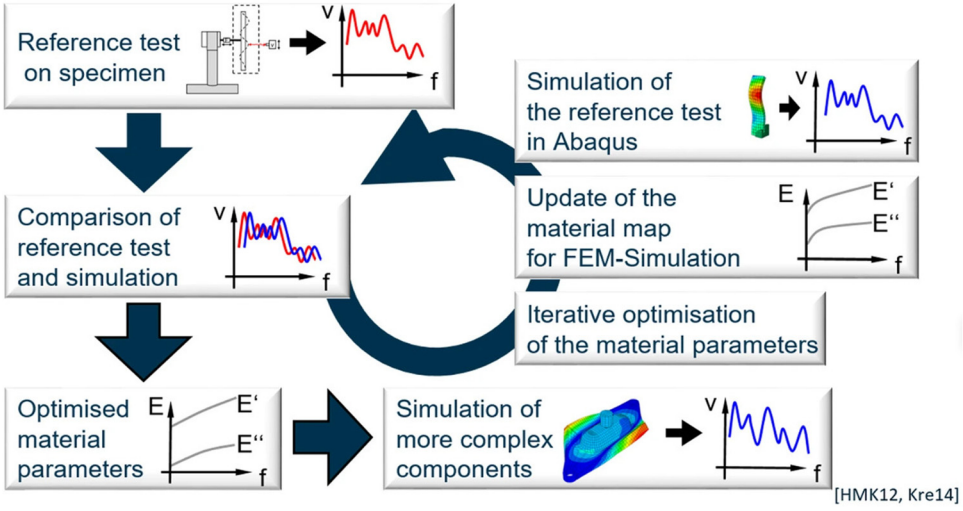

Figure 79: The schematic of material data determination overview based on reverse engineering approach [350].

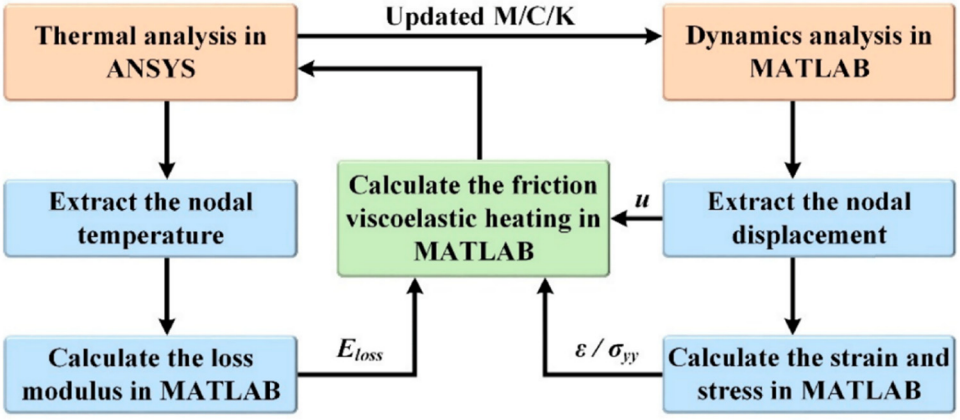

Figure 80: The computational methodology model for analyzing the thermal mechanical coupling [351].

the quality of welding. The range of process parameters, including power, energy, holding time, welding time, vibration time, holding time, vibrational amplitude, and frequency, are different based on the type of USW machine. Furthermore, accurate joint designs are ideal for concentrating ultrasonic energy at the welding interface. The USW process features are also strictly connected, demonstrating unusual sensitivity to the holding and tolerances of the components required to weld. The mechanical test shows that by comparing the LSS findings of coupling layers made of PEI and PEEK, both have the same thickness in dissimilar welding of CF/Ep and CF/PEEK, both materials show nearly comparable LSS values. In contrast, the USW process did not lead to any substantial damage in the mechanical properties in the interphase or the adherend in dissimilar welding. Based on the

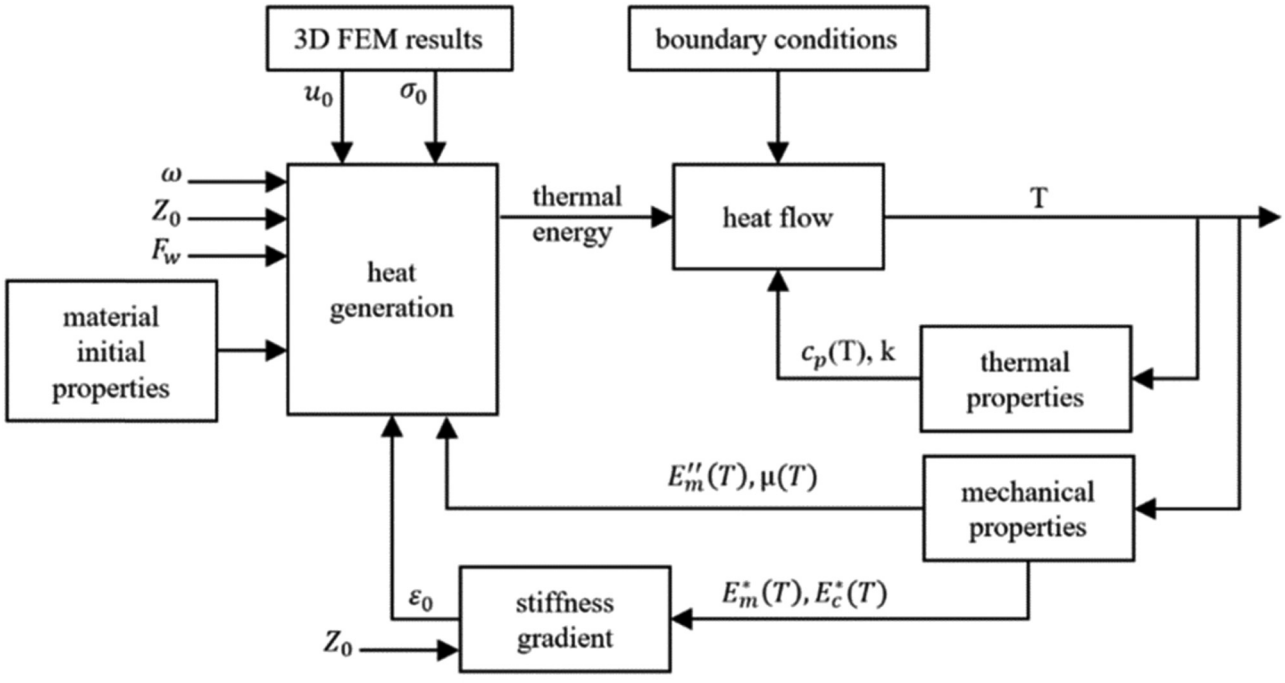

Figure 81: The numerical modeling by using the explicit finite difference method for various spots in USW: ω is the angular frequency, Z_0 is the applied displacement amplitude, F_w is the applied static weld pressure, u_0 is the interfacial slippage amplitude, $\mu(T)$ is the friction coefficient, ε_0 is the resolving strain amplitude, σ_0 is the interface pressure amplitude, T is temperature value, $E''_m(T)$ is the matrix loss modulus, $E^*m(T)$ is the matrix complex modulus, $c_p(T)$ is the composite specific heat capacity, k is the thermal conductivity of the composite, and $E^*c(T)$ is the composite complex modulus [352].

literature, some welding processes are controlled by other process parameters, such as welding energy, which may affect the required welding time and vibration time. Also, some parameters impact welding strength and mechanical properties more than the rest of the USW process parameters such as, welding time and welding force. Meanwhile, some parameters, such as frequency, are considered as a constant in most studies. However, raising the vibration time may cause an additional concentration of heat at the interface, and the temperature would reach the melting temperature of the polymer matrix. Moreover, an adequate flow in the resin at the interface was noticeable. Consequently, the interfacial bonding formed the intermediate between the two specimens of base materials by the resin fusion. Simultaneously, extreme heat can also be applied to the CFRP matrix. Owing to the significant variance amongst the thermal expansion coefficients, the voids appeared at the interface of the polymer resin and the CF and cracks. Consequently, in many cases, the bonding cannot be achieved without using ED or interlayer in USW. The energy-controlling mode is recommended for welding strength, and the displacement-controlling mode is preferable for welding quality. Nevertheless, one of the most significant essential rewards of USW, above short welding time, is that it is an environmentally benign method, and the joined welded pieces, after the USW, do not require any additional cleaning or treatment. Due to the nature of the process, which entails a very high strain due to the high vibrational frequency, USW is expected to have a very high instantaneous strain rate, which will affect the crystallization accordingly. Furthermore, the unique influences of fiber types and matrix scatterings on USW weldability are still unclear, and owing to the numerous physical properties of various materials, USW may have a more substantial impact on mechanical behavior and welding strength than others, including their melting and acoustic features. Besides, the weldability of various materials is identical.

The USW is a very effective method for joining CFRTPCs and CFRTSCs, whether by single or multiple spot welding. It can fabricate joints in comparably quick cycle times, and they are distinguished by performance

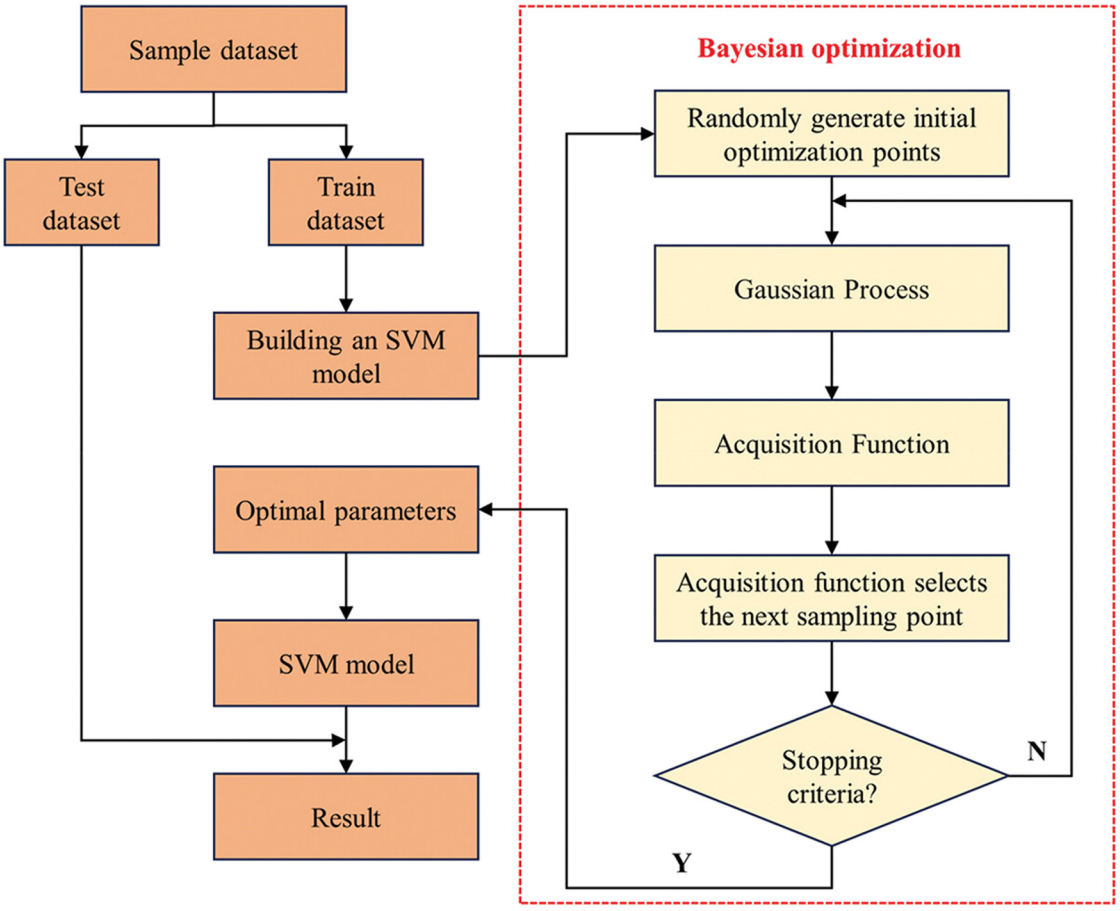

Figure 82: The BO-SVM flowchart [353].

that is equivalent to or better than that of mechanically or adhesively fastened joints. In order to achieve either growing welding pressure in a very short welding time or *vice versa*, a longer duration with less welding pressure is required; in this manner, the USW technique creates the entire joint between the layers. However, welding with high welding pressure and a short welding period causes insufficient heat dispersion, which prevents the acquisition of any anticipated junction. Furthermore, modern USW has made displacement-controlled welding possible, and this technique has numerous advantages over time, including energy-controlled welding. The surface friction causes the ED to heat up, and the time it takes to melt the EDs can vary. Unwelded portions occasionally have shiny, smooth mating fracture surfaces, which was indicative of an adhesive failure at the welding interface, which was caused by the interaction of rapid heating and relatively low temperatures in the overlap's center. While there is a large variety of resin volumes for which welds with a reasonable strength level can be achieved, an excessive quantity of resin at the welding interface causes a reduction in welding strength, as proven by previous studies. As an observation from the literature, most researchers have used PEEK, PEI, PE, Nylon (PA6, and PA66), and a few studies investigate the CFRTP (Elium®) and PPS. There are still some restrictions since when heating the polymers, poisonous gases can be generated; besides, despite the developed interest in natural fiber owing to its eco-friendly advantages, no records have been found on welding natural FRPs by USW.

7 Conclusion

This state-of-the-art review investigates the similar and dissimilar welded CFRP by the USW technology and discusses the welding process parameters and the pretreatment impact on the performed joint's mechanical properties and microstructure characterizations, while highlighting the recyclability of CFRPs and the fabrication process of polymer matrixes. Besides, the improvement of USW process by using ED and the challenges of USW were also addressed. The USW is considered as the fastest joining process, capable of joining either metal matrix/polymer matrix, polymer matrix/polymer matrix, or metal/metal. The main principle of USW is to transfer the vibrational motion into heat between the two adherend surfaces.

Based on the literature reviewed, the most favorable PCs matrix to be used in USW are CF/PEEK and Nylon (CF/PA6, CF/PA66); where significant mechanical and microstructure observations were noticeable, above other types of CFRP in similar/dissimilar welding. Moreover, using an appropriate type and orientation of ED enhances the welding process, weldment strength, and weldment quality. However, some restrictions must be considered while choosing the ED, such as its melting temperature, which must be less than the melting temperature of the CFRP to be welded, and optimum design geometry of ED.

There is a direct relation between the number of spots and welding strength and quality in all types of welded matrices. While the geometry of the sonotrode primarily affects the welded area, limited studies concentrated on studying the consequence of changing the geometry of the sonotrode on welding strength and quality due to its high cost, which may lead to unclear information about the effect of sonotrode geometry as the process parameter. Most studies that focused on investigating the impact of changing process parameters considered single or dual parameters as variable, and the remaining process parameters had constant values, in order to make the investigation easier and finding the optimum values in a more straightforward manner. Based on this perspective, the welding energy, vibration amplitude and welding time are the most critical parameters that enhance the weldment performance and welding quality.

The welding strength was found by investigating the mechanical properties through a mechanical test. Commonly, only two types of mechanical tests are processed: LSS or tensile tests. However, only a few studies were interested in a fatigue test. There are no recorded data about further mechanical tests, such as hardness or impact tests. The microstructure observation found the welding quality, usually through the SEM, after failure or fracture. Besides, the FE analysis and mathematical modeling are still limited. Additionally, the welding quality is directly influenced by material qualities and the temperature distribution within the welded adherend. Nonetheless, there is still an essential need for optimum EDs for similar and dissimilar joints by USW. A review of ML for ultrasonically welded CFRP may be considered in upcoming work. The vibrational and thermal tests of the joined CFRP were not considered in this review and can be covered in further work.

Acknowledgments: The authors extend their appreciation to the KEGA grant 009TUKE-4/2023 of the Slovak Grant Agency.

Funding information: This work was supported by KEGA grant 009TUKE-4/2023 of the Slovak Grant Agency.

Author contributions: All authors have accepted responsibility for the entire content of this manuscript and approved its submission.

Conflict of interest: David Hui, who is the co-author of this article, is a current Editorial Board member of *Reviews on Advanced Materials Science*. This fact did not affect the peer-review process. The authors declare no other conflict of interest.

Data availability statement: All data generated or analyzed during this study are included in this published article.

References

[1] Thapliyal, S. Ultrasonic welding – a modern welding technology for metals and plastics. *Advanced Welding and Deforming*, 2021, pp. 1–22.

[2] Ageorges, C., L. Ye, and M. Hou. Advances in fusion bonding techniques for joining thermoplastic matrix composites: a review. *Composites Part A: Applied Science and Manufacturing*, Vol. 32, 2001, pp. 839–857.

[3] Villegas, I. F. and H. E. N. Bersee. Ultrasonic welding of advanced thermoplastic composites: An investigation on energy-directing surfaces. *Advanced Polymer Technology*, Vol. 29, 2010, pp. 112–121.

[4] Benatar, A. Ultrasonic welding of plastics and polymeric composites. *Power Ultrasonics Applications of High-Intensity Ultrasound*, 2015, pp. 295–312.

[5] Villegas, I. F. and R. van Moorleghem. Ultrasonic welding of carbon/epoxy and carbon/PEEK composites through a PEI thermoplastic coupling layer. *Composites Part A: Applied Science and Manufacturing*, Vol. 109, 2018, pp. 75–83.

[6] Goto, K., K. Imai, M. Arai, and T. Ishikawa. Shear and tensile joint strengths of carbon fiber-reinforced thermoplastics using ultrasonic welding. *Composites Part A: Applied Science and Manufacturing*, Vol. 116, 2019, pp. 126–137.

[7] Tierney, J. J., J. W. Gillespie, and J. R. P-EB. Ultrasonic heating. *Comprehensive composite materials*, In: A. K. Zweben, Ed., 2000, pp. 1029–1047.

[8] Zhang, Z., X. Wang, Y. Luo, Z. Zhang, and L. Wang. Study on heating process of ultrasonic welding for thermoplastics. *Journal of Thermoplastic Composite Materials*, Vol. 23, 2010, pp. 647–664.

[9] Tolunay, M. N., P. R. Dawson, and K. K. Wang. Heating and bonding mechanisms in ultrasonic welding of thermoplastics. *Polymer Engineering and Science*, Vol. 23, 1983, pp. 726–733.

[10] Devine, J. Ultrasonic plastics welding basics. *Welding Journal (Miami, Fla)*, Vol. 80, 2001, pp. 29–33.

[11] Grewell, D. A., A. Benatar, J. B. Park, and C. Hanser. *Plastics and composites welding handbook*, 2003.

[12] Chuah, Y. K., L. H. Chien, B. C. Chang, and S. J. Liu. Effects of the shape of the energy director on far-field ultrasonic welding of thermoplastics. *Polymer Engineering and Science*, Vol. 40, 2000, pp. 157–167.

[13] Benatar, A., R. V. Eswaran, and S. K. Nayar. Ultrasonic welding of thermoplastics in the near-field. *Polymer Engineering and Science*, Vol. 29, 1989, pp. 1689–1698.

[14] Delzendehrooy, F., A. Akhavan-Safar, A. Q. Barbosa, R. Beygi, D. Cardoso, R. J. C. Carbas, et al. A comprehensive review on structural joining techniques in the marine industry. *Composite Structures*, Vol. 289, 2022, id. 115490.

[15] INSIGHT BR. *Ultrasonic Welding Systems Market Size, Share, Growth, Forecast 2030*, 2023.

[16] Zion market research. *Ultrasonic Welding Systems Market Size, Share, Growth, Forecast 2030*. 2023.

[17] Benatar, A. and T. G. Gutowski. Ultrasonic welding of PEEK graphite APC-2 composites. *Polymer Engineering and Science*, Vol. 29, 1989, pp. 1705–1721.

[18] Barnes, T. A. and I. R. Pashby. Joining techniques for aluminium spaceframes used in automobiles: Part II — adhesive bonding and mechanical fasteners. *Journal of Materials Processing Technology*, Vol. 99, 2000, pp. 72–79.

[19] Lu, H. M., A. Benatar, and F. G. C. He. Sequential ultrasonic welding of PEEK/Graphite composites plates. *Annual Technical Conference – ANTEC, Conference Proceedings*, Vol. 37, 1991.

[20] Bhudolia, S. K., G. Gohel, K. F. Leong, and A. Islam. Advances in ultrasonic welding of thermoplastic composites: A review. *Materials (Basel)*, Vol. 13, 2020, pp. 1284–1310.

[21] Sandeep, R. and A. Natarajan. Advances in joining technologies for the innovation of 21st century lightweight aluminium-CFRP hybrid structures. *Proceedings of the Institution of Mechanical Engineers, Part E: Journal of Process Mechanical Engineering*, Vol. 236, 2022.

[22] Liu, Z., Y. Li, Z. Liu, Y. Yang, Y. Li, and Z. Luo. Ultrasonic welding of metal to fiber-reinforced thermoplastic composites: A review. *Journal of Manufacturing Processes*, Vol. 85, 2023, pp. 702–712.

[23] Abbas, Z., L. Zhao, J. Deng, S. Wang, and W. Hong. Advances in ultrasonic welding of lightweight alloys: A review. *High Temperature Materials and Processes*, Vol. 42, 2023, pp. 1–25.

[24] Pramanik, A., A. K. Basak, Y. Dong, P. K. Sarker, M. S. Uddin, G. Littlefair, et al. Joining of carbon fibre reinforced polymer (CFRP) composites and aluminium alloys – A review. *Composites Part A: Applied Science and Manufacturing*, Vol. 101, 2017, pp. 1–29.

[25] Fan, Z., K. Bai, and C. Chen. The application of ultrasound in Joining: Principles, processes and properties. *Journal of Manufacturing Processes*, Vol. 101, 2023, pp. 269–299.

[26] Jiao, J., J. Xu, C. Jing, L. Sheng, H. Ru, and H. Xia. Laser welding process and strength enhancement of carbon fiber reinforced thermoplastic composites and metals dissimilar joint: A review. *Chinese Journal of Aeronautics*, Vol. 36, No. 12, 2023, pp. 13–31.

[27] Acherjee, B. Laser transmission welding of polymers – A review on welding parameters, quality attributes, process monitoring, and applications. *Journal of Manufacturing Processes*, Vol. 64, 2021, pp. 421–443.

[28] Li, W. and G. Palardy. Damage monitoring methods for fiber-reinforced polymer joints: A review. *Composite Structures*, Vol. 299, 2022, id. 116043.

[29] Li, J., Z. Zhang, J. Fu, Z. Liang, and K. R. Ramakrishnan. Mechanical properties and structural health monitoring performance of carbon nanotube-modified FRP composites: A review. *Nanotechnology Reviews*, Vol. 10, 2021, pp. 1438–1468.

[30] Silverman, E., R. Griese, E. M. Silverman, and R. A. Griese. Joining methods for graphite/PEEK thermoplastic composites. *Society for the Advancement of Material and Process Engineering*, Vol. 25, 1989, pp. 34–38.

[31] Forintos, N. and T. Czigany. Multifunctional application of carbon fiber reinforced polymer composites: Electrical properties of the reinforcing carbon fibers – A short review. *Composites, Part B: Engineering*, Vol. 162, 2019, pp. 331–343.

[32] Zeng, L., W. Tao, J. Zhao, Y. Li, and R. Li. Mechanical performance of a CFRP composite reinforced via gelatin-CNTs: A study on fiber interfacial enhancement and matrix enhancement. *Nanotechnology Reviews*, Vol. 11, 2022.

[33] Amanat, N., N. L. James, and D. R. McKenzie. Welding methods for joining thermoplastic polymers for the hermetic enclosure of medical devices. *Medical Engineering & Physics*, Vol. 32, 2010, pp. 690–699.
[34] Hamza, A. A. and S. R. Jalal. A review on manufacturing the polymer composites by friction stir processing. *European Polymer Journal*, Vol. 178, 2022, id. 111495.
[35] Asmael, M., B. Safaei, O. Kalaf, Q. Zeeshan, F. Aldakheel, T. Nasir, et al. Recent developments in tensile properties of friction welding of carbon fiber-reinforced composite: A review. *Nanotechnology Reviews*, Vol. 11, 2022, pp. 1408–1436.
[36] El-Sayed, M. M., A. Y. Shash, M. Abd-Rabou, and M. G. ElSherbiny. Welding and processing of metallic materials by using friction stir technique: A review. *Journal of Advanced Joining Processes*, Vol. 3, 2021, id. 100059.
[37] Wang, Y., Z. Rao, S. Liao, and F. Wang. Ultrasonic welding of fiber reinforced thermoplastic composites: Current understanding and challenges. *Composites Part A: Applied Science and Manufacturing*, Vol. 149, 2021, pp. 1–13.
[38] Zhao, P., S. Jia, C. Xiao, and J. Wang. Research progress in ultrasonic welding of fiber-reinforced polymeric composites. *Cailiao Gongcheng/Journal Materials Engineering*, Vol. 51, 2023, id. 21.
[39] Nagarajan, B. M. and M. Manoharan. Assessment of dissimilar joining between metal and polymer hybrid structure with different joining processes. *Journal of Thermoplastic Composite Materials*, Vol. 36, 2023, pp. 2169–2211.
[40] Ni, Z. L. and F. X. Ye. Ultrasonic spot welding of aluminum alloys: A review. *Journal of Manufacturing Processes*, Vol. 35, 2018, pp. 580–594.
[41] Bose, S., H. Chelladurai, and K. Ponappa. A review on recent developments in ultrasonic welding of polymers and polymeric composites. *Welding in the World*, Vol. 68, 2024, pp. 1–23.
[42] Mirzaahmadi, S., D. Akbari, and I. Ahadzadeh. Ultrasonic welding of glass fiber-reinforced epoxy composite using thermoplastic nanocomposites interlayer. *Transactions of the Indian Institute of Metals*, Vol. 77, 2024, pp. 1229–1238.
[43] Mahato, K. K., K. Dutta, and B. C. Ray. Static and dynamic behavior of fibrous polymeric composite materials at different environmental conditions. *Journal of Polymers and the Environment*, Vol. 26, 2018, pp. 1024–1050.
[44] Meschut, G., M. Merklein, A. Brosius, D. Drummer, L. Fratini, U. Füssel, et al. Review on mechanical joining by plastic deformation. *Journal of Advanced Joining Processes*, Vol. 5, 2022, id. 100113.
[45] Luckachan, G. E. and C. K. S. Pillai. Biodegradable polymers- a review on recent trends and emerging perspectives. *Journal of Polymers and the Environment*, Vol. 19, 2011, pp. 637–676.
[46] Paul, D., M. Gaff, D. Tesařová, D. Hui, and H. Li. Recent advancements in nanotechnology application on wood and bamboo materials: A review. *Nanotechnology Reviews*, Vol. 12, 2023, pp. 321–382.
[47] Alhijazi, M., Q. Zeeshan, B. Safaei, M. Asmael, and Z. Qin. Recent developments in palm fibers composites: a review. *Journal of Polymers and the Environment*, Vol. 28, 2020, pp. 3029–3054.
[48] Odesanya, K. O., R. Ahmad, M. Jawaid, S. Bingol, G. O. Adebayo, and Y. H. Wong. Natural fibre-reinforced composite for ballistic applications: a review. *Journal of Polymers and the Environment*, Vol. 29, 2021, pp. 3795–3812.
[49] Sun, H., X. Li, H. Li, D. Hui, M. Gaff, and R. Lorenzo. Nanotechnology application on bamboo materials: A review. *Nanothecnology Reviews*, Vol. 11, 2022, pp. 1–26.
[50] Gandini, A. and M. N. Belgacem. Recent contributions to the preparation of polymers derived from renewable resources. *Journal of Polymers and the Environment*, Vol. 10, 2002, pp. 105–114.
[51] Hosseini, S. B., M. Gaff, H. Li, and D. Hui. Effect of fiber treatment on physical and mechanical properties of natural fiber-reinforced composites: A review. *Reviews on Advanced Materials Science*, Vol. 62, 2023, pp. 1–17.
[52] Rafiee, R. and R. Shahzadi. Mechanical properties of nanoclay and nanoclay reinforced polymers: a review. *Polymer Composites*, Vol. 40, 2019, pp. 431–445.
[53] Hosseini, M., M. Gaff, H. Li, P. Konvalinka, J. Lair, D. Hui, et al. A review of the performance of fibre-reinforced composite laminates with carbon nanotubes. *Nanotechnology Reviews*, Vol. 12, 2023, id. 20230164.
[54] Francisco, D. L., L. B. Paiva, and W. Aldeia. Advances in polyamide nanocomposites: A review. *Polymer Composites*, Vol. 40, 2019, pp. 851–870.
[55] Gu, J. G. and J. D. Gu. Methods currently used in testing microbiological degradation and deterioration of a wide range of polymeric materials with various degree of degradability: A review. *Journal of Polymers and the Environment*, Vol. 13, 2005, pp. 65–74.
[56] Anugrahwidya, R., B. Armynah, and D. Tahir. Bioplastics starch-based with additional fiber and nanoparticle: characteristics and biodegradation performance: a review. *Journal of Polymers and the Environment*, Vol. 29, 2021, pp. 3459–3476.
[57] SJ, A. and A. Natarajan. Review on the advancements and relevance of emerging joining techniques for aluminium to polymers/carbon fibre-reinforced polymer lightweight hybrid structures. *Proceedings of the Institution of Mechanical Engineers, Part L: Journal of Materials: Design and Applications*, Vol. 236, No. 12, 2022, pp. 2394–2435.
[58] Xiao, H., M. T. H. Sultan, F. S. Shahar, M. Gaff, and D. Hui. Recent developments in the mechanical properties of hybrid fiber metal laminates in the automotive industry: A review. *Reviews on Advanced Materials Science*, Vol. 62, 2023, pp. 328–348.
[59] Zhang, C., G. Zhang, J. Xu, X. P. Shi, and X. Wang. Review of curing deformation control methods for carbon fiber reinforced resin composites. *Polymer Composites*, Vol. 43, 2022, pp. 3350–3370.
[60] Yu, T., S. A. Soomro, F. Huang, W. Wei, B. Wang, Z. Zhou, et al. Naturally or artificially constructed nanocellulose architectures for epoxy composites: A review. *Nanotechnology Reviews*, Vol. 9, 2020, pp. 1643–1659.
[61] Zhang, J., V. S. Chevali, H. Wang, and C. H. Wang. Current status of carbon fibre and carbon fibre composites recycling. *Composites, Part B: Engineering*, Vol. 193, 2020, id. 108053.
[62] Global Market Insights. *Carbon fiber composite market*, 2022.
[63] Bhudolia, S. K., G. Gohel, L. Kah Fai, and R. J. Barsotti. Fatigue response of ultrasonically welded carbon/Elium® thermoplastic composites. *Materials Letters*, Vol. 264, 2020, id. 127362.
[64] Villegas, I. F. Strength development versus process data in ultrasonic welding of thermoplastic composites with flat energy directors and its application to the definition of optimum processing parameters. *Composites Part A: Applied Science and Manufacturing*, Vol. 65, 2014, pp. 27–37.
[65] Villegas, I. F. In situ monitoring of ultrasonic welding of thermoplastic composites through power and displacement data. *Journal of Thermoplastic Composite Materials*, Vol. 28, 2015, pp. 66–85.

[66] Bhudolia, S. K., G. Gohel, L. K. Fai, and R. J. Barsotti. Investigation on ultrasonic welding attributes of novel carbon/elium® composites. *Materials (Basel)*, Vol. 13, 2020, pp. 1–18.
[67] Van Tooren, M. J. L. Method for bonding a thermoplastic polymer to a thermosetting polymer component. Pat., PCT/NL2012/OOOO3S. *Eur Pat Off*, 2012, pp. 1–21.
[68] Hou, M. Thermoplastic adhesive for thermosetting composites. *Materials Science Forum*, Vol. 706–709, 2012, pp. 2968–2973.
[69] Adams, R. D. and P. Cawley. A review of defect types and nondestructive testing techniques for composites and bonded joints. *NDT International*, Vol. 21, 1988, pp. 208–222.
[70] Zhang, G. P., J. C. Li, Z. X. Liu, and P. C. Wang. Application of ultrasonic welding to repair adhesively bonded short carbon fiber reinforced Nylon 6 composites. *International Journal of Adhesion and Adhesives*, Vol. 100, 2020, pp. 1–12.
[71] Tian, Z. G., L. Y. Chen, G. P. Zhang, Z. X. Liu, and P. C. Wang. Nondestructive evaluation of bond quality of adhesively joined carbon fiber/nylon 6 composites. *Journal of Adhesion*, Vol. 94, 2018, pp. 668–688.
[72] Zhao, T., G. Palardy, I. F. Villegas, C. Rans, M. Martinez, and R. Benedictus. Mechanical behaviour of thermoplastic composites spot-welded and mechanically fastened joints: A preliminary comparison. *Composites, Part B: Engineering*, Vol. 112, 2017, pp. 224–234.
[73] Schwartz, M. M. *Joining of composite-matrix materials*, ASM International, Michigan, USA, 1994.
[74] Stavrov, D. and H. E. N. Bersee. Resistance welding of thermoplastic composites-an overview. *Composites Part A: Applied Science and Manufacturing*, Vol. 36, 2005, pp. 39–54.
[75] Davies, P., W. J. Cantwell, P. Y. Jar, P. E. Bourban, V. Zysman, and H. H. Kausch. Joining and repair of a carbon fibre-reinforced thermoplastic. *Composites*, Vol. 22, 1991, pp. 425–431.
[76] Siddique, A., Z. Iqbal, Y. Nawab, and K. Shaker. A review of joining techniques for thermoplastic composite materials. *Journal of Thermoplastic Composite Materials*, Vol. 36, 2022, pp. 3417–3454.
[77] Li, W. and G. Palardy. Electro-mechanical response of ultrasonically welded thermoplastic composite interfaces under static and cyclic flexural loads using nanocomposites. *CS Applied Polymer Materials*, Vol. 4, 2022, pp. 5209–5223.
[78] Ochôa, P., I. F. Villegas, R. M. Groves, and R. Benedictus. Diagnostic of manufacturing defects in ultrasonically welded thermoplastic composite joints using ultrasonic guided waves. *NDT E International*, Vol. 107, 2019, pp. 1–10.
[79] Rohart, V., L. Laberge Lebel, and M. Dubé. Improved adhesion between stainless steel heating element and PPS polymer in resistance welding of thermoplastic composites. *Composites, Part B: Engineering*, Vol. 188, 2020, id. 107876.
[80] Yousefpour, A., M. Hojjati, and J. P. Immarigeon. Fusion bonding/welding of thermoplastic composites. *Journal of Thermoplastic Composite Materials*, Vol. 17, 2004, pp. 303–341.
[81] Yusoff, S. N., H. Ramli, N. F. Zainal, S. I. Halim, and C. H. Chan. Thermoplastic-based polymer blend nanocomposites for energy storage. *Polymer Blend Nanocomposites for Energy Storage Applications*, 2023.
[82] Ahmad, Z., M. K. Abdullah, M. Zeshan, and M. Z. Ali. Introduction to polymers. *Polymers in Electronics*, 2023, pp. 3–31.
[83] Bhudolia, S. K., P. Perrotey, and S. C. Joshi. Mode I fracture toughness and fractographic investigation of carbon fibre composites with liquid Methylmethacrylate thermoplastic matrix. *Composites, Part B: Engineering*, Vol. 134, 2018, pp. 246–253.
[84] Bhudolia, S. K., S. C. Joshi, and Y. D. Boon. Experimental and microscopic investigation on mechanical performance of textile spread-tow thin ply composites. *Fibers and Polymers*, Vol. 20, 2019, pp. 1036–1045.
[85] Bhudolia, S. K., P. Perrotey, and S. C. Joshi. Experimental investigation on suitability of carbon fibre thin plies for racquets. *Journal of Sports Engineering and Technology*, Vol. 230, 2015, pp. 64–72.
[86] Bhudolia, S. K., S. C. Joshi, A. Bert, B. Yi Di, R. Makam, and G. Gohel. Flexural characteristics of novel carbon methylmethacrylate composites. *Composites Communications*, Vol. 13, 2019, pp. 129–133.
[87] Bhudolia, S. K. and S. C. Joshi. Low-velocity impact response of carbon fibre composites with novel liquid methylmethacrylate thermoplastic matrix. *Composite Structures*, Vol. 203, 2018, pp. 696–708.
[88] Bhudolia, S. K., S. C. Joshi, A. Bert, G. R. Gohel, and M. Raama. Energy characteristics and failure mechanisms for textile spread tow thin ply thermoplastic composites under low-velocity impact. *Fibers and Polymers*, Vol. 20, 2019, pp. 1716–1725.
[89] Bhudolia, S. K., P. Perrotey, and S. C. Joshi. Enhanced vibration damping and dynamic mechanical characteristics of composites with novel pseudo-thermoset matrix system. *Composite Structures*, Vol. 179, 2017, pp. 502–513.
[90] Shogren, R. L., G. Selling, and J. L. Willett. Effect of Orientation on the Morphology and Mechanical Properties of PLA/Starch Composite Filaments. *Journal of Polymers and the Environment*, Vol. 19, 2011, id. 19.
[91] Chen, C. W., H. I. Mao, H. K. Lee, J. Y. Chou, and S. P. Rwei. Upcycling recycled epoxy-based vitrimer for enhancing toughness of poly(ethylene terephthalate). *Journal of Polymers and the Environment*, Vol. 32, 2023, pp. 621–631.
[92] Luan, C., X. Yao, and J. Fu. Fabrication and characterization of in situ structural health monitoring hybrid continuous carbon/glass fiber-reinforced thermoplastic composite. *The International Journal of Advanced Manufacturing Technology*, Vol. 116, 2021, pp. 3207–3215.
[93] Kord, B., M. Jamshidi, and S. K. Hosseinihashemi. Effect of multiwalled carbon nanotubes on viscoelastic properties of PP/reed flour composites. *Journal of Polymers and the Environment*, Vol. 25, 2017, pp. 1313–1320.
[94] Shi, H., J. Sinke, and R. Benedictus. Surface modification of PEEK by UV irradiation for direct co-curing with carbon fibre reinforced epoxy prepregs. *International Journal of Adhesion and Adhesives*, Vol. 73, 2017, pp. 51–57.
[95] Talbott, M. F., G. S. Springer, and L. A. Berglund. The effects of crystallinity on the mechanical properties of PEEK polymer and graphite fiber reinforced PEEK. *Journal of Composite Materials*, Vol. 21, 2016, pp. 1056–1081.
[96] Li, C. S., C. Vannabouathong, S. Sprague, and M. Bhandari. The use of carbon-fiber-reinforced (CFR) peek material in orthopedic implants: A systematic review. *Clinical Medicine Insights Arthritis and Musculoskeletal Disorders*, Vol. 8, 2014, pp. 33–45.
[97] Crevecoeur, G. and G. Groeninckx. Binary blends of poly(ether ether ketone) and poly(ether imide). Miscibility, crystallization behavior, and semicrystalline morphology. *Macromolecules*, Vol. 24, 1991, pp. 1190–1195.
[98] Muthuraj, R., Y. Grohens, and B. Seantier. Mechanical and thermal insulation properties of elium acrylic resin/cellulose nanofiber based composite aerogels. *Nano-Structures and Nano-Objects*, Vol. 12, 2017, pp. 68–76.

[99] Malyuta, D. A. I., K. L. Matteson, C. Ryan, M. P. Berry, and D. Bajwa. An investigation into the tensile properties of recycled high-density polyethylene (rHDPE) blended with talc filler. *Results in Materials*, Vol. 17, 2023, pp. 1–9.

[100] Greene, J. P. Microstructures of polymers. *Automotive Plastic Components*, 2021.

[101] Liyana Bekri, N., I. Idris, A. Md Som, M. Nazri Murat, F. Sholahudin Rohman, R. Ahmad Ilyas, et al. Study of input parameter changes toward low density polyethylene's product properties. *Materials Today: Proceedings*, Vol. 74, 2023, pp. 425–432.

[102] Kumar, V., I. S. Ahuja, and R. Singh. Multi-factor optimization for preparation of mechanical blended and chemical assisted mechanical blended ABS-graphene composite for 3D printing. *Encyclopedia of Materials Plastics & Polymers*, 2022, pp. 281–287.

[103] Duleba, B., E. Spišák, and F. Greškovič. Mechanical properties of PA6/MMT polymer nanocomposites and prediction based on content of nanofiller. *Procedia Engineering*, Vol. 96, 2014, pp. 75–80.

[104] Marais, S., Q. Lozay, N. Follain, J. Soulestin, N. Couvrat, and E. Dargent. Multinanolayered PA6/Cloisite and PE/PA6/Cloisite composites: Structure, mechanical and barrier properties. *Composites, Part B: Engineering*, Vol. 271, 2024, id. 111167.

[105] Sastri, V. R. Engineering thermoplastics: Acrylics, polycarbonates, polyurethanes, polyacetals, polyesters, and polyamides. *Plastics in Medical Devices*, 2022, pp. 167–232.

[106] Truckenmüller, R., Y. Cheng, R. Ahrens, H. Bahrs, G. Fischer, and J. Lehmann. Micro ultrasonic welding: joining of chemically inert polymer microparts for single material fluidic components and systems. *Microsystem Technologies*, Vol. 12, 2006, pp. 1027–1029.

[107] Maddock, N. A., N. L. James, D. R. McKenzie, and J. F. Patrick. Technological advances for polymers in active implantable medical devices. *The Design and Manufacture of Medical Devices*, 2012, pp. 239–272.

[108] Jiang, S., G. Liao, D. Xu, F. Liu, W. Li, Y. Cheng, et al. Mechanical properties analysis of polyetherimide parts fabricated by fused deposition modeling. *High Performance Polymers*, Vol. 31, 2019, pp. 97–106.

[109] Chowdhury, S., B. Pal, and P. Datta. *Composite biomaterials for bone grafting and other biomedical applications*, Elsevier, West Bengal, India, 2022.

[110] Chen, X. Y., A. Romero, A. Paton-Carrero, M. P. Lavin-Lopez, L. Sanchez-Silva, J. L. Valverde, et al. Functionalized graphene-reinforced foams based on polymer matrices: Processing and applications. *Functionalized Graphene Nanocomposites and their Derivatives Synth Process Appl*, 2018.

[111] Al-Haydari, I. S. and H. S. Al-Haidari. Mechanical properties of polyethylene terephthalate-modified pavement mixture. *IOP Conference Series: Materials Science and Engineering*, Vol. 870, 2020, id. 012073.

[112] Hamdi, D. A. Investigating the mechanical and microstructure properties of ceramic-PMMA polymer composite. *AIP Conference Proceedings*, Vol. 2213, 2020, id. 020043.

[113] Agrawal, S., D. Patidar, M. Dixit, K. Sharma, and N. S. Saxena. Investigation of thermo-mechanical properties of PMMA. *AIP Conference Proceedings*, Vol. 1249, 2010, pp. 79–82.

[114] Özkan Gülsoy, H. and M. Taşdemir. Physical and mechanical properties of polypropylene reinforced with Fe particles. *International Journal of Polymeric Materials and Polymeric Biomaterials*, Vol. 55, 2006, pp. 619–626.

[115] Hassan Awad, A., R. El Gamasy, A. Abd El Wahab, and M. Hazem Abdellatif. Mechanical and physical properties of PP and HDPE. *Engineering and Science*, Vol. 4, 2019, id. 34.

[116] Balani, K., V. Verma, A. Agarwal, and R. Narayan. Physical, thermal, and mechanical properties of polymers. *Biosurfaces*, 2015, pp. 329–344.

[117] Sun, Z., L. Sun, C. Zhu, W. Tian, L. Shao, X. Feng, et al. Effect of polyphenylene sulphide particles and films on the properties of polyphenylene sulphide composites. *Materials (Basel)*, Vol. 15, 2022, pp. 1–13.

[118] Yan, Y. Developments in fibers for technical nonwovens. *Advances in technical nonwovens*, 2016.

[119] Park, S. J. and M. K. Seo. Element and processing. *Interface science and technology*, 18th ed., Elsevier, Incheon, South Korea, 2011, pp. 431–499.

[120] Al-Shalchy, S. I., K. M. Shabeeb, A. M. Hasan, and R. F. Hasan. Mechanical properties of polyvinyl chloride and polypropylene hybrid polymeric nanocomposites for structural applications. *International Journal of Nanoelectronics & Materials*, Vol. 13, 2020, pp. 249–262.

[121] Sterzyński, T., J. Tomaszewska, J. Andrzejewski, and K. Skórczewska. Evaluation of glass transition temperature of PVC/POSS nanocomposites. *Composites Science and Technology*, Vol. 117, 2015, pp. 398–403.

[122] Reding, F. P., E. R. Walter, and F. J. Welch. Glass transition and melting point of poly(vinyl chloride). *Journal of Polymer Science*, Vol. 56, 1962, pp. 225–231.

[123] Gaur, A., D. Rana, and P. Maiti. Mechanical and wear behaviour of poly(vinylidene fluoride)/clay nanocomposite. *Journal of Materials Research and Technology*, Vol. 8, 2019, pp. 5874–5881.

[124] Feiring, A. E. Fluorine-containing polymers. *Encyclopedia of Materials: Science and Technology*, 2001.

[125] Koerner, G. R., Y. G. Hsuan, and R. M. Koerner. The durability of geosynthetics. *Geosynthetics in Civil Engineering*, 2006, pp. 36–65.

[126] Goudarzian, N., M. Esmaeli, S. M. Mousavi, S. A. Hashemi, M. Zarei, A. Gholami, et al. Preparation physical, mechanical properties and biodegradable study of SAN/EOC/nanoclay/proteins nanocomposite. *Polymers from Renewable Resources*, Vol. 12, 2020, pp. 19–34.

[127] Solakoglu, I., S. Ataoglu, A. N. Gulluoglu, and N. Kadioglu. Temperature dependent mechanical characterisation of styrene-acrylonitrile. *Polymers and Polymer Composites*, Vol. 17, 2009, pp. 247–252.

[128] Offringa, A. R. Thermoplastic composites – rapid processing applications. *Composites Part A: Applied Science and Manufacturing*, Vol. 27, 1996, pp. 329–336.

[129] Singh, R., R. Kumar, L. Feo, and F. Fraternali. Friction welding of dissimilar plastic/polymer materials with metal powder reinforcement for engineering applications. *Composites, Part B: Engineering*, Vol. 101, 2016, pp. 77–86.

[130] Rizzolo, R. H. and D. F. Walczyk. Ultrasonic consolidation of thermoplastic composite prepreg for automated fiber placement. *Journal of Thermoplastic Composite Materials*, Vol. 29, 2016, pp. 1480–1497.

[131] Balle, F., S. Emrich, G. Wagner, D. Eifler, A. Brodyanski, and M. Kopnarski. Improvement of ultrasonically welded aluminum/carbon fiber reinforced polymer-joints by surface technology and high resolution analysis. *Advanced Engineering Materials*, Vol. 15, 2013, pp. 814–820.

[132] Anaç, N. The mechanical properties of dissimilar/similar polymer materials joined by friction stir welding. *Heliyon*, Vol. 9, 2023, id. e17627.
[133] Jagadeesh, P., M. Puttegowda, O. P. Oladijo, C. W. Lai, S. Gorbatyuk, D. Matykiewicz, et al. A comprehensive review on polymer composites in railway applications. *Polymer Composites*, Vol. 43, 2022, pp. 451–464.
[134] Han, S., X. Guang, Z. Li, and Y. Li. Joining processes of CFRP-Al sheets in automobile lightweighting technologies: A review. *Polymer Composites*, Vol. 43, 2022, pp. 8622–8633.
[135] Qiao, Y., L. D. Fring, M. R. Pallaka, and K. L. Simmons. A review of the fabrication methods and mechanical behavior of continuous thermoplastic polymer fiber–thermoplastic polymer matrix composites. *Polymer Composites*, Vol. 44, 2023, pp. 694–733.
[136] Bhat, A., S. Budholiya, S. A. Raj, M. T. H. Sultan, D. Hui, A. U. M. Shah, et al. Review on nanocomposites based on aerospace applications. *Nanotechnology Reviews*, Vol. 10, 2021, pp. 237–253.
[137] Gopinath, S., N. N. Adarsh, P. Radhakrishnan Nair, and S. Mathew. Recent trends in thermo-responsive elastomeric shape memory polymer nanocomposites. *Polymer Composites*, Vol. 44, 2023, pp. 4433–4458.
[138] Gopinath, S., N. N. Adarsh, P. R. Nair, and S. Mathew. Shape-memory polymer nanocomposites of poly(ϵ-caprolactone) with the polystyrene- block-polybutadiene- block-polystyrene-tri-block copolymer encapsulated with metal oxides. *ACS Omega*, Vol. 6, 2021, pp. 6261–6273.
[139] Cao, Y. Z., H. B. Wei, J. Wang, Z. Yu, and D. H. Li. Application of polyetheretherketone and its composite as frameworks in fixed dental prostheses. *Zhonghua kou qiang yi xue za zhi*, Vol. 54, 2019, pp. 773–777.
[140] Popp, J. and D. Drummer. Joining of continuous fiber reinforced thermoplastic/steel hybrid parts via undercutting pin structures and infrared heating. *Journal of Advanced Joining Processes*, Vol. 5, 2022, id. 100084.
[141] Hussen, M. S., Y. Kyosev, K. Pietsch, T. Pilling, J. Boll, and A. K. Kabish. Uncovering the peel strength performance of multi-layer ultrasonic weld seams in PVC-coated hybrid textiles for weather protection. *Journal of Advanced Joining Processes*, Vol. 8, 2023, id. 100151.
[142] Wang, F., P. Zhang, J. Luo, B. Li, G. Liu, and X. Zhan. Effect of heat input on temperature characteristics and fusion behavior at bonding interface of CFRTP induction welded joint with carbon fiber susceptor. *Polymer Composites*, Vol. 44, 2023, pp. 1586–1602.
[143] Liu, A., Y. Zou, Y. Chen, J. Hu, and B. Wang. Experimental investigation of impact resistance and compression behavior of CF/PEEK laminates after hot-press fusion repair with different stacking sequences. *Polymer Composites*, Vol. 32, 2023, pp. 621–631.
[144] Takeda, N. Characterization of microscopic damage in composite laminates and real-time monitoring by embedded optical fiber sensors. *International Journal of Fatigue*, Vol. 24, 2002, pp. 281–289.
[145] Lin, L. Y., J. H. Lee, C. E. Hong, G. H. Yoo, and S. G. Advani. Preparation and characterization of layered silicate/glass fiber/epoxy hybrid nanocomposites via vacuum-assisted resin transfer molding (VARTM). *Composites Science and Technology*, Vol. 66, 2006, pp. 2116–2125.
[146] Francis, J. N., I. Banerjee, A. Chugh, and J. Singh. Additive manufacturing of polyetheretherketone and its composites: A review. *Polymer Composites*, Vol. 43, 2022, pp. 5802–5819.
[147] Darji, V., S. Singh, and H. S. Mali. Mechanical characterization of additively manufactured polymer composites: A state-of-the-art review and future scope. *Polymer Composites*, Vol. 44, 2023, pp. 4370–441.
[148] Iwata, K., A. Suzuki, S. G. Kim, N. Takata, and M. Kobashi. Enhancing the solid-state joinability of A5052 and CFRTP via an additively manufactured micro-structure. *Journal of Materials Processing Technology*, Vol. 306, 2022, id. 117629.
[149] Pinto, G. M., J. M. O. Cremonezzi, H. Ribeiro, R. J. E. Andrade, N. R. Demarquette, and G. J. M. Fechine. From two-dimensional materials to polymer nanocomposites with emerging multifunctional applications: A critical review. *Polymer Composites*, Vol. 44, 2023, pp. 1438–1470.
[150] Azizli, M. J., A. Ghadami, E. Vafa, K. Rezaeeparto, S. Parham, M. Mokhtary, et al. Compatibilization of immiscible PA6/PLA nanocomposites using graphene oxide and PTW compatibilizer for high thermal and mechanical applications. *Journal of Polymers and the Environment*, Vol. 31, 2023, pp. 4193–4209.
[151] Murariu, M., A. L. Dechief, Y. Paint, S. Peeterbroeck, L. Bonnaud, and P. Dubois. Polylactide (PLA)-halloysite nanocomposites: Production, morphology and key-properties. *Journal of Polymers and the Environment*, Vol. 20, 2012, pp. 932–943.
[152] Naik, T. P., I. Singh, and A. K. Sharma. Processing of polymer matrix composites using microwave energy: A review. *Composites Part A: Applied Science and Manufacturing*, Vol. 156, 2022, id. 106870.
[153] Melentiev, R., A. Yudhanto, R. Tao, T. Vuchkov, and G. Lubineau. Metallization of polymers and composites: State-of-the-art approaches. *Materials & Design*, Vol. 221, 2022, id. 110958.
[154] Gupta, S., A. Sharma, R. K. Varma, and V. Kushvaha. A review on performance of near-surface mounted-carbon fiber-reinforced polymer laminates bonded into slits. *Polymer Composites*, Vol. 43, 2022, pp. 6782–6802.
[155] Eratbeni, M. G., and Y. Rostamiyan. Vibration behavior of a carbon fiber-reinforced polymer composite sandwich panel: rhombus core versus elliptical core. *Polymer Composites*, Vol. 44, No. 3, 2023, pp. 1741–1751.
[156] Miranda Campos, B., S. Bourbigot, G. Fontaine, and F. Bonnet. Thermoplastic matrix-based composites produced by resin transfer molding: A review. *Polymer Composites*, Vol. 43, 2022, pp. 2485–2506.
[157] Takahashi, J. and T. Ishikawa. Current Japanese activity in CFRTP for industrial application. *Composites WEEK LEUVEN TEXCOMP-11 Conf*, 2013.
[158] Ishikawa, T., K. Amaoka, Y. Masubuchi, T. Yamamoto, A. Yamanaka, M. Arai, et al. Overview of automotive structural composites technology developments in Japan. *Composites Science and Technology*, Vol. 155, 2018, pp. 221–246.
[159] Duflou, J. R., J. De Moor, I. Verpoest, and W. Dewulf. Environmental impact analysis of composite use in car manufacturing. *CIRP Annals – Manufacturing Technology*, Vol. 58, 2009, pp. 9–12.
[160] Mubashir, S. and S. B. Muttana. Carbon fibre composites: Outlook for the automobile sector. *Auto Tech Review*, Vol. 1, 2012, pp. 18–23.
[161] Sawpan, M. A. Experimental investigation of long term seawater durability and shear properties of pultruded GFRP composite. *Journal of Polymers and the Environment*, Vol. 29, 2021, pp. 3574–3586.

[162] Kafodya, I., G. Xian, and H. Li. Durability study of pultruded CFRP plates immersed in water and seawater under sustained bending: Water uptake and effects on the mechanical properties. *Composites, Part B: Engineering*, Vol. 70, 2015, pp. 138–148.

[163] Bazli, M., H. Ashrafi, and A. V. Oskouei. Effect of harsh environments on mechanical properties of GFRP pultruded profiles. *Composites, Part B: Engineering*, Vol. 99, 2016, pp. 203–215.

[164] Cheng, H., H. Huang, Z. Liu, and J. Zhang. Reaction kinetics of CFRP degradation in supercritical fluids. *Journal of Polymers and the Environment*, Vol. 26, 2018, pp. 2153–2165.

[165] Jongbloed, B., J. Teuwen, R. Benedictus, and I. F. Villegas. On differences and similarities between static and continuous ultrasonic welding of thermoplastic composites. *Composites, Part B: Engineering*, Vol. 203, 2020, pp. 1–14.

[166] Jaeschke, P., D. Herzog, H. Haferkamp, C. Peters, and A. S. Herrmann. Laser transmission welding of high-performance polymers and reinforced composites – a fundamental study. *Journal of Reinforced Plastics and Composites*, Vol. 29, 2010, pp. 3083–3094.

[167] Bayerl, T., M. Duhovic, P. Mitschang, and D. Bhattacharyya. The heating of polymer composites by electromagnetic induction – A review. *Composites Part A: Applied Science and Manufacturing*, Vol. 57, 2014, pp. 27–40.

[168] Kumar, R., R. Singh, I. P. S. Ahuja, R. Penna, and L. Feo. Weldability of thermoplastic materials for friction stir welding- A state of art review and future applications. *Composites, Part B: Engineering*, Vol. 137, 2018, pp. 1–15.

[169] Kumar, S., C. S. Wu, G. K. Padhy, and W. Ding. Application of ultrasonic vibrations in welding and metal processing: A status review. *Journal of Manufacturing Processes*, Vol. 26, 2017, pp. 295–322.

[170] Zhao, T., C. Broek, G. Palardy, I. F. Villegas, and R. Benedictus. Towards robust sequential ultrasonic spot welding of thermoplastic composites: Welding process control strategy for consistent weld quality. *Composites Part A: Applied Science and Manufacturing*, Vol. 109, 2018, pp. 355–367.

[171] Gutnik, V. G., N. V. Gorbach, and A. V. Dashkov. Some characteristics of ultrasonic welding of polymers. *Fibre Chemistry*, Vol. 34, 2002, pp. 426–432.

[172] Sackmann, J., K. Burlage, C. Gerhardy, B. Memering, S. Liao, and W. K. Schomburg. Review on ultrasonic fabrication of polymer micro devices. *Ultrasonics*, Vol. 56, 2015, pp. 189–200.

[173] Hongoh, M., M. Yoshikuni, H. Miura, T. Ueoka, and J. Tsujino. Configuration of a 20-mm-diameter 150 kHz ultrasonic longitudinal vibration system for plastic welding. *Proceedings – IEEE Ultrasonics Symposium*, Vol. 3, 2004, pp. 2326–2329.

[174] Nonhof, C. J. and G. A. Luiten. Estimates for process conditions during the ultrasonic welding of thermoplastics. *Polymer Engineering and Science*, Vol. 36, 1996, pp. 1177–1183.

[175] Stokes, V. K. Joining methods for plastics and plastic composites: An overview. *Polymer Engineering and Science*, Vol. 29, 1989, pp. 1310–1324.

[176] Patel, V. K., S. D. Bhole, and D. L. Chen. Ultrasonic spot welding of dissimilar 2024Al alloy and SiCp/2009Al composite. *Journal of Materials: Design and Applications*, Vol. 233, 2018, pp. 531–538.

[177] Patel, V. K., S. D. Bhole, and D. L. Chen. Microstructure and mechanical properties of dissimilar welded Mg–Al joints by ultrasonic spot welding technique. *Science and Technology of Welding and Joining*, Vol. 17, 2012, pp. 202–206.

[178] Abbas, Z., J. Deng, L. Zhao, and M. S. Islam. Surface-conformed approach for mechanical property analysis using ultrasonic welding of dissimilar metals. *The International Journal of Advanced Manufacturing Technology*, Vol. 132, 2024, pp. 3447–3466.

[179] Shimada, S., H. Tanaka, K. Hasebe, N. Hayashi, Y. Ochi, T. Matsui, et al. Ultrasonic welding of polymer optical fibres onto composite materials. *Electronics Letters*, Vol. 52, 2016, pp. 1472–1474.

[180] Kempe, G., H. Krauss, and G. Korger-Roth. Adhesion and welding of continuous carbon-fiber reinforced polyether etherketone (CF-PEEK/APC2). *Developments in the Science and Technology of Composite Materials*, 1990, pp. 105–112.

[181] Biswal, A. K., A. Nandi, H. Wang, and A. Vashisth. Ultrasonic welding of fiber reinforced vitrimer composites. *Composites Science and Technology*, Vol. 242, 2023, id. 110202.

[182] Sadeghi, M., M. Golzar, D. Akbari, and M. R. Karafi. Ultrasonic welding of composite laminate GF/PA6: Weldability and weld quality by current and strength. *Journal of Reinforced Plastics and Composites*, 2024.

[183] BRANSON. *Polymers: Characteristics and compatibility for ultrasonic assembly*, 2009.

[184] Staab, F., M. Liesegang, and F. Balle. Local shear strength distribution of ultrasonically welded hybrid Aluminium to CFRP joints. *Composite Structures*, Vol. 248, 2020, pp. 1–7.

[185] Wagner, G., F. Balle, and D. Eifler. Ultrasonic welding of aluminum alloys to fiber reinforced polymers. *Advanced Engineering Materials*, Vol. 15, 2013, pp. 792–803.

[186] Balle, F. and D. Eifler. Statistical test planning for ultrasonic welding of dissimilar materials using the example of aluminum-carbon fiber reinforced polymers (CFRP) joints. *Materialwissenschaft und Werkstofftechnik*, Vol. 43, 2012, pp. 286–292.

[187] Kawakami, K. and K. Yasuda. Utrasonic joining of carbon fiber reinforced thermoplastic and magnesium alloy. *2019 IEEE CPMT Symp Japan, ICSJ 2019*, 2019, pp. 135–137.

[188] Volkov, S. S., G. A. Bigus, and A. L. Remizov. Ultrasonic welding of dissimilar plastics. *Russian Engineering Research*, Vol. 38, 2018, pp. 281–284.

[189] Tsiangou, E., S. Teixeira de Freitas, I. F. Villegas, and R. Benedictus. Ultrasonic welding of epoxy- to polyetheretherketone-based composites: Investigation on the material of the energy director and the thickness of the coupling layer. *Journal of Composite Materials*, Vol. 54, 2020, pp. 3081–3098.

[190] Fernandez Villegas, I. and P. Vizcaino Rubio. On avoiding thermal degradation during welding of high-performance thermoplastic composites to thermoset composites. *Composites Part A: Applied Science and Manufacturing*, Vol. 77, 2015, pp. 172–180.

[191] Deng, S., L. Djukic, R. Paton, and L. Ye. Thermoplastic–epoxy interactions and their potential applications in joining composite structures – A review. *Composites Part A: Applied Science and Manufacturing*, Vol. 68, 2015, pp. 121–132.

[192] Oliver Schieler, U. B. Induction welding of hybrid thermoplastic-thermoset composite parts. *Applied Science and Engineering Progress*, Vol. 9, 2015, pp. 27–36.

[193] Vandi, L. J., M. Hou, M. Veidt, R. Truss, M. Heitzmann, and R. Paton. Interface diffusion and morphology of aerospace grade epoxy co-cured with thermoplastic polymers. *28th Congress of the International Council of the Aeronautical Sciences 2012, ICAS*, Vol. 3, 2012, pp. 1–9.

[194] Lestriez, B., J. P. Chapel, and J. F. Gérard. Gradient interphase between reactive epoxy and glassy thermoplastic from

dissolution process, reaction kinetics, and phase separation thermodynamics. *Macromolecules*, Vol. 34, 2001, pp. 1204–1213.
[195] Heitzmann, M. T., M. Hou, M. Veidt, L. J. Vandi, and R. Paton. Morphology of an interface between polyetherimide and epoxy prepreg. *Advances in Materials Research*, Vol. 393–395, 2012, pp. 184–188.
[196] Lionetto, F., M. N. Morillas, S. Pappadà, G. Buccoliero, I. Fernandez Villegas, and A. Maffezzoli. Hybrid welding of carbon-fiber reinforced epoxy based composites. *Composites Part A: Applied Science and Manufacturing*, Vol. 104, 2018, pp. 32–40.
[197] Liu, Z., Y. Li, Y. Wang, B. I. Epureanu, and M. Banu. Nonlinear friction behavior in ultrasonic welding of aluminum alloy to carbon fiber reinforced PA6 composite. *Journal of Materials Processing Technology*, Vol. 296, 2021, id. 117230.
[198] Lionetto, F., F. Balle, and A. Maffezzoli. Hybrid ultrasonic spot welding of aluminum to carbon fiber reinforced epoxy composites. *Journal of Materials Processing Technology*, Vol. 247, 2017, pp. 289–295.
[199] Shi, R., Z. Liu, W. Liu, S. Ao, Z. Luo, and Y. Li. Effect of PA6 coating on the ultrasonic welding of CF/PA66 to 6061 aluminum alloy. *Journal of Materials Science*, Vol. 59, 2024, pp. 2328–2339.
[200] Kalyan Kumar, R. and M. Omkumar. Ultrasonic welding of CF/PA6 composite to 6061Al alloy utilizing an interfacial coating as energy director. *Journal of Adhesion Science and Technology*, Vol. 38, 2024, pp. 1–15.
[201] Huang, Z., S. Sugiyama, and J. Yanagimoto. Hybrid joining process for carbon fiber reinforced thermosetting plastic and metallic thin sheets by chemical bonding and plastic deformation. *Journal of Materials Processing Technology*, Vol. 213, 2013, pp. 1864–1874.
[202] Reisgen, U., A. Schiebahn, J. Lotte, C. Hopmann, D. Schneider, and J. Neuhaus. Innovative joining technology for the production of hybrid components from FRP and metals. *Journal of Materials Processing Technology*, Vol. 282, 2020.
[203] Xue, Y. Q., T. A. Tervoort, S. Rastogi, and P. J. Lemstra. Welding behavior of semicrystalline polymers. 2. Effect of cocrystallization on autoadhesion. *Macromolecules*, Vol. 33, 2000.
[204] Lamèthe, J. F., P. Beauchêne, and L. Léger. Polymer dynamics applied to PEEK matrix composite welding. *Aerospace Science and Technology*, Vol. 9, 2005.
[205] Kurtz, S. M. and J. N. Devine. PEEK biomaterials in trauma, orthopedic, and spinal implants. *Biomaterials*, Vol. 28, 2007, pp. 4845–4869.
[206] Awaja, F. Autohesion of polymers. *Polymer*, Vol. 97, 2016, pp. 387–407.
[207] Maffezzoli, A., J. M. Kenny, and L. Nicolais. A macrokinetic approach to crystallization modelling of semicrystalline thermoplastic matrices for advanced composites. *Journal of Materials Science*, Vol. 28, 1993, pp. 4994–5001.
[208] Schulz, E., G. Kalinka, and W. Auersch. Effect of transcrystallization in carbon fiber reinforced poly(p-phenylene sulfide) composites on the interfacial shear strength investigated with the single fiber pull-out test. *Journal of Macromolecular Science, Part B: Physics*, Vol. 35, 2006, pp. 527–546.
[209] Howarth, J., S. S. R. Mareddy, and P. T. Mativenga. Energy intensity and environmental analysis of mechanical recycling of carbon fibre composite. *Journal of Cleaner Production*, Vol. 81, 2014, pp. 46–50.
[210] Li, H. and K. Englund. Recycling of carbon fiber-reinforced thermoplastic composite wastes from the aerospace industry. *Journal of Composite Materials*, Vol. 51, 2017, pp. 1265–1273.
[211] Karuppannan Gopalraj, S. and T. Kärki. A review on the recycling of waste carbon fibre/glass fibre-reinforced composites: fibre recovery, properties and life-cycle analysis. *SN Applied Sciences*, Vol. 2, 2020, id. 433.
[212] Dauguet, M., O. Mantaux, N. Perry, and Y. F. Zhao. Recycling of CFRP for high value applications: Effect of sizing removal and environmental analysis of the Super Critical Fluid Solvolysis. *Procedia Cirp*, Vol. 29, 2015, pp. 734–739.
[213] Nguyen, P. N. D., M. Kubouchi, T. Sakai, S. A. Roces, F. T. Bacani, P. Yimsiri, et al. Relationship of mechanical properties and temperature of carbon fiber-reinforced plastics under microwave irradiation. *Clean Technologies and Environmental Policy*, Vol. 14, 2012, pp. 943–951.
[214] Pakdel, E., S. Kashi, R. Varley, and X. Wang. Recent progress in recycling carbon fibre reinforced composites and dry carbon fibre wastes. *Resources, Conservation and Recycling*, Vol. 166, 2021, id. 105340.
[215] Borjan, D., Ž. Knez, and M. Knez. Recycling of carbon fiber-reinforced composites— difficulties and future perspectives. *Materials (Basel)*, Vol. 14, 2021, id. 4191.
[216] Chen, P. Y., R. Feng, Y. Xu, and J. H. Zhu. Recycling and reutilization of waste carbon fiber reinforced plastics: Current status and prospects. *Polymers (Basel)*, Vol. 15, 2023, id. 3508.
[217] Vidal, J., C. Hornero, R. Garcia, J. Cuartero, A. Beaucamp, M. N. Collins, et al. Use of covalent dynamic networks as binders on epoxy-based carbon fiber composites: Effect on properties, processing, and recyclability. *Polymer Composites*, Vol. 44, 2023, pp. 7444–7456.
[218] Shuaib, N. A. and P. T. Mativenga. Energy demand in mechanical recycling of glass fibre reinforced thermoset plastic composites. *Journal of Cleaner Production*, Vol. 120, 2016, pp. 198–206.
[219] Witik, R. A., R. Teuscher, V. Michaud, C. Ludwig, and J. A. E. Månson. Carbon fibre reinforced composite waste: An environmental assessment of recycling, energy recovery and landfilling. *Composites Part A: Applied Science and Manufacturing*, Vol. 49, 2013, pp. 89–99.
[220] Bachmann, J., C. Hidalgo, and S. Bricout. Environmental analysis of innovative sustainable composites with potential use in aviation sector – A life cycle assessment review. *Science China: Technological Sciences*, Vol. 60, 2017, pp. 1301–1317.
[221] Yang, Y., R. Boom, B. Irion, D. J. van Heerden, P. Kuiper, and H. de Wit. Recycling of composite materials. *Chemical Engineering and Processing: Process Intensification*, Vol. 51, 2012, pp. 53–68.
[222] Unnikrishnan, T. G. and P. Kavan. A review study in ultrasonic-welding of similar and dissimilar thermoplastic polymers and its composites. *Materials Today: Proceedings*, Vol. 56, 2022, pp. 3294–3300.
[223] Yao, Y., Y. Pan, and S. Liu. Power ultrasound and its applications: A state-of-the-art review. *Ultrasonics Sonochemistry*, Vol. 62, 2020, pp. 1–20.
[224] Gu, X., D. Liu, and J. Liu. Effect of post-weld heat treatment on the dissimilar Cu/Al joints produced by high power ultrasonic spot welding. *ISIJ International*, Vol. 58, 2018, pp. 1721–1726.
[225] Shah, U. and X. Liu. Effect of ultrasonic energy on the spot weldability of aluminum alloy AA6061. *Materials & Design*, Vol. 192, 2020, id. 108690.
[226] Patel, V. K., S. D. Bhole, and D. L. Chen. Microstructure and mechanical properties of dissimilar welded Mg-Al joints by ultrasonic spot welding technique. *Science and Technology of Welding and Joining*, Vol. 17, 2012, pp. 202–206.

[227] Li, H., C. Chen, R. Yi, Y. Li, and J. Wu. Ultrasonic welding of fiber-reinforced thermoplastic composites: a review. *International Journal of Advanced Manufacturing Technology*, Vol. 120, 2022, pp. 29–57.

[228] Bhudolia, S. K., G. Gohel, K. F. Leong, and A. Islam. Advances in ultrasonic welding of thermoplastic composites: a review. *Materials (Basel)*, Vol. 13, 2020, pp. 1284–1310.

[229] Lee, S. *Process and quality characterization for ultrasonic welding of lithium-ion batteries*, University of Michigan, Michigan, USA, 2013. https://hdl.handle.net/2027.42/99803.

[230] Al-Sarraf, Z. S. *A study of ultrasonic metal welding*, University of Glasgow, Glasgow, United Kingdom, 2013. https://eleanor.lib.gla.ac.uk/record=b2982130.

[231] Zhao, T., Q. Zhao, W. Wu, L. Xi, Y. Li, Z. Wan, et al. Enhancing weld attributes in ultrasonic spot welding of carbon fibre-reinforced thermoplastic composites: Effect of sonotrode configurations and process control. *Composites, Part B: Engineering*, Vol. 211, 2021, pp. 1–11.

[232] Yang, Y., Y. Y. Li, Z. Liu, Y. Y. Li, S. Ao, and Z. Luo. Ultrasonic welding of short carbon fiber reinforced PEEK with spherical surface anvils. *Composites, Part B: Engineering*, Vol. 231, 2022, pp. 1–10.

[233] Zhi, Q., Y. H. Gao, L. Lu, Z. X. Liu, and P. C. Wang. Online inspection of weld quality in ultrasonic welding of carbon fiber/polyamide 66 without energy directors. *Welding Journal*, Vol. 97, 2018, pp. 65–74.

[234] Gao, Y. H., Q. Zhi, L. Lu, Z. X. Liu, and P. C. Wang. Ultrasonic welding of carbon fiber reinforced nylon 66 composite without energy director. *Journal of Manufacturing Science and Engineering*, Vol. 140, 2018, pp. 1–11.

[235] Jongbloed, B., J. Teuwen, and I. F. Villegas. On the use of a rounded sonotrode for the welding of thermoplastic composites. *Journal of Advanced Joining Processes*, Vol. 7, 2023, id. 100144.

[236] Zhao, T., C. Rans, I. Fernandez Villegas, and R. Benedictus. On sequential ultrasonic spot welding as an alternative to mechanical fastening in thermoplastic composite assemblies: A study on single-column multi-row single-lap shear joints. *Composites Part A: Applied Science and Manufacturing*, Vol. 120, 2019, pp. 1–11.

[237] Zhao, Q., H. Wu, X. Chen, Y. Ni, X. An, W. Wu, et al. Insights into the structural design strategies of multi-spot ultrasonic welded joints in thermoplastic composites: A finite element analysis. *Composite Structures*, Vol. 299, 2022, id. 115996.

[238] Palardy, G. and I. F. Villegas. On the effect of flat energy directors thickness on heat generation during ultrasonic welding of thermoplastic composites. *Composite Interfaces*, Vol. 24, 2017, pp. 203–214.

[239] Zhi, Q., X. R. Tan, and Z. X. Liu. Effect of moisture on the ultrasonic welding of carbon-fiber-reinforced polyamide 66 composite. *Polymers (Basel)*, Vol. 14, 2017, pp. 1–13.

[240] Lee, T. H., H. T. Fan, Y. Li, D. Shriver, J. Arinez, G. Xiao, et al. Enhanced performance of ultrasonic welding of short carbon fiber polymer composites through control of morphological parameters. *Journal of Manufacturing Science and Engineering*, Vol. 142, 2020, pp. 1–12.

[241] Gomer, A., W. Zou, N. Grigat, J. Sackmann, and W. K. Schomburg. Low-cost fabrication of fiber reinforced plastics by ultrasonic processing. *ECCM 2018 – 18th European Conference on Composite Materials*, 2020.

[242] Gomer, A., W. Zou, N. Grigat, J. Sackmann, and W. K. Schomburg. Fabrication of fiber reinforced plastics by ultrasonic welding. *Journal of Composites Science*, Vol. 2, 2018, pp. 1–14.

[243] Zhi, Q., X. R. Tan, Z. X. Liu, W. H. Liu, Y. Liu, B. L. Ou, et al. The effect of a hollow fixture on energy dissipation of ultrasonic welded carbon fiber/polyamide 66 composite. *Welding Journal*, Vol. 100, 2021, pp. 371–378.

[244] Palardy, G., H. Shi, A. Levy, S. Le Corre, and I. Fernandez Villegas. A study on amplitude transmission in ultrasonic welding of thermoplastic composites. *Composites Part A: Applied Science and Manufacturing*, Vol. 113, 2018, pp. 339–349.

[245] Koutras, N., J. Amirdine, N. Boyard, I. Fernandez Villegas, and R. Benedictus. Characterisation of crystallinity at the interface of ultrasonically welded carbon fibre PPS joints. *Composites Part A: Applied Science and Manufacturing*, Vol. 125, 2019, pp. 1–11.

[246] Jongbloed, B., R. Vinod, J. Teuwen, R. Benedictus, and I. F. Villegas. Improving the quality of continuous ultrasonically welded thermoplastic composite joints by adding a consolidator to the welding setup. *Composites Part A: Applied Science and Manufacturing*, Vol. 155, 2022, pp. 1–13.

[247] Brito, C. B., J. Teuwen, C. A. Dransfeld, and I. F. Villegas. The effects of misaligned adherends on static ultrasonic welding of thermoplastic composites. *Composites Part A: Applied Science and Manufacturing*, Vol. 155, 2022, pp. 1–13.

[248] Wang, Y., Z. Rao, S. Bao, W. Ma, and S. Liao. Process and strength analysis of joining CF/PA6 composite plates without energy director by a servo-driven ultrasonic welder. *Journal of Materials Research and Technology*, Vol. 19, 2022, pp. 4613–4626.

[249] Li, Y., B. Yu, B. Wang, T. H. Lee, and M. Banu. Online quality inspection of ultrasonic composite welding by combining artificial intelligence technologies with welding process signatures. *Materials & Design*, Vol. 194, 2020, pp. 1–10.

[250] Sun, L., S. J. Hu, and T. Freiheit. Feature-based quality classification for ultrasonic welding of carbon fiber reinforced polymer through Bayesian regularized neural network. *Journal of Manufacturing Systems*, Vol. 58, 2021, pp. 335–347.

[251] Wang, B., Y. Li, Y. Luo, X. Li, and T. Freiheit. Early event detection in a deep-learning driven quality prediction model for ultrasonic welding. *Journal of Manufacturing Systems*, Vol. 60, 2021, pp. 325–336.

[252] Wang, K., D. Shriver, Y. Li, M. Banu, S. J. Hu, G. Xiao, et al. Characterization of weld attributes in ultrasonic welding of short carbon fiber reinforced thermoplastic composites. *Journal of Manufacturing Processes*, Vol. 29, 2017, pp. 124–132.

[253] Natesh, M., L. Yun, S. Arungalai Vendan, K. A. Ramesh Kumar, L. Gao, X. Niu, et al. Experimental and numerical procedure for studying strength and heat generation responses of ultrasonic welding of polymer blends. *Measurement*, Vol. 132, 2019, pp. 1–10.

[254] Hargou, K., K. Pingkarawat, A. P. Mouritz, and C. H. Wang. Ultrasonic activation of mendable polymer for self-healing carbon–epoxy laminates. *Composites, Part B: Engineering*, Vol. 45, 2013, pp. 1031–1039.

[255] Wang, K., Y. Li, M. Banu, J. Li, W. Guo, and H. Khan. Effect of interfacial preheating on welded joints during ultrasonic composite welding. *Journal of Materials Processing Technology*, Vol. 246, 2017, pp. 116–122.

[256] Tao, W., X. Su, H. Wang, Z. Zhang, H. Li, and J. Chen. Influence mechanism of welding time and energy director to the thermoplastic composite joints by ultrasonic welding. *Journal of Manufacturing Processes*, Vol. 37, 2019, pp. 196–202.

[257] Williams, S. and G. Palardy. Ultrasonic consolidation of dry carbon fiber and polyphenylene sulfide film. *Society for the Advancement of Material and Process Engineering*, 2020, pp. 1–12.

[258] Villegas, I. F., L. Moser, A. Yousefpour, P. Mitschang, and H. E. N. Bersee. Process and performance evaluation of ultrasonic, induction and resistance welding of advanced thermoplastic composites. *Journal of Thermoplastic Composite Materials*, Vol. 26, 2013, pp. 1007–1024.

[259] Liu, S. J., I. T. Chang, and S. W. Hung. Factors affecting the joint strength of ultrasonically welded polypropylene composites. *Polymer Composites*, Vol. 22, 2001, pp. 132–141.

[260] Fernandez Villegas, I., B. Valle Grande, H. E. N. Bersee, and R. Benedictus. A comparative evaluation between flat and traditional energy directors for ultrasonic welding of CF/PPS thermoplastic composites. *Composite Interfaces*, Vol. 22, 2015, pp. 717–729.

[261] Tsiangou, E., S. Teixeira de Freitas, I. Fernandez Villegas, and R. Benedictus. Investigation on energy director-less ultrasonic welding of polyetherimide (PEI)- to epoxy-based composites. *Composites, Part B: Engineering*, Vol. 173, 2019, pp. 1–11.

[262] Van Wijk, H., G. A. Luiten, P. G. Van Engen, and C. J. Nonhof. Process optimization of ultrasonic welding. *Polymer Engineering and Science*, Vol. 36, 1996, pp. 1165–1176.

[263] Müller, F. W., C. Mirz, S. Weil, A. Schiebahn, B. Corves, and U. Reisgen. Weld quality characterization by vibration analysis for ultrasonic metal welding processes. *Journal of Advanced Joining Processes*, Vol. 8, 2023, id. 100149.

[264] Gaurav, A. and K. K. Singh. Fatigue behavior of FRP composites and CNT-Embedded FRP composites: A review. *Polymer Composites*, Vol. 39, 2018, pp. 1785–1808.

[265] Radakovic, D. J. and M. Tumuluru. An evaluation of the cross-tension test of resistance spot welds in high-strength dual-phase steels. *Welding Journal*, Vol. 91, 2012, pp. 8–15.

[266] Szlosarek, R., T. Karall, N. Enzinger, C. Hahne, and N. Meyer. Mechanical testing of flow drill screw joints between fibre-reinforced plastics and metals. *Materials Testing*, Vol. 55, 2013, pp. 737–742.

[267] Haque, R. and Y. Durandet. Strength prediction of self-pierce riveted joint in cross-tension and lap-shear. *Materials & Design*, Vol. 108, 2016, pp. 666–678.

[268] Kairouz, K. C. and F. L. Matthews. Strength and failure modes of bonded single lap joints between cross-ply adherends. *Composites*, Vol. 24, 1993, pp. 475–484.

[269] Harras, B., K. C. Cole, and T. Vu-Khanh. Optimization of the Ultrasonic Welding of PEEK-Carbon Composites. *Journal of Reinforced Plastics and Composites*, Vol. 15, 2016, pp. 174–182.

[270] DMslon, C. Graphite composite truss welding and cap section forming subsystems. *Program Results*, Vol. 2, 1980, pp. 1–105.

[271] Zhi, Q., X. R. Tan, L. Lu, L. Y. Chen, J. C. Li, and Z. X. Liu. Decomposition of ultrasonically welded carbon fiber/polyamide 66 and its effect on weld quality. *Welding in the World*, Vol. 61, 2017, pp. 1017–1028.

[272] Zhang, J., K. K. Chawla, and U. K. Vaidya. Ultrasonic welding of glass fiber reinforced polypropylene. *Advances in Materials Research*, Vol. 557–559, 2012, pp. 1313–1316.

[273] Wang, T., Y. Li, Z. Dong, Y. Yang, Z. Liu, and Y. Li. Ultrasonic welding of CFRTP based on structured surfaces. Cailiao Gongcheng/Journal. *Materials Engineering*, Vol. 51, 2023, pp. 33–41.

[274] Wang, K., D. Shriver, M. Banu, S. Jack Hu, G. Xiao, J. Arinez, et al. Performance prediction for ultrasonic spot welds of short carbon fiber-reinforced composites under shear loading. *Journal of Manufacturing Science and Engineering*, Vol. 139, 2017, pp. 1–10.

[275] Kalyan Kumar, R. and M. Omkumar. Investigation and characterization of ultrasonically welded GF/PA6T composites. *Materials Today: Proceedings*, Vol. 26, 2020, pp. 282–286.

[276] Choudhury, M. R. and K. Debnath. Analysis of tensile failure load of single-lap green composite specimen welded by high-frequency ultrasonic vibration. *Materials Today: Proceedings*, Vol. 28, 2020, pp. 739–744.

[277] Zhang, G. and J. Qiu. Ultrasonic thermal welding of immiscible thermoplastics via the third phase. *Journal of Materials Processing Technology*, Vol. 299, 2022, pp. 1–9.

[278] Villegas, I. F. and G. Palardy. Ultrasonic welding of CF/PPS composites with integrated triangular energy directors: melting, flow and weld strength development. *Composite Interfaces*, Vol. 24, 2016, pp. 515–528.

[279] Zhang, G., J. Qiu, E. Sakai, and Z. Zhou. Interface investigation between dissimilar materials by ultrasonic thermal welding by the third phase. *International Journal of Adhesion and Adhesives*, Vol. 104, 2021, pp. 1–8.

[280] Alexenko, V. O., S. V. Panin, S. A. Bochkareva, T. Defang, and I. L. Panov. Ultrasonic welding of lap joints of PEI plates with PEI/CF-fabric prepregs. *Fracture & Structural Integrity/Frattura ed Integrità Strutturale*, Vol. 18, 2024, pp. 390–409.

[281] Calabrese, L., G. Cicala, G. Di Bella, E. Proverbio, C. Tosto, and L. Saitta. Optimisation of ultrasonic welding process of carbon/epoxy composites using Nylon-based or PES thermoplastic interlayers. *Composites, Part B: Engineering*, Vol. 275, 2024, id. 111318.

[282] Tsiangou, E., S. T. de Freitas, R. Benedictus, and I. F. Villegas. On the sensitivity of the ultrasonic welding process of epoxy- to polyetheretherketone (PEEK)-based composites to the welding force and amplitude of vibrations. *Compos Part C Open Access*, Vol. 5, 2021, pp. 1–12.

[283] Tateishi, N., T. H. North, and R. T. Woodhams. Ultrasonic welding using tie-layer materials. part I: Analysis of process operation. *Polymer Engineering and Science*, Vol. 32, 1992, pp. 600–611.

[284] Gohel, G., S. K. Bhudolia, J. Kantipudi, K. F. Leong, and R. J. Barsotti. Ultrasonic welding of novel Carbon/Elium® with carbon/epoxy composites. *Composites Communications*, Vol. 22, 2020, pp. 1–5.

[285] Parmar, U. and D. H. Pandya. Experimental investigation of ultrasonic welding on non-metallic material. *Procedia Technology*, Vol. 23, 2016, pp. 551–557.

[286] Wang, J., C. Lu, C. Xiao, J. Cheng, R. Ren, and X. Xiong. Heat distribution simulation and effects of ultrasonic welding amplitude on carbon fiber/polyetherimide composite joint properties. *Materials Letters*, Vol. 340, 2023, id. 134148.

[287] Sánchez-Cabrera, V. M., C. Rubio-González, J. I. Ruíz-Vela, and C. Ramírez-Baltazar. Effect of preheating temperature and filler metal type on the microstructure, fracture toughness and fatigue crack growth of stainless steel welded joints. *Materials Science & Engineering, A: Structural Materials: Properties, Microstructure and Processing*, Vol. 452–453, 2007, pp. 235–243.

[288] Grouve, W. J. B., L. L. Warnet, B. Rietman, and R. Akkerman. On the weld strength of in situ tape placed reinforcements on weave reinforced structures. *Composites Part A: Applied Science and Manufacturing*, Vol. 43, 2012, pp. 1530–1536.

[289] Qu, H., Z. Wu, L. Hou, Z. Zhang, and W. Wu. Ultrasonic-assisted reinforcement and annealing treatment of additive manufacturing polyether-ether-ketone. *Polymer Composites*, Vol. 44, 2023, pp. 1684–1695.

[290] Karger-Kocsis, J. and K. Friedrich. Temperature and strain-rate effects on the fracture toughness of poly(ether ether ketone) and its short glass-fibre reinforced composite. *Polymer*, Vol. 27, 1986, pp. 1753–1760.

[291] Gao, S. L. and J. K. Kim. Cooling rate influences in carbon fibre/PEEK composites. Part II: Interlaminar fracture toughness. *Composites Part A: Applied Science and Manufacturing*, Vol. 32, 2001, pp. 763–774.

[292] Sacchetti, F., W. J. B. Grouve, L. L. Warnet, and I. F. Villegas. Effect of cooling rate on the interlaminar fracture toughness of unidirectional Carbon/PPS laminates. *Engineering Fracture Mechanics*, Vol. 203, 2018, pp. 126–136.

[293] Li, L., M. Zheng, D. Guo, and Q. He. Advantage of quantum heating on double-vibrator ultrasonic welding of polymers. *Hanjie Xuebao/Transactions China Welding Institution*, Vol. 44, 2023, pp. 78–83.

[294] Barkley, K. M., J. S. Arner, T. A. Pike, P. Diwakar, and C. M. Birrenkott. Correlation of surface and interfacial temperature during differential ultrasonic spot welding. *Journal of Advanced Joining Processes*, Vol. 7, 2023, id. 100142.

[295] Grimm, R. A. Welding processes for plastics. *Advanced Materials & Processes*, Vol. 147, 1995, pp. 27–30.

[296] Tsujino, J., M. Hongoh, M. Yoshikuni, H. Hashii, and T. Ueoka. Welding characteristics of 27, 40 and 67 kHz ultrasonic plastic welding systems using fundamental- and higher-resonance frequencies. *Ultrasonics*, Vol. 42, 2004, pp. 131–137.

[297] Tsujino, J., M. Hongoh, R. Tanaka, R. Onoguchi, and T. Ueoka. Ultrasonic plastic welding using fundamental and higher resonance frequencies. *Ultrasonics*, Vol. 40, 2002, pp. 375–378.

[298] Chien, M. C. and R. A. Weiss. Strain-induced crystallization behavior of poly(ether ether ketone) (PEEK). *Polymer Engineering and Science*, Vol. 28, 1988, pp. 6–12.

[299] Rao, I. J. and K. R. Rajagopal. A study of strain-induced crystallization of polymers. *International Journal of Solids and Structures*, Vol. 38, 2001, pp. 1149–1167.

[300] Yoon, W. J., H. S. Myung, B. C. Kim, and S. S. Im. Effect of shearing on crystallization behavior of poly(ethylene naphthalate). *Polymer*, Vol. 41, 2000, pp. 4933–4942.

[301] Zhang, R. C., Y. Xu, A. Lu, K. Cheng, Y. Huang, and Z. M. Li. Shear-induced crystallization of poly(phenylene sulfide). *Polymer*, Vol. 49, 2008, pp. 2604–2613.

[302] Benatar, A. and T. G. Gutowski. Review of methods for fusion bonding thermoplastic composites. *SAMPE Journal*, Vol. 23, 1987, pp. 1–10.

[303] Zach, T., J. Lew, T. H. North, and R. T. Woodhams. Joining of high strength oriented polypropylene using electromagnetic induction bonding and ultrasonic welding. *Materials Science and Technology*, Vol. 5, 1989, pp. 281–287.

[304] Tateishi, N., T. B. Zach, R. T. Woodhams, and T. H. North. Ultrasonic bonding of roll-drawn polypropylene using tie-layers. *Annual Technical Conference of the Society of Plastics Engineers*, 1989, pp. 198–496.

[305] Grouve, W. J. B., G. Vanden Poel, L. L. Warnet, and R. Akkerman. On crystallisation and fracture toughness of poly(phenylene sulphide) under tape placement conditions. *Plast Rubber and Composites*, Vol. 42, 2013, pp. 282–288.

[306] Spruiell, J. E. *A review of the measurement and development of crystallinity and its relation to properties in neat poly(phenylene sulfide) and its fiber reinforced composites*, U.S. Department of Energy (DOE) Information Bridge, Oak Ridge, TN, 2005.

[307] Wise, R. J. and A. D. H. Bates. Ultrasonic welding of PES to aluminum alloy. *Annual Technical Conference – ANTEC, Conference Proceedings*, Vol. 1, San Diago, 1996, pp. 1203–1207.

[308] Singh Rana, R., I. Singh, and A. Kumar Sharma. Ultrasonic welding of printed/molded sustainable polymer specimens with energy directors. *Ultrasonics*, Vol. 134, 2023, id. 107078.

[309] Potente, H. Ultrasonic welding – Principles & theory. *Materials & Design*, Vol. 5, 1984, pp. 228–234.

[310] Eveno, E. C. and J. W. Gillespie. Experimental investigation of ultrasonic welding of graphite reinforced polyetheretherketone composites. *National SAMPE Tech Conferences*, Vol. 21, New Jersey, 1989, pp. 923–934.

[311] Huang, Y. Study on design of welding-joint and structure of welding based on ultrasonic welding technology. *Applied Mechanics and Materials*, Vol. 101–102, 2012, pp. 871–875.

[312] Khatri, B., M. F. Roth, and F. Balle. Ultrasonic welding of additively manufactured PEEK and carbon-fiber-reinforced PEEK with integrated energy directors. *Journal of Manufacturing and Materials Processing*, Vol. 7, 2023, id. 2.

[313] Levy, A., S. Le Corre, and A. Poitou. Ultrasonic welding of thermoplastic composites: A numerical analysis at the mesoscopic scale relating processing parameters, flow of polymer and quality of adhesion. *International Journal of Material Forming*, Vol. 7, 2014, pp. 39–51.

[314] Koyanagi, J., M. Takamura, K. Wakayama, K. Uehara, and S. Takeda. Numerical simulation of ultrasonic welding for CFRP using energy director. *Advanced Composite Materials*, Vol. 31, 2022, pp. 428–441.

[315] Cilento, F., A. Bassano, L. Sorrentino, A. Martone, M. Giordano, and B. Palmieri. PVB nanocomposites as energy directors in ultrasonic welding of epoxy composites. *Journal of Composites Science*, Vol. 7, 2023, id. 160.

[316] Li, Y., Y. Li, Z. Liu, Y. Yang, S. Ao, and Z. Luo. Investigation of ultrasonic welding of CF/PA66 using stainless steel mesh energy directors. *Thin-Walled Structures*, Vol. 188, 2023, id. 110795.

[317] Tian, D., V. O. Alexenko, S. V. Panin, A. A. Bogdanov, and D. G. Buslovich. Effect of the energy director material on the structure and properties of ultrasonic welded lap joints of PEI plates with CF fabric/PEI prepreg. *Journal of Composites Science*, Vol. 8, 2024, pp. 1–22.

[318] Korycki, A., F. Carassus, C. Garnier, F. Chabert, and T. Djilali. Effect of energy director thickness on thermal diffusion and joint quality during ultrasonic welding of CF/PEEK composites. *Materials Research Proceedings*, Vol. 28, 2023, pp. 1819–1828.

[319] Wang, T., K. Yasuda, and H. Nishikawa. Study on the SPCC and CFRTP hybrid joint performance produced with additional nylon-6 interlayer by ultrasonic plastic welding. *Polymers (Basel)*, Vol. 14, 2022, id. 5235.

[320] Levy, A., S. Le Corre, N. Chevaugeon, and A. Poitou. A level set based approach for the finite element simulation of a forming process involving multiphysics coupling: Ultrasonic welding of thermoplastic composites. *European Journal of Mechanics-A/Solids*, Vol. 30, 2011, pp. 501–509.

[321] Levy, A., S. Le Corre, and I. Fernandez Villegas. Modeling of the heating phenomena in ultrasonic welding of thermoplastic composites with flat energy directors. *Journal of Materials Processing Technology*, Vol. 214, 2014, pp. 1361–1371.

[322] Li, Y., J. Arinez, Z. Liu, T. Hwa Lee, H. T. Fan, G. Xiao, et al. Ultrasonic welding of carbon fiber reinforced composite with

variable blank holding force. *Journal of Manufacturing Science and Engineering*, Vol. 140, 2018, pp. 1–11.

[323] Cilento, F., B. Palmieri, L. Sorrentino, M. Giordano, and A. Martone. Insights on the use of PVB nanocomposites as energy directors in ultrasonic welding of epoxy composites. *Materials Research Proceedings*, Vol. 28, 2023, pp. 1851–1860.

[324] Wang, Y., Z. Rao, D. Wang, W. Ma, and S. Liao. Investigation of the weldability of PA6 and CF/PA6 based on a servo-driven ultrasonic welder without using energy director. *Journal of Materials Research and Technology*, Vol. 26, 2023, pp. 2465–2480.

[325] Senders, F., M. van Beurden, G. Palardy, and I. F. Villegas. Zero-flow: a novel approach to continuous ultrasonic welding of CF/PPS thermoplastic composite plates. *Advanced Manufacturing: Polymer & Composites Science*, Vol. 2, 2016, pp. 83–92.

[326] Wang, J., S. Jia, Y. Yuan, L. Xia, F. Wang, R. Ren, et al. Optimization and mechanism of ultrasonic welding process of CF/PEI composite. *Cailiao Gongcheng/Journal of Materials and Engineering*, Vol. 51, 2023, pp. 42–49.

[327] Wang, T., R. Shi, Z. Liu, S. Ao, Z. Luo, K. Wang, et al. Effect of ultrasonic embossing and welding time on the joint performance of ultrasonically welded short carbon fiber reinforced PEEK. *Journal of Materials Research and Technology*, Vol. 28, 2024, pp. 3258–3266.

[328] Rubino, F., H. Parmar, T. Mancia, and P. Carlone. Ultrasonic welding of glass reinforced epoxy composites using thermoplastic hybrid interlayers. *Composite Structures*, Vol. 314, 2023, id. 116980.

[329] Tian, Z., Q. Zhi, G. Zhang, X. Tan, L. Lu, P. Wang, et al. Influence of pre-pressing ring on the weld quality of ultrasonically welded short carbon fiber reinforced nylon 6 composite. *Polymers (Basel)*, Vol. 14, 2022, id. 3115.

[330] Liu, S. J. and I. T. Chang. Optimizing the weld strength of ultrasonically welded nylon composites. *Journal of Composite Materials*, Vol. 36, 2002, pp. 611–624.

[331] Jongbloed, B., J. Teuwen, G. Palardy, I. Fernandez Villegas, and R. Benedictus. Continuous ultrasonic welding of thermoplastic composites: Enhancing the weld uniformity by changing the energy director. *Journal of Composite Materials*, Vol. 54, 2020, pp. 2023–2035.

[332] Brito, C. B., J. Teuwen, C. A. Dransfeld, and I. F. Villegas. On improving process efficiency and weld quality in ultrasonic welding of misaligned thermoplastic composite adherends. *Composite Structures*, Vol. 304, 2023, id. 116342.

[333] Suresh, K. S., M. R. Rani, K. Prakasan, and R. Rudramoorthy. Modeling of temperature distribution in ultrasonic welding of thermoplastics for various joint designs. *Journal of Materials Processing Technology*, Vol. 186, 2007, pp. 138–146.

[334] Bose, S., H. M. Chelladurai, and K. Ponappa. Submerged ultrasonic welding of fused filament fabricated short carbon-fibre-reinforced polyamide plates with energy directors. *Proceedings of the Institution of Mechanical Engineers, Part L: Journal of Materials: Design and Applications*, Vol. 238, 2023, pp. 857–874.

[335] Bose, S., H. M. Chelladurai, and P. Kanaiyaram. An experimental investigation on feasibility of submerged ultrasonic spot welding of thermoplastics. *Proceedings of the Institution of Mechanical Engineers, Part L: Journal of Materials: Design and Applications*, Vol. 238, 2024, pp. 2043–2057.

[336] Bonmatin, M., F. Chabert, G. Bernhart, T. Cutard, and T. Djilali. Ultrasonic welding of CF/PEEK composites: Influence of welding parameters on interfacial temperature profiles and mechanical properties. *Composites Part A: Applied Science and Manufacturing*, Vol. 162, 2022, pp. 1–12.

[337] Köhler, F., I. F. Villegas, C. Dransfeld, and A. Herrmann. Static ultrasonic welding of carbon fibre unidirectional thermoplastic materials and the influence of heat generation and heat transfer. *Journal of Composite Materials*, Vol. 55, 2021, pp. 2087–2102.

[338] Tsiangou, E., J. Kupski, S. Teixeira de Freitas, R. Benedictus, and I. F. Villegas. On the sensitivity of ultrasonic welding of epoxy- to polyetheretherketone (PEEK)-based composites to the heating time during the welding process. *Composites Part A: Applied Science and Manufacturing*, Vol. 144, 2021, pp. 1–13.

[339] Isozaki, M., M. Takamura, S. Takeda, and J. Koyanagi. Comprehensive evaluation method of bond strength in ultrasonic welding for CFRTP. *Procedia Structural Integrity*, Vol. 52, 2024, pp. 176–186.

[340] Smeets, E. T. B., C. D. Rans, S. G. P. Castro, and I. F. Villegas. To measure is to know: Evaluating indirect measurement techniques for observing the damage tolerance behaviour of spot welded thermoplastic composites. *Journal of Advanced Joining Processes*, Vol. 8, 2023, id. 100152.

[341] Ward, A. A., Y. Zhang, and Z. C. Cordero. Junction growth in ultrasonic spot welding and ultrasonic additive manufacturing. *Acta Materialia*, Vol. 158, 2018, pp. 393–406.

[342] Nikoi, R., M. M. Sheikhi, and N. B. M. Arab. Experimental analysis of effects of ultrasonic welding on weld strength of polypropylene composite samples. *International Journal of Engineering*, Vol. 28, 2015, pp. 447–453.

[343] Tirband, H., D. Akbari, and P. Faraji Kalajahi. Improving the quality of the ultrasonic welded thermoset-based composites using laser surface treatment. *Proceedings of the Institution of Mechanical Engineers, Part L: Journal of Materials: Design and Applications*, 2024.

[344] Chan, W. X., S. H. Ng, K. H. H. Li, W. T. Park, and Y. J. Yoon. Micro-ultrasonic welding using thermoplastic-elastomeric composite film. *Journal of Materials Processing Technology*, Vol. 236, 2016, pp. 183–188.

[345] Meng, Y., D. Peng, Q. Nazir, G. Kuntumalla, M. C. Rajagopal, H. C. Chang, et al. Ultrasonic welding of soft polymer and metal: A preliminary study. *ASME 2019 14th International Manufacturing Science and Engineering Conference MSEC 2019*, Vol. 2, 2019.

[346] Galiana, S., M. Moradi, P. Wierach, and D. Zarouchas. Innovative welding integration of acousto-ultrasonic composite transducers onto thermoplastic composite structures. *Structural Health Monitoring*, 2024, pp. 1–15.

[347] Sancaktar, E. Polymer adhesion by ultrasonic welding. *Journal of Adhesion Science and Technology*, Vol. 13, 1999.

[348] Quader, R., L. Klinstein, D. Grewell, and L. K. Narayanan. Evaluation of the influence of ultrasonic vibration on physical, tensile, and morphological properties of fused deposition modeled specimens. *The International Journal of Advanced Manufacturing Technology*, 2024.

[349] Zhang, C. and L. Li. A coupled thermal-mechanical analysis of ultrasonic bonding mechanism. *Metallurgical and Materials Transactions B*, Vol. 40, 2009, pp. 196–207.

[350] Hopmann, C., R. Dahlmann, M. Weihermüller, J. Wipperfürth, and J. Sommer. Determination of the frequency- and temperature-dependent stiffness and damping properties of thermoplastics for the prediction of the vibration and heating behaviour during ultrasonic welding. *Welding in the World*, Vol. 67, 2023, pp. 435–445.

[351] Yang, Y., Z. Liu, Y. Wang, and Y. Li. Numerical study of contact behavior and temperature characterization in ultrasonic welding of CF/PA66. *Polymers (Basel)*, Vol. 14, 2022, id. 683.
[352] Tutunjian, S., M. Dannemann, N. Modler, M. Kucher, and A. Fellermayer. A numerical analysis of the temporal and spatial temperature development during the ultrasonic spot welding of fibre-reinforced thermoplastics. *Journal of Manufacturing and Materials Processing*, Vol. 4, 2020, id. 30.
[353] Zhu, Y., Z. Tian, D. Zhang, and Z. Liu. Classification of weld quality in ultrasonic composite welding using vibration information. *Nondestructive Testing and Evaluation*, 2024.
[354] Zhu, J. and C. Wang. Biodegradable plastics: Green hope or greenwashing? *Marine Pollution Bulletin*, Vol. 161, 2020, id. 111774.
[355] Oulidi, O., A. Nakkabi, A. Bouymajane, I. Elaraaj, F. R. Filali, M. Fahim, et al. Biodegradation of polyamide 6 by Lysinibacillus sp, Alcaligene faecalis and Enterococcus faecalis. *Cleaner Chemical Engineering*, Vol. 3, 2022, id. 100054.
[356] Luo, K., J. Liu, K. Abbay, Y. Mei, X. Guo, Y. Song, et al. The relationships between the structure and properties of PA56 and PA66 and their fibers. *Polymers (Basel)*, Vol. 15, 2023, id. 2877.
[357] Rafiqah, S. A., A. Khalina, A. S. Harmaen, I. A. Tawakkal, K. Zaman, M. Asim, et al. A review on properties and application of bio-based poly(Butylene succinate). *Polymers (Basel)*, Vol. 13, 2021, id. 1436.
[358] Gregor-Svetec, D. Polymers in printing filaments. *Polymers for 3D Printing Methods, Properties, and Characteristics*, 2022.
[359] Samir, A., F. H. Ashour, A. A. A. Hakim, and M. Bassyouni. Recent advances in biodegradable polymers for sustainable applications. *Npj Materials Degradation*, Vol. 6, 2022, id. 68.
[360] Shaikh, S., M. Yaqoob, and P. Aggarwal. An overview of biodegradable packaging in food industry. *Current Research in Food Science*, Vol. 4, 2021, pp. 503–520.
[361] Almasi B. G. Biodegradable polymers. *Biodegradation - Life of Science. Edited vol*, In: R.Chamy, Ed., InTech, Tabriz, Iran, 2013.